Doctoral Dissertation
Doctoral Program in Civil and Environmental Engineering (33rd Cycle)

Community Resilience and Seismic Performance of Physical Infrastructures

Alessandro Cardoni
* * * * * *

Supervisor
Prof. Gian Paolo Cimellaro

Doctoral Examination Committee:
Prof. Joan Ramon Casas, Referee, Universitat Politecnica de Catalunya
Prof. Andrea Dall'Asta, Referee, University of Camerino
Prof. Camillo Nuti, Committee, Roma Tre University
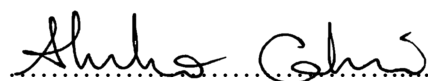Prof. Paolo Gardoni, Committee, University of Illinois Urbana-Champaign
Prof. Giuseppe Carlo Marano, Committee, Politecnico di Torino

Politecnico di Torino
July 9, 2021

I hereby declare that, the contents and organisation of this dissertation constitute my own original work and does not compromise in any way the rights of third parties, including those relating to the security of personal data.

Alessandro Cardoni
Turin, July 9, 2021

Abstract

Over the years, community resilience has attracted tremendous attention due to the increasing number of natural and man-made disasters. The lack of a concise and methodical approach makes it challenging to evaluate resilience, especially on large scale applications. This dissertation proposes new tools to evaluate seismic resilience at the regional and urban level. The proposed method to quantify regional resilience is inspired by existing indicator-based frameworks. In the analysis, only publicly available statistical census data has been used. For each Italian regions, three different indexes are calculated. The first is a measure of resilience in normal conditions, while the others are related to the emergency and the restoration phases following an earthquake. Results highlight those aspects and indicators that influence regional resilience the most and can be used to better distribute funds among the various regions.

The testbed for the performance and resilience assessment of infrastructure systems is a virtual city resembling a typical medium size European city. The analyzed infrastructures are the road transportation system, the power, and the telecommunication network. The transportation network has been modelled using graph theory. This allows to define different metrics that help to quantify the seismic performance. Moreover, the interdependence with the building portfolio has been considered. Once the level of the damage to the buildings is estimated, the footprint of the generated debris is determined. Thus, for a given seismic scenario, blocked roads can be identified. The information on roads blocked by debris is used to update evacuation paths and calculate the travel time of injured people to the closest hospital. The power grid is designed implicitly modeling the interdependency with the building portfolio. The fragility of the power network's substations is linked to the buildings' seismic fragility, as electrical substations are likely to fail because of the damages that occur to the buildings hosting them. As a result of the analysis, damaged substations and users not supplied can be

determined. A new resilience index that considers redundancy and resourcefulness is introduced and compared to others available in the literature. The telecommunication network has been modelled based on publicly available information and visual inspection. The connectivity is based on a three-layer hierarchical approach. The most significant damages suffered by this system are due to the interdependency with the built environment. Collapses of buildings where servers and towers are installed yield to the failure of those nodes. The performance metrics for resilience of this infrastructure are evaluated in terms of damage to telecommunication towers, throughput, and number of users per antenna.

The results of this research provide practical and replicable solutions to evaluate infrastructure performances and quantify resilience. The methodologies and tools proposed could help decision-makers not only in the emergency management phase but also in the allocation of resources for implementing preventive measures.

Acknowledgments

Contents

List of Tables

List of Figures

3

Chapter 1

1 Introduction

1.1 Background and problem definition

In recent years, extreme events have been increasing and their impact has been catastrophic for several communities worldwide. Strong ground motions are among the most disruptive events, often causing thousands of casualties and billions of dollars of economic losses, let alone the long and strenuous recovery process which generates serious social repercussions. Urban areas are particularly vulnerable due to the high concentration of people and economic assets, and in some cases, their hazard-prone location. The world is witnessing a rapid pace urbanization phenomenon, mainly because of industrialization and rationalization processes. According to United Nations, in 2008 about 50% of the world's population lived in urban areas. Current estimates speculate this number is expected to reach 69% by 2050. Without effective measures, overpopulation could increase vulnerability even further.

With cities becoming the center of economic activities and innovations, urban communities have become progressively more dependent on infrastructure systems. Nowadays, these are essential to provide all the services needed by the community. The efficiency of these systems heavily relies on their interdependencies. The interdependence might be of various nature such as logical, functional, geographical, etc. As a consequence, a system cannot properly operate without the one it is interconnected to. Such relationships expose infrastructures to potential cascading effects and long restoration time. Events like the 2011 Christchurch earthquake and the 2011 Great East Japan earthquake have shown disproportionate effects related to infrastructure interdependencies and the issues faced in the recovery phase. Infrastructure systems are essential in the post-disaster phase to ensure a prompt and efficient emergency management. Nonetheless, in many cases existing infrastructures are already overloaded and not capable of accommodating

the service demand in normal conditions. If the overall performance and resilience of these systems is not improved, disasters of larger proportions are likely to happen again in the future.

To prevent disproportionate effects from happening, the topic of resilience evaluation of communities and infrastructure systems has attracted close attention. More resilient environments would reduce losses and the time to reach full recovery. The first step consists in finding ways to quantify performances and resilience under a given scenario. The approach could be predictive, meaning decision-makers could see the response of the system under different scenarios and decide how to improve it, or retrospective, to analyze the causes of failures and understand how to intervene in the future. The quantification of the initial resilience would represent the baseline from which starting to implement planning and strategies. Currently, this baseline is missing in most of communities. Not having a starting point makes it even questionable to develop strategies to improve resilience since there would not be a way of determining whether they would actually be effective. Resilience measurement tools would certainly help communities figuring out the benefits and the cost of implementing actions, evaluate their effectiveness, and track progresses by means of different policies and approaches.

Several frameworks and methodologies have been proposed to measure resilience. However, many of them are extremely complicated and therefore difficult to apply. On the contrary, some approaches might not be adequate for the specific case study, leading to a coarse assessment. However, having communities to develop their own measurement systems would not be useful to compare the results across different communities. A solid method for quantifying resilience at the community level should be clear, easy to apply, replicable over time, versatile enough to be adjusted based on the application. A unique all-purpose, all-scale approach is not able to fit all case studies. Depending on the scale of the application, the methodology should be adapted. The outcome of large-scale simulations is strictly based on the quality and the availability of the required input data. Often times, it is not possible to have access to all the needed information. Therefore, simulation models should be adapted or allow for a probabilistic analysis introducing uncertainties. Although the various attempts, the main challenges that still remain in the resilience evaluation process are: (i) the need for practical models that can be applied on different scales; (ii) data collection and processing on a large scale (e.g., reconnaissance reports, census data); (iii) the need for models that can analyze multiple systems considering their interdependencies.

The shortcomings in methods to practically quantify resilience and the lack of models that take infrastructure interdependencies into account have motivated this research. The main objectives and an overview of the research approach are summarized in the following section.

1.2 Research objectives and approach

The first objective of this research is to propose a simplified indicator-based approach to evaluate resilience of regional communities. This objective is achieved through an indicator-based approach that quantifies resilience using a weighting procedure to combine the indicators. The method is inspired by existing resilience frameworks. Hence, it considers different aspects and dimensions of resilience. However, the application of existing framework on a large scale is usually overwhelming as most of the required information is not accessible. The idea was to implement a procedure that is practical and replicable. To this purpose, only publicly available input data was used. The methodology is intended to be used for a preliminary resilience assessment, which would serve as baseline for further and more detailed investigations. Decision makers could benefit from such analysis to allocate resources and national funds.

The second objective is to develop an integrated simulation tool to assess the resilience of some of the most important physical infrastructures of urban communities. To achieve this objective, a virtual case study representative of a medium-size European city was developed. By means of different simulation techniques, the seismic vulnerability, damage, and resilience of the community's infrastructures could be investigated. The specific aspects addressed by this research are the following:

- Modeling techniques for large-scale road transportation networks, power networks, and telecommunication networks.
- Inclusion of interdependencies between the building portfolio and each of the aforementioned networks.
- Metrics to quantify the resilience of the networks.
- Decision support tools that can be used to optimize and prioritize the emergency response actions after an earthquake.
- Evaluation of the community response under scenarios with different intensity.

1.3 Thesis organization

Chapter 2 presents a literature review on disaster resilience. First, some of the most relevant definitions are reported, followed by a general resilience formulation. Then, an overview of the main existing frameworks is presented. Finally, some applications of resilience quantification methods are described, and the importance of the scale discussed.

Chapter 3 introduces a methodology to quantify resilience for communities at the regional level. The approach is based on indicators collected from publicly available census data. The proposed weighting method to combine the indicators

allows a straightforward and practical solution for a preliminary analysis. It was applied to measure the resilience of Italian regions in normal conditions, during the emergency, and during the recovery phase.

In chapter 4 an introduction to Ideal City, the virtual case study, is presented. The building portfolio database and the numerical simulation strategy adopted to evaluate the seismic response are described. The results of the simulation are used to define the damage state of each building. This chapter also describes the four seismic scenarios used as benchmark to assess the resilience of all infrastructures.

Chapter 5 presents the model of the road transportation network. This was analyzed using graph theory principles. The interdependence with the building portfolio was considered by developing a machine learning algorithm that estimates the extension of the debris caused by collapses. The extension of debris is then used to determine which roads are blocked.

Chapter 6 describe the model and resilience analysis of the power network. The vulnerability of its components is related to the vulnerability of the buildings where they are installed. A new resilience index is proposed and after the simulation the number of users without power was calculated.

Chapter 7 deals with the model and analysis of the telecommunication network. Its performance is evaluated in terms of throughput and three different indexes are proposed to measure resilience. A resilience improvement strategy is also presented.

Chapter 8 summarizes the work highlighting the main conclusions and findings. Suggestions for relevant future work are also discussed.

Chapter 2

2 Literature review on disaster resilience

2.1 Definition of resilience

In the past two decades, due to the increasing number of natural disasters, many researchers have been studying methods to address the resilience of communities, systems, and networks at various scales. Resilient communities are more likely to be able to absorb the effects of a disaster and recover in a short time. Despite great progresses in science and technologies, most communities worldwide are still extremely vulnerable, causing extreme human and economic losses. The concept of resilience involves different subjects and features such as awareness and preparedness, regulation enforcement, and hazard mitigation (Cimellaro et al. 2016; Cimellaro 2010). It can be applied at any scale, from individual (e.g., person, building) to global applications (e.g., regions, countries). For these reasons, many definitions of resilience can be found in the literature and they have been changing over the years. (Folke et al. 2002) defined resilience it as the speed to return to the initial condition after a perturbation. One of the most accredited definitions was provided by (Bruneau et al. 2003) who said that it is "the ability of social units (e.g., organizations, communities) to mitigate hazards, contain the effects of disasters when they occur, and carry out recovery activities in ways to minimize social disruption and mitigate the effects of further earthquakes". A slightly different meaning was given by (Allenby and Fink 2005): "the ability of a system to remain in a practical state and to degrade gracefully in the face of internal and outside changes". Resilience can be seen as the ability to "withstand stress, survive, adapt, and bounce back from a crisis or disaster and rapidly move on" (Wagner and Breil 2013). Other researchers proposed a more inclusive meaning which extends to other disciplines. (Cutter et al. 2014) describe it as "the ability of a community to prepare

and plan for, absorb, recover from, and more successfully adapt to actual or potential adverse events in a timely and efficient manner including the restoration and improvement of basic functions and structures". Given the available definitions in the scientific literature, resilience can be deemed as a process aiming at enhancing current conditions. This might translate to a safer city, a more robust infrastructure, a cost-effective policy, etc. However, it is still difficult to find a comprehensive, specific, and generally accepted definition.

2.2 Resilience assessment

Several authors have explored approaches to develop a resilience formulation. However, the broad nature of the concept makes it challenging to define a precise and methodical procedure. As previously mentioned, one of the earliest and most accredited resilience definitions was the one provided by (Bruneau et al. 2003). They inferred that the resilience of a system depends on its serviceability performance. The serviceability performance (Q) of a system can range from 0 to 100%, where 100% means that it is functioning at an impaired level and 0% implies that no service is available. The strike of a disaster at time t_0 causes a certain level of damage which produces an instant drop in the system's serviceability (ΔQ). Over time, the system is being restored to its initial state. This period of time is called recovery period (t_1-t_0). The degradation of the service over the recovery period represents the loss of resilience (*LOR*). This concept is mathematically defined as:

$$LOR = \int_{t0}^{t1}\left[100 - Q\left(t\right)\right]dt \qquad (2\text{-}1)$$

where the function *Q(t)* is the serviceability function of the system at a given time *t*. Figure 2-1 shows a conceptual representation of the formulation. By definition, this approach implies the initial serviceability is at 100% (Q_0=100). However, this might not be the case and during the system's recovery strategic actions can be taken to increase the functionality beyond the initial conditions.
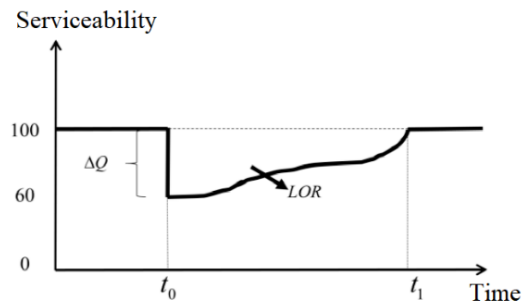
Figure 2-1. Graphic representation of the loss of resilience.

The recovery period (t_1-t_0) and the path taken for the recovery are crucial components. They depend on many variables like available resources, system preparedness, planning, etc. Different types of restoration paths can be found in the literature. Examples are linear, exponential, step, and random functions. However, due to complexity, most common resilience assessment models, such as HAZUS (FEMA 2011), use a linear function to describe the recovery phase. The linear trend is typically adopted when there is not enough information about system resources and recovery plans.

(Cimellaro 2010) improved the formulation provided by Bruneau et al. (2003) by introducing the control time T_C. The control time is the period of time for which the functionality of the system is being observed. The control time is usually decided by owners, or society, and usually coincides with the life cycle of the system. Hence, resilience (R) can be analytically identified as the integral of the serviceability function $Q(t)$ divided by the considered control time T_C:

$$R = \int_{ts}^{tr} \frac{Q(t)}{T_C} \, dt \qquad\qquad (2\text{-}2)$$

Where t_s is the time before the disaster occurs and t_r represents the time after the system completely recovered. Figure 2-2 illustrates the idea of this formulation. The area underneath the serviceability function denotes the resilience of the system.
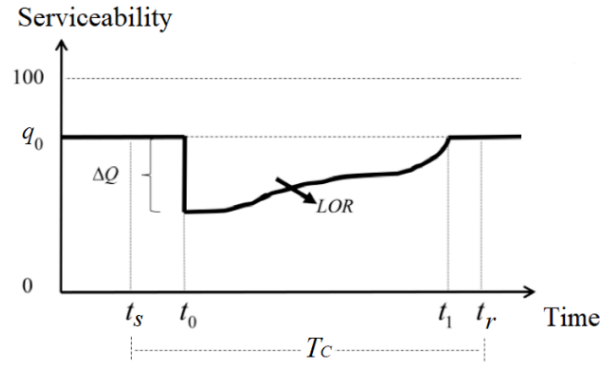
Figure 2-2. Graphic representation of the loss of resilience considering the initial conditions and control time.

2.3 Resilience frameworks

To include the various aspects that underpin the concept of resilience, different frameworks were developed. San Francisco Planning and Urban Research Association (SPUR) is a framework at the city level (Planning and Association 2009). The main goal of this framework was to make the city of San Francisco more resilient through mitigation strategies and new policies. It defines different performance targets based on the intensity of the seismic scenario. In addition, the

methodology is broken down into three phases, namely prior, during, and after the earthquake. Each type of infrastructures (e.g., hospitals, emergency housing, strategic facilities, etc.) is associated with different goals. Consequently, a recovery time is defined for each infrastructure so that their functionality can return to acceptable levels. However, the framework does not directly include a metric for economic and social dimensions, which are crucial in the aftermath of a disaster.

The United Nations International Strategy for Disaster Reduction (UNISDR) is a framework to evaluate the resilience of an urban community subject to natural disasters (Maskrey et al. 2011). The methodology is based on scorecards in form of checklists to measure the current level of cities, identify priorities for investment and action, and to monitor the progress over the recovery time. Nevertheless, it does not offer a theoretical approach which clearly explains how to apply these methods in practice. Additional information is required to assess the performance of critical networks and their interdependencies. Furthermore, it does not detail how to assess the recovery time considering all community dimensions such as social and economic aspects.

Another city-scale framework is the National Institute of Standards and Technology (NIST 2015), which describes several tools and metrics to assess community resilience against different types of hazards and hazard intensities. The framework addresses strategies for improving resilience prior and after disaster events. Preparedness and adaptation capacity are fundamental in preparation for a disaster. Recovery time, economic, and social indexes are the three core elements of this framework. The recovery time estimates the restoration time for the built environment. The economic metric represents the business network that supports the growth of the community. The social metric characterizes human needs such as safety, security, and sense of belonging. However, these metrics are presented without a specific indication on how to apply them. It is also worth noting that, despite not presenting any applicability limitations, the framework was specifically designed for cities across United States.

At the state level, the Oregon resilience plan was derived from the SPUR framework (OSSPAC 2013). It provides guidelines and suggestions to increase the community resilience in terms of human losses, damaged buildings, and marketplaces. It also provides policy recommendations to protect critical infrastructures such as transportation, power, telecommunication, water and wastewater specific to coastal communities. An acceptable time frame to achieve the expected performance goals is provided for each critical network. Compared to the original framework, it is better at evaluating economic resilience, but it does not quantitively account for the social dimension. Furthermore, the methodology is limited to earthquakes and tsunamis.

Hazus methodology is a national framework implemented by the Federal Emergency Management Agency (FEMA 2011). It proposes several models for fragility and loss estimation caused by earthquakes, hurricanes, and floods. Although the methodology can be extended, it was designed according to typical community and infrastructure systems of the United States. The models exploit

Geographic Information System (GIS) technology to evaluate the physical, social, and economic impact of a disaster. The framework allows to calculate performance levels and recovery times, which are normalized and also presented in terms of economic losses. Nonetheless, losses are considered independently, neglecting the relationship between different resilience dimensions.

PEOPLES is a multi-dimensional framework that can be applied for communities of different sizes, from city to country level (Cimellaro et al. 2016). This framework allows to take into account different types of hazards and to model possible responses of a community considering the interdependency between the different community layers. The acronym PEOPLES stands for its seven dimensions, which are:

1. Population and demographics: parameters that describe the social-economic composition of the community. This dimension accounts for the social vulnerability that could compromise the emergency and recovery phases (e.g., population density, age distribution, social integration of minorities, socio-economic status).

2. Environment and ecosystem: capability of the ecosystem to return to its pre-disaster conditions. It includes quality of water, air, and soil, as well as a measure of the biodiversity and sustainability.

3. Organized government services: services that the government is supposed to ensure before and after an extreme event. Mitigation and recovery processes, which include the preparedness to hazards and risk reduction measures, assume a great importance.

4. Physical infrastructure: buildings and facilities that are essential to provide the community with the necessary services. Two different aspects are considered: facilities, i.e., housing and services which are not crucial during the emergency, and lifelines, which consists of services that are vital for the management of the post-disaster phase.

5. Lifestyle and community competence: capability of a community to face problems by means of political partnerships. This includes both the skills of the community's components and how these are perceived by the community itself.

6. Economic development: the economic situation of the community. It can be viewed as a static component, which measures the current economic state, and a dynamic component, which represents the development and economic growth of the community.

7. Social-cultural capital: evaluation of the community's attitude to response to adverse situations and bounce back to the initial conditions. Several subcategories are included in this dimension. They are aimed at assessing the community's commitment and the socio-cultural heritage.

PEOPLES framework provides an innovative approach that can facilitate decision-making under critical situations. However, it does not indicate a procedure

to quantify resilience in a practical way. Furthermore, there is no metric to evaluate the recovery time for social and economic aspects.

2.4 Resilience applications on different scales

Despite there is not a unique or prevalent methodology to quantify resilience, the available approaches can be categorized into four groups. The first uses scorecards to evaluate the performance of the analyzed system. Scorecards are similar to checklists where the presence or absence of certain features is investigated. A score is given to each question and the resilience is measured by adding scores. The second group consists of indicator-based methods. Indicators are meant to capture specific properties of a system that are collected through statistics. By combining the selected indicators, it is possible to measure resilience. The third group combines scorecards and indicators, providing tools such as guidelines and surveys. Lastly, the fourth group consists of mathematical models that describe the relationships among the characteristics of the considered system. All system dimensions can be modelled through computational simulations (Renschler et al. 2010).

Reviewing existing measurement tools, another distinction can be found between top-down and bottom-up approaches. Top-down approaches deconstruct a system to gain more insight into its sub-systems in a reverse engineering way. For instance, a top-down approach would break down the components of a building into columns, beams, plumbing, heating system, etc. Each of these components is then further deconstruct until the lowest level sub-components can be described and assessed independently. On the other hand, bottom-up approaches put together small systems to produce more complex systems (Crowder et al. 2016). They are usually qualitative assessments mainly designed by communities themselves to help them predict and plan for resilience.

Top-down approaches include PEOPLES framework, which starts from the overall resilience and then breaks down more specific subsets. Each subsystem is then refined in greater detail, until the entire specification is reduced to basic elements (Cimellaro et al. 2016). Another top-down tool is the Baseline Resilience Indicator for communities (BRIC) (Cutter et al. 2014). This measurement tool is both qualitative and quantitative, but it focuses on resilience in normal conditions. Unlike the PEOPLES framework, BRIC is practically oriented towards the fieldwork. Other examples of this category of approaches are the SPUR framework, the Hyogo Framework for Action (HFA) (UNISDR 2007), the UK Department for International Development (DFID) Interagency Group (Twigg 2007), ResilUS (Miles and Chang 2011). Bottom-up approaches are less common. Some examples are the Conjoint Community Resiliency Assessment Measure (CCRAM) (Cohen et al. 2013), the Communities Advancing Resilience Toolkit (CART) (Pfefferbaum et al. 2013), the Community Resilient System (White et al. 2015).

The idea introduced by these approaches have been further extended and adapted focusing on more specific applications. (Guidotti et al. 2019) highlighted the importance of the social component and how to include it in the resilience analysis of physical infrastructures through probabilistic models. (Chang and Shinozuka 2004) introduced a measurement framework to quantitatively assess the disaster resilience of communities. They proposed a series of probabilistic resilience measures based on the research done by Bruneau et al. (2003). The proposed framework has been applied to the Memphis water system under a seismic event. (Cimellaro et al. 2016) introduced an index to evaluate the resilience water distribution networks. It was then used to compare different restoration plans in a town in the South of Italy. To quantify the economic resilience, (Gilbert and Ayyub 2016) proposed microeconomic models and metrics that represent a viable solution for effective decision-making aiming at bringing significant savings through risk reduction and fast recovery measures. (Liu et al. 2017) introduced a method that combines dynamic modeling with resilience analysis. Interdependent critical infrastructures were analyzed by means of numerical analysis of the resilience conditions in terms of design, operation, and control for a given failure scenario. (Kammouh et al. 2018) introduced a quantitative method that works at the state level based on the Hyogo Framework for Action. Several other works have been carried out to define and quantify the resilience, mostly with a focus on engineering systems (Hosseini et al. 2016; Park et al. 2013; Sharma et al. 2018). Virtual case studies are a powerful tool to assess the resilience of a community. They allow to specifically model each component of the system and perform targeted analyses as well as global analyses considering the interdependencies among the components. For instance, the Center of Excellence for Risk-Based Community Resilience Planning developed a computational platform that includes the interdependencies between buildings and other networks (Ellingwood et al. 2016). The methodology revolves around a virtual testbed called "Centerville". The city was designed based on a typical medium city of a Midwestern State. The effects of extreme events were estimated through different physics-based models. The methodology allows scalability in community infrastructure modeling and can also be used to evaluate the interaction between the physical and social infrastructures of a community.

The spatial scale plays a key role in the definition of the methodology to evaluate resilience. Depending on the size of the system being analyzed, some solutions might be more suitable than others. For example, on a regional or country scale, indicator-based approaches are probably the most practical. Information that can be collected on those scales is often generic and incomplete. Consequently, running detailed analyses is not viable. However, defining a standard set of resilience indicators is clearly challenging for the dynamic nature and peculiarities of each system. On the other hand, large-scale simulations are often time-consuming and efficient measures to limit the computational effort without losing accuracy must be implemented. On an urban scale, existing simulation models to assess the seismic vulnerability make use of pre-defined fragility curves grouped by typological characteristics. This approximation might lead to inconsistent

results. Considering the single building as a system, its response is significantly dependent on various parameters such as building geometry, mechanical characteristics, construction details, etc. Therefore, depending on the scale of application, resilience measurement tools should be able to accurately model the main characteristics influencing the resilience of the analyzed system and limit the number of input parameters and computational effort at the same time.

Chapter 3

3 Regional resilience assessment

3.1 Introduction

Even though remarkable efforts have already been made to boost research on community resilience (Cutter et al. 2010; Norris et al. 2008; Twigg 2009), there is still not a universally accepted methodology (Abeling et al. 2019). The resilience evaluation process involves a variety of aspects and parameters, which make it prone to subjective interpretations. Chang and Shinozuka (2004) proposed a probabilistic formulation of a series of resilience metrics based on the research done by Bruneau et al. (2003). More recently, Ayyub (2015) introduced straightforward resilience measurements derived from reliability and risk concepts. Liu et al. (2017) presented a method to combine resilience with dynamic modeling. The response of interdependent infrastructures was studied through numerical analyses aimed at assessing their conditions under a given failure scenario. Overall, existing methodologies seems to be specific to the case study. The main concepts vary across different resilience frameworks, especially regarding social aspects (Saja et al. 2019).

The use of indicator-based approaches represents a viable solution to measure the resilience. Nonetheless, the development of a standardized method to identify a set of indicators is a complex task, given the dynamic and context-dependent nature of resilience. This is especially evident on a large scale such as regions or countries. Moreover, in large-scale analyses, the lack of data is an additional issue to address.

This chapter presents a novel indicator-based method to assess regional resilience using only publicly available data. The main source for this application was census data collected by a national institution. The choice of the indicators was inspired by PEOPLES framework's dimensions and components (Cimellaro et al. 2016). Indicators were combined using weighting factors, which were obtained considering their interdependency and importance. The methodology was applied

to the Italian regions. For each of them seismic resilience was evaluated in three circumstances: normal conditions, emergency, and restoration phase.

3.2 Data collection

Gathering input data for resilience analyses is always a challenging task. Not only the quality of information might be an issue, but also scarcity. Indeed, in many cases it is often incomplete, inaccessible or not available. In large scale applications, it is likely that the necessary data is owned by private institutions and stakeholders that are not allowed to share it.

This research aims at performing a regional resilience analysis using publicly available data. The methodology consists of an indicator-based approach. The reason for this choice is that indices have proved to be quite effective in existing applications. They also allow to keep track of the progress of a certain aspect over the years. The resulting resilience index illustrates the multi-layer nature of resilience by condensing multiple indicators into a numeric value. Indicators should be quantifiable variables that are representative of a certain characteristic that affects resilience. Several factors can determine the type and number of these indicators. Some studies are geographically specific, others focus on a certain infrastructure, others look at the restoration capacity of an essential service. However, the goal is to filter the information so that only those indicators that have a positive or negative impact on regional resilience are considered.

For the selection of relevant indicators, any framework can be used as reference. It is worth noting that existing methodologies might propose metrics which are not always computable given the data found in public databases. Thus, some adjustments to the chosen reference framework may be required (Scherzer et al. 2019).

3.3 Selected indicators

The case study for the methodology are the 20 Italian regions. Input data was gathered searching in the public census database. ISTAT is the Italian largest institution that carries out statistical surveys. It periodically collects information about demographics, economics, social and environmental aspects, healthcare, etc. The results of their surveys are structured in a freely accessible database (ISTAT 2020). PEOPLES framework was chosen as a guideline to select relevant indicators (Kammouh et al. 2019).

First, a list of all indicators found in the database was generated. Then, a time span for the analysis was defined, selecting the period from 2007 to 2017. This choice was the best compromise to include more parameters. Before 2007, fewer data had been collected while after 2017 the results of the surveys have not been published for all regions yet. The so obtained statistical records were examined to identify their possible impact on resilience. It was found that only a few were

relevant to a resilience analysis. Consequently, the screening process led to the definition of only 12 indicators for each year of the imposed time span. Due to the limited number of variables, the correlation among them was not considered necessary. In fact, a correlation analysis could lead to misleading results. The indicators selected are the following:

1) Population density: percentage of inhabitants per square kilometer.
2) Elders' index: ratio between elders (more than 65 years old) and young people (less than 14 years old).
3) Number of foreigners: number of non-Italian residents living in the region.
4) People with middle school education: population who have attained a middle school diploma (8th grade) as their highest education.
5) People with higher education: number of people with a Bachelor's or Master's degree.
6) GDP: gross domestic product of each region in million euros.
7) Relative poverty index: ratio between the number of families with a total spending minor or equal to the Italian poverty threshold (defined each year by ISTAT) and the total of resident families.
8) Unemployment rate: percentage of unemployed people.
9) Number of doctors: number of doctors per 10,000 inhabitants
10) Number of hospital beds: number of hospital beds per 1,000 inhabitants
11) Families with Internet access: percentage of families who have access to the Internet.
12) People living in damaged houses: percentage of people who declared to live in damaged buildings.

Figure 3-1 shows an example of the obtained choropleth maps for each indicator relative to the year 2017.

(a)   (b)   (c)   (d)

(e)   (f)   (g)   (h)

<p style="text-align:center">(i)   (j)   (k)   (l)</p>
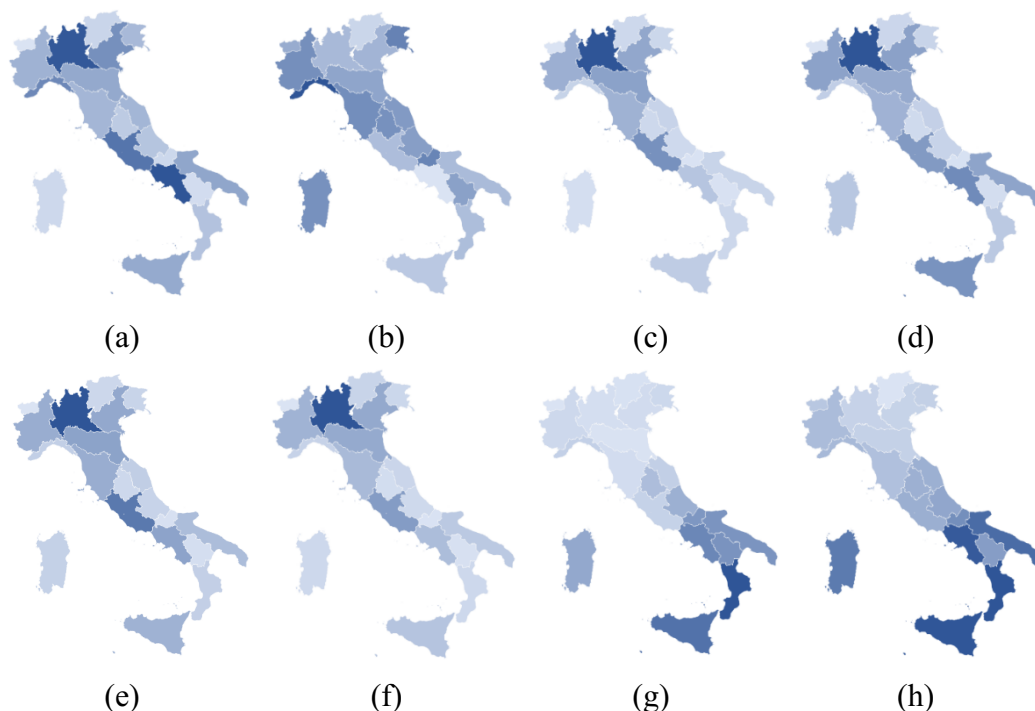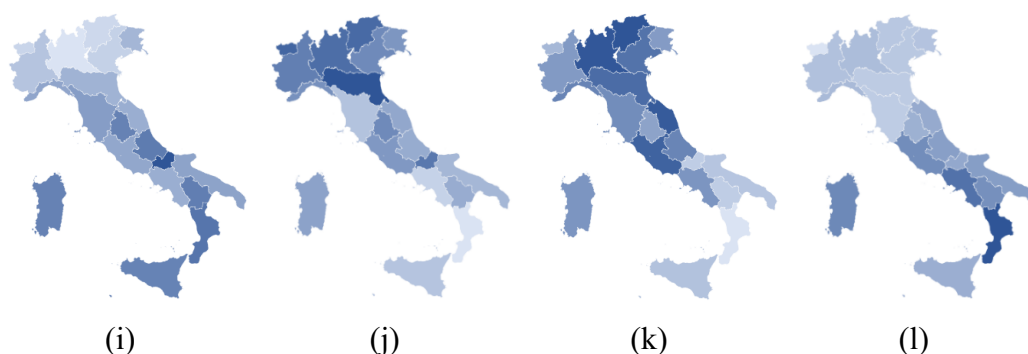
Figure 3-1. Choropleth maps showing the 2017 (a) population density, (b) elders' index, (c) number of foreigners, (d) people holding a middle school diploma, (e) people holding a degree, (f) GDP, (g) relative poverty index, (h) unemployment rate, (i) number of doctors, (j) number of hospital beds, (k) families with Internet access, and (l) people living in damaged houses.

Table 3-1 compares the selected indicators to some of those proposed by PEOPLES methodology. As previously discussed, it is unlikely to obtain a perfect correspondence with the framework chosen as reference. However, a strong similarity could still be achieved. The available information falls in different categories of PEOPLES framework, except for indicator number 12, i.e., people living in damaged houses. It was decided to consider it anyway since it represents a socio-economic aspect with a relevant impact on resilience.

Based on their definition, the indicators' effect on resilience should be determined. Some indicators have a positive effect while others contribute negatively. This is explicated in the last column of Table 3-1. The letter "P" indicates a positive effect, which means the higher the value the greater the resilience. On the contrary, the letter "N" indicates a negative effect, meaning that a high value implies low resilience. For instance, a region with a high "elders' index" is less resilient that a region with a younger population since old people contribute less to the growth of the community, they are prone to illness, and resistant to change.

Table 3-1. Comparison between PEOPLES' and selected indicators.

No.	Selected indicator at regional level	PEOPLES framework indicator	PEOPLES component	PEOPLES framework definition	Indicator effect
1	Population density	Population density	Distribution/Density	Average number of people per area ÷ SV	P
2	Elders' index	Age	Composition	% population whose age is between 18 and 65	N

3	Number of foreigners	Place attachment-not recent immigrants	Composition	% population whose age is between 18 and 65	N
4	People holding a middle school diploma	Educational attainment equality	Socio-Economic Status	% population with college education – % population with less than high school education	P
5	People holding a degree	Educational attainment equality	Socio-Economic Status	% population with college education – % population with less than high school education	P
6	Gross domestic product (GDP)	Income	Socio-Economic Status	Capita household income ÷ SV	P
7	Relative poverty index	Poverty	Socio-Economic Status	% population whose income is below minimum wage	N
8	Unemployment rate	Occupation	Socio-Economic Status	Employment rate %	N
9	Number of doctors	Medical care capacity	Lifelines	Number of physicians per population ÷ SV	P
10	Number of hospital beds	Physician access	Lifelines	Number of hospital beds per population ÷ SV	P
11	Families with Internet access	High-speed internet infrastructure	Lifelines	% population with access to broadband internet service	P
12	People living in damaged houses	-	-	-	N

3.4 Discussion on the selected indicators

Existing methodologies exploit several input parameters as they aim at being as comprehensive as possible. Generally, the larger the number of indicators the more reliable the result. However, a clear indication about the minimum number of

indicators is not provided. It is also not possible to determine whether and how using fewer indicators affects the results.

At the same time, existing methodologies frequently use multiple indicators to better outline a certain characteristic of a system. For instance, a number of indicators could be used to describe the economic status of a community (e.g., annual income, median household income, percentage of households covered by insurance, tax revenues, wealthy retirees, etc.). There is no consistent and systematic definition of the concepts underlying resilience. This is due to the vast range of figures, environments, disciplines, and assets involved. Consequently, depending on the case study, characteristics and number of indicators may vary consistently.

Regardless of the number of input parameters, the interesting aspect is that, when comparing existing frameworks and methodologies, several concepts and variables tend to overlap (Cutter 2016). By comparing different case studies, Cutter found out that there were ten categories of variables that are used in more than 40% of empirical studies on resilience assessment. These categories include social education, income, civic organizations, health access, mitigation plans, religious affiliations, community attributes, emergency management assets, mitigation activities, infrastructures, and buildings. However, some of the proposed indicators are unlikely to be consistently collected, especially at the regional level. In addition, some of them are context-dependent and might be extraneous to the analyzed community and therefore impossible to collect. Examples are preparedness, number of religious organizations, number of nonprofit organizations, population covered by hazard mitigation plans, etc. In this application, the 12 indicators belong to the major and most common of the above-mentioned categories, i.e., social education, income, health access, community attributes, infrastructures and buildings. Other categories refer to parameters that are challenging to measure on a regional scale or not applicable to the specific case study or not relevant to resilience towards seismic events.

3.5 Normalization criteria of the indicators

Since they are defined differently, indicators cannot be combined until they are normalized so that values range between 0 and 1. Ideally, the best way to normalize them would be to divide each value by an optimal value. The introduction of a standard value (SV) for each indicator would provide a benchmark to measure regional resilience. This can be seen as a comparison between the system's functionality at a given time and its optimal performance, which quantifies the system's functionality deficiency. For example, considering the indicator "number of doctors per 10,000 inhabitants", the output would be an absolute number. This quantity could not be combined with the others unless it was normalized. Therefore, dividing the parameter by SV, which ideally represents the "best" number of doctors per 10,000 people, the performance of the region with regard to this aspect

could be evaluated. If the ratio between the value of the measure and SV is less than one, it means that the indicator can still be improved. In case it is greater than one, the region is overperforming, and a value of 1 is assigned to the parameter.

The definition of SVs is a challenging task. Usually, they can be defined by the competent authority or assumed from best practices. However, finding references for each indicator is unattainable given the large scale and multidisciplinary nature of the problem. Therefore, it was decided to normalize indicators with respect to the value of the best performing region. For instance, since Lombardy is the region with the largest gross domestic product, the GDP of all other regions was divided by Lombardy's GDP, meaning that this is regarded as the optimal value.

To combine the indicators that have a negative impact on resilience, the complement of the normalized value was considered. More specifically, the complement value was calculated for: elders' index, number of foreigners, relative poverty index, unemployment rate, people living in damaged houses.

3.6 Combination of the indicators

The approach adopted for the combination of the indicators takes into account two aspects, namely interdependence and importance. Interdependent indicators, meaning that variations of one indicator imply changes on others, could alter the resilience assessment. Therefore, an interdependence analysis was carried out by assign different coefficients to each indicator. The procedure is based on generating an interdependence matrix, as suggested by POEPLES methodology (Cimellaro et al. 2016). An indicator with many interdependencies on others is deemed to have a higher impact on resilience. Additionally, variations of such indicator lead to different values of the others depending on it, changing the overall resilience index. On the other hand, if a parameter changes and the others are not affected, it has less weight. Ideally, the best scenario for evaluating resilience would be having all independent indicators. In such case the impact of each indicator could be clearly defined, variations on one indicator would not be as significant, and targeted measures to improve resilience could be defined. The interdependency matrix is an $[n \times n]$ square matrix where the dimension n corresponds to the number of indicators. Each cell contains a value expressing the level of interdependency. In this application, three interdependency levels were assumed, so that possible values are *0*, *0.5* or *1*, indicating no dependence, medium dependence, and full dependence, respectively, as shown in Equation (3-1):

$$\mathbf{I} = \begin{bmatrix} a_{11} & \cdots & a_{1n} \\ \vdots & \ddots & \vdots \\ a_{n1} & \cdots & a_{nn} \end{bmatrix} \quad a_{ij} = \begin{cases} 0 \\ 0.5 \\ 1 \end{cases} \qquad (3\text{-}1)$$

where a_{ij} expresses the interdependency between the *i-th* and the *j-th* variable. The definition of these value is qualitative and subjective. The best practice to get meaningful data would be to ask a group of experts to fill a questionnaire. Experts would be able to give their opinion on the level of dependency of each pair of indicators based on their knowledge. The larger the number of responses the better for decreasing possible biases. Results could also be statistically analyzed to consider uncertainties and a probability distribution function so that the measure of resilience could be provided in terms of mean and standard deviation.

It is worth noting that matrix *I* is not symmetrical. If a variable is dependent on another one, it does not imply that the opposite is also true. As an example, one can say the indicator "GDP" is deeply dependent on the "elder's index", while the latter does not depend on the value of "GDP".

From the interdependence matrix it is possible to obtain the interdependence vector (λ). This contains interdependency factors, which are calculated by normalizing the sum of each column of the matrix to the maximum value of all columns' sum. A large factor means high dependence of the considered indicator to the others. Equation (3-2) shows how interdependency factors are calculated.

$$\boldsymbol{\lambda} = \{\lambda_1, \ldots, \lambda_n\}, \ n = 1, \ldots, 12$$

$$\lambda_i = \frac{\displaystyle\sum_{j=1}^{n} a_{ji}}{\max\left(\displaystyle\sum_{j=1}^{n} a_{j1}, \ldots, \sum_{j=1}^{n} a_{jn}\right)} \tag{3-2}$$

The type of community (e.g., urban, rural, etc.) has a great influence on the interdependency level. For example, if the case study is a rural community, economic indicators would be scarcely dependent on indicators related to infrastructures. On the other hand, that dependency would be strong when considering an urban environment. In modern communities, the economic development plays a key role, and many indicators are dependent on it. Therefore, to reduce the recovery time after a catastrophic event, a huge number of resources should be primarily allocated to infrastructures. As far as this research is concerned, no distinctions about the type of community have been made and all regions have been treated equally. Nonetheless, when there is sufficient information about the type of communities, it would be beneficial to introduce correction factors to account for specific regional traits.

The importance aspect was introduced to consider that some indicators may have a larger impact on the overall resilience. Also in this case, the type of community is a crucial factor to determine the importance of indicators. For instance, in rural communities, indicators related to lifestyle and economics have a lower impact on resilience than other environment-related parameters. Another

important factor influencing the importance of each indicator is the type of hazard. Depending on the potential damage and the necessary resources in the recovery phase, some variables might gain or lose their relevancy.

An importance factor (c) is assigned to each variable. This that can assume three values, i.e., 1, 2, or 3, where 1 equals low importance, 2 medium importance, and 3 high importance (Equation (3-3)). The evaluation of these factors is also subjective, as for the case of the interdependency factors. Therefore, an estimate provided by experts and decision-makers is required.

$$\mathbf{c} = \{c_1, \ldots, c_n\} \quad c_i = \begin{cases} 1 \\ 2 \\ 3 \end{cases} \tag{3-3}$$

Given a community and selected the type of hazard, some indicators may vary their importance depending on the phase resilience is being calculated for. In this application, resilience is calculated based on the seismic hazard in three different cases. The first is the evaluation of global resilience (Rg) under ordinary conditions, the second is resilience during the emergency (Re), and the third consists in the resilience assessment in the restoration phase (Rr).

Interdependency and importance factors are combined into a weighting factor (w), which is calculated as shown in Equation (3-4):

$$\mathbf{w} = \{w_1, \ldots, w_n\}, \, n = 1, \ldots, 12$$
$$w_i = \frac{\lambda_i \cdot c_i}{\sum\limits_{j=1}^{n} \lambda_j \cdot c_j} \cdot n \tag{3-4}$$

Once weighting factors are calculated for all indicators, the resilience metric (R_i) is obtained for each region by aggregating the weighted measures for all indicators (Equation (3-5)).

$$R_i = \frac{\sum\limits_{i=1}^{n} w_i m_i}{n}, \quad n = 12 \tag{3-5}$$

where m_i is the normalized value for the *i-th* indicator.

3.7 Results

Interdependence and importance factors were determined by asking a group of experts to fill out a questionnaire (Figure 3-2, Figure 3-3). The group of experts consists of 20 people (11 females and 9 males) from 30 to 50 years old. 30% of them are doctors in public hospitals, while 70% of the group works in municipalities and regions as administrative officers. In the analysis, the average value of each response was taken. Due to the limited number of experts who took part to the survey, it was not possible to carry on a statistical analysis of the results.

Full Name: _____ Title: _____

Company: _____ Date: _____

PART I

Please fill the following table based on your expertise. Each cell represents the level of dependency of one indicator upon the others. Please find the description of each indicator in the following page. Allowed values are **0**, for no dependency, **0.5**, for partial dependency, and **1**, for full dependency.

Indicators	Population density	Elders' index	Number of foreigners	People holding a middle school diploma	People holding a degree	GDP	Relative poverty index	Unemployment rate	Number of doctors	Number of hospital beds	Families with Internet access	People living in damaged houses
Population density	1											
Elders' index		1										
Number of foreigners			1									
People holding a middle school diploma				1								
People holding a degree					1							
GDP						1						
Relative poverty index							1					
Unemployment rate								1				
Number of doctors									1			
Number of hospital beds										1		
Families with Internet access											1	
People living in damaged houses												1

Figure 3-2. Part I of the questionnaire – interdependence matrix.

PART II

Please fill the following table based on your expertise. Each cell represents the importance of each parameter under normal conditions (NORMAL), during an emergency caused by an earthquake (EMERGENCY), in the restoration phase after an earthquake (RESTORATION). Please find the description of each indicator in the following page. Allowed values are **1**, for low importance, **2**, for moderate importance, and **3**, for high importance.

	NORMAL	EMERGENCY	RESTORATION
Population density			
Elders' index			
Number of foreigners			
People holding a middle school diploma			
People holding a degree			
GDP			
Relative poverty index			
Unemployment rate			
Number of doctors			
Number of hospital beds			
Families with Internet access			
People living in damaged houses			

Figure 3-3. Part II of the questionnaire – resilience importance factors.

The average interdependency factors and the calculated interdependence vector (λ) are reported in Table 3-2. From the collected responses it is possible to notice that "GDP" is the most interdependent variable, closely followed by the "elders' index". On the contrary, the most independent indicators are "people living in damaged houses" and "families with Internet access".

The average importance factors in normal, emergency, and restoration conditions are summarized in Table 3-3. It is possible to observe that under different conditions the importance of a given indicator may change significantly. The gross domestic product was deemed to be the most important in normal conditions and one of the most important during the restoration phase, while its importance in the emergency phase is quite low. This can be explained by the fact that during emergencies resources are managed by the government at a higher level. Conversely, in the emergency phase the number of doctors and hospital beds acquire a crucial importance, while their relevance during the restoration phase is reduced.

Table 3-2. Interdependence matrix.

	1	2	3	4	5	6	7	8	9	10	11	12
1	1.00	0.08	0.03	0.05	0	0.48	0.53	0.15	0	0	0	0.03
2	0.15	1.00	0.05	0.08	0.03	0.50	0.05	0.13	0.08	0.03	0	0
3	0.50	0.15	1.00	0.03	0.08	0.45	0.53	0.45	0.03	0	0	0
4	0.03	0.88	0.03	1.00	0.10	0.48	0.08	0.08	0.05	0	0.08	0
5	0.08	0.45	0.03	0.83	1.00	0.50	0.03	0.10	0.03	0.08	0.08	0
6	0.88	0.50	0.48	0.50	0.43	1.00	0	0.98	0.15	0.15	0.03	0.03
7	0.08	0.08	0.13	0.03	0.05	0.50	1.00	0.93	0.03	0	0.08	0.18
8	0.43	0.03	0.18	0.53	0.53	0.98	0.03	1.00	0.03	0	0.12	0.08
9	0.55	0.73	0	0.08	0.08	0.03	0	0.08	1.00	0.65	0	0
10	0.50	0.93	0	0.05	0.03	0.43	0.45	0.13	0.25	1.00	0	0
11	0.43	0.53	0.10	0.45	0.98	0.08	0.98	0.50	0	0	1.00	0
12	0.08	0.03	0.18	0.08	0.05	0.48	1.00	0.03	0	0	0.03	1.00
λ	0.80	0.91	0.37	0.63	0.57	1.00	0.79	0.77	0.28	0.32	0.24	0.22

Table 3-3. Importance factors in normal, emergency, and restoration conditions.

		NORMAL	EMERGENCY	RESTORATION
1	Population density	1.15	1.35	1.30
2	Elders' index	1.95	2.90	1.75
3	Number of foreigners	1.10	1.15	1.15
4	People holding a middle school diploma	1.05	2.00	2.00
5	People holding a degree	1.85	1.75	2.10
6	GDP	2.95	1.25	2.80
7	Relative poverty index	2.00	1.15	2.85
8	Unemployment rate	2.05	1.15	2.85
9	Number of doctors	2.20	3.00	1.30
10	Number of hospital beds	1.85	3.00	1.15
11	Families with Internet access	1.15	1.65	1.05
12	People living in damaged houses	2.25	2.85	1.15

Interdependency and importance factors were combined to obtain the weights of each indicator. Table 3-4 shows the weighting factors relative to year 2017, calculated as per Equation (3-4). Therefore, it was possible to calculate the resilience metric for each region. This is illustrated by the choropleth maps in Figure 3-4. This graphic visualization allows to have a straightforward idea of the resilience and to compare regions' performances thanks to the different color intensity. It can be noted that the most resilient region is Lombardy (no. 4). This is the case in all three conditions. The obtained numerical values are reported in Table

3-5 to further analyze the performance of each region in different circumstances and make comparisons with other regions. For instance, it can be observed that Molise (region no. 14) has the lowest value of resilience in both normal and emergency conditions. The worst performing region in the restoration phase is Calabria (no. 18).

The proposed preliminary resilience analysis, albeit simplified, allows to point out critical aspects. Interestingly, Lombardy proved to be resilient towards earthquakes, despite being one of the regions with the lowest seismicity. Conversely, Calabria, together with other regions in the Apennines area, characterized by high seismicity, proved to be scarcely resilient. This result is validated by the consequences of the 2009 L'Aquila earthquake and the 2016 Central Italy earthquake. Both events caused sever economic and human losses and still to these days they have not completed the reconstruction phase. Additionally, socio-economic activities are struggling to return to pre-event levels. Overall, results showed that northern regions are more resilient. This can be attributed to aspects such as better economics, advanced services, and lower unemployment rates. Nonetheless, Campania and Sicily showed encouraging results, which are mostly due to solid indicators in terms of young population, population density, and number of doctors. Decision-makers and public authorities could use the obtained results to make more detailed evaluations and comparisons through an in-depth analysis of the selected indicators.

Table 3-4. Weighting factors for normal, emergency, and restoration conditions.

		NORMAL	EMERGENCY	RESTORATION
1	Population density	0.85	1.05	0.89
2	Elders' index	1.65	2.59	1.37
3	Number of foreigners	0.38	0.42	0.37
4	People holding a middle school diploma	0.61	1.23	1.07
5	People holding a degree	0.97	0.97	1.02
6	GDP	2.75	1.22	2.40
7	Relative poverty index	1.47	0.89	1.94
8	Unemployment rate	1.47	0.87	1.88
9	Number of doctors	0.57	0.81	0.31
10	Number of hospital beds	0.56	0.95	0.32
11	Families with Internet access	0.26	0.39	0.21
12	People living in damaged houses	0.46	0.62	0.22
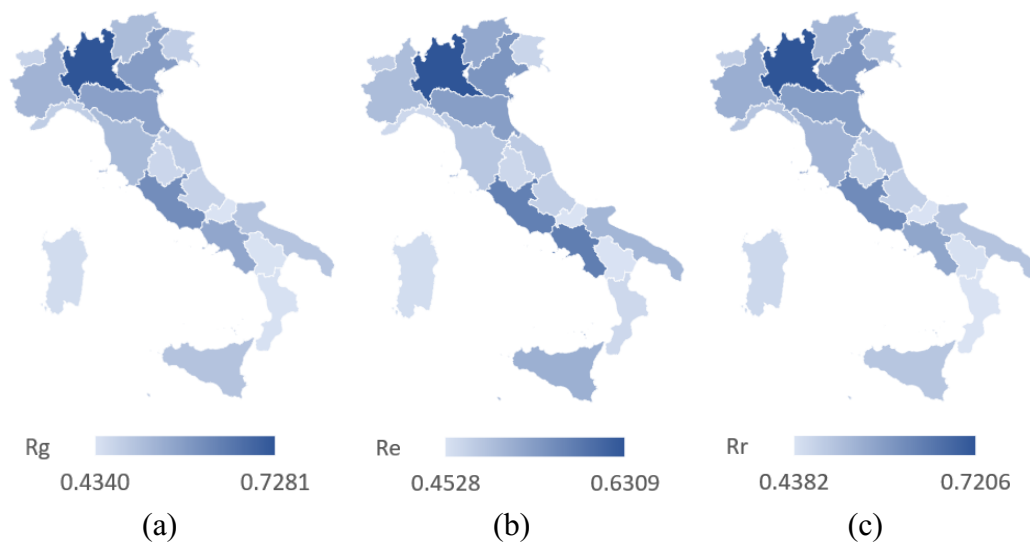
Figure 3-4. Choropleth maps illustrating the (a) global (b) emergency and (c) restoration resilience for 2017.

The procedure was repeated over the 2007-2017 period for each year in order to evaluate the performance of the regions over time. Then, the results in terms of resilience were averaged and compared to the 2017 results. Table 3-5 summarizes the resilience measures for 2017, those for the 2007-2017 period, and the percentage variation between them. As it can be seen, in most cases resilience decreased with respect to the average in all scenarios, with Calabria and Apulia showing the worst performance. Exceptions to this trend are Lombardy, Emilia Romagna, and Trentino South Tyrol which reported an improvement in all scenarios.

The proposed methodology is meant to be used at the early stage of a resilience analysis. In this application, regions were considered homogeneous in terms of demographics, economics, infrastructures, etc., which is not always the case. In fact, it is likely that within a region the areas around the biggest cities are the most resilient ones and usually those areas represent just a small fraction of the entire region. Moreover, geographical characteristics play a key role. Most of the Italian regions have a large variety of territories and small, hardly accessible mountain villages are certainly going to be less resilient due to the inferior services and infrastructures. However, these analyses on a large geographic scale have some advantages. First, they are fast, free, and require negligible computational effort. Second, public funds are distributed at the regional level, and this is probably the main motivation and utility of this work. To date, in virtually all cases, resilience is not considered in the decision-making process aimed at fund redistribution. Economics, socio-demographical aspects and past events are the leading factors in this process which often results in unwise decisions. Preliminary resilience analyses on a regional scale could assist decision-makers in this process and significantly improve resource allocation. After this first step, the single regions should carry on more detailed analyses to identify the resilience of each neighborhood and decide

how to spend the money they have been given. Therefore, the proposed methodology for the resilience assessment could help decision-makers to improve resource allocation significantly.

Table 3-5. Global, emergency, and restoration resilience for each Italian region over the considered time span.

No.	Region	2017			2007 – 2017			Variation (%)		
		Rg	Re	Rr	Rg	Re	Rr	Rg	Re	Rr
1	Piedmont	0.53	0.50	0.54	0.54	0.51	0.55	-1.0	-0.8	-0.7
2	Aosta Valley	0.47	0.48	0.48	0.47	0.48	0.48	0.0	-0.2	0.2
3	Liguria	0.48	0.47	0.50	0.48	0.47	0.50	-0.8	-0.1	-0.7
4	Lombardy	0.73	0.63	0.72	0.73	0.63	0.72	0.1	0.1	0.2
5	Veneto	0.58	0.55	0.59	0.59	0.56	0.59	-0.8	-0.8	-0.7
6	Friuli Venezia Giulia	0.48	0.47	0.50	0.48	0.48	0.50	-1.0	-1.5	-0.6
7	Emilia Romagna	0.57	0.54	0.58	0.57	0.53	0.57	1.2	2.0	1.0
8	Trentino South Tyrol	0.52	0.53	0.53	0.51	0.53	0.52	0.5	0.1	0.5
9	Tuscany	0.52	0.49	0.53	0.52	0.49	0.53	-0.5	-0.1	-0.5
10	Umbria	0.46	0.47	0.47	0.46	0.46	0.48	-0.5	1.1	-1.2
11	Marche	0.48	0.48	0.50	0.49	0.49	0.50	-1.3	-1.1	-1.2
12	Lazio	0.61	0.58	0.61	0.62	0.59	0.62	-1.8	-1.8	-1.2
13	Abruzzo	0.47	0.48	0.48	0.47	0.48	0.48	-1.2	-0.8	-1.2
14	Molise	0.43	0.45	0.44	0.44	0.46	0.45	-2.3	-2.6	-2.4
15	Campania	0.56	0.58	0.56	0.58	0.59	0.58	-2.8	-2.5	-2.7
16	Apulia	0.50	0.51	0.50	0.51	0.53	0.52	-3.1	-3.5	-2.7
17	Basilicata	0.44	0.45	0.44	0.44	0.46	0.44	-0.6	-1.6	0.2
18	Calabria	0.44	0.47	0.44	0.46	0.48	0.46	-4.2	-3.2	-4.7
19	Sicily	0.50	0.52	0.50	0.51	0.53	0.51	-2.8	-1.9	-2.8
20	Sardinia	0.45	0.46	0.46	0.46	0.48	0.49	-2.4	-3.4	-1.7

3.8 Conclusions

This chapter presented an indicator-based method to evaluate regional resilience. When dealing with resilience analyses at the regional level, input data could be missing or inaccessible due to privacy issues. Since existing resilience frameworks require several input parameters, it is often impossible to apply them thoroughly. The proposed methodology was implemented with the objective of using only public census data. The seismic resilience of the Italian regions in normal, emergency, and restoration conditions was estimated. After a screening process of the available data, twelve relevant indicators were selected. They were then combined using a weighting formulation that takes into account their

importance and interdependency, which were drawn by asking experts to fill out questionnaires.

The calculated resilience values allowed to evaluate the performance of the a given region in different circumstances and to compare it to other regions. The analysis was performed over a ten-year period and showed that resilience decreased for most regions. The proposed method is a simple and valid tool for preliminary analyses. It can be used to highlight which indicators are solid and which need to be improved for each region. In addition, it could be used by decision-makers to deeper investigate the impact of the indicators. It could also facilitate the allocation of resources to improve features that increase resilience, both in terms of importance and interdependency. With this information better recovery plans could be implemented.

Chapter 4

4 Resilience of urban communities: Ideal City

4.1 Introduction to Ideal City

The resilience assessment of an urban community starts with the definition of all its principal components. Typically, the main components are infrastructures and social networks. An effective way of approaching the problem is to consider the community as a series of multiple layers, one for each component. These layers are not separate, as infrastructures are interdependent (Pamungkas et al. 2014).

Common approaches to evaluate the vulnerability of a community to a given hazard can categorized as: empirical, agent-based, system dynamics, economic theory-based, network, and others (Ouyang 2014). Empirical methods are based on historical data from past disasters. In agent-based approaches systems are adaptive and their complex behavior is described by the interaction of agents (Cimellaro et al. 2017). System dynamic approaches aim at modeling the evolutionary relation of interdependent infrastructures by describing the causes and effects of a perturbation. In network-based approaches infrastructures are schematized into nodes and links, while interdependencies between infrastructures are defined through interlinks. Approaches based on economic models implement market rules to account for interdependencies. Other approaches include Bayesian networks, hierarchical methods, and hybrid models, which combine two or more methods (Kammouh et al. 2018).

In order to perform these types of analyses on an urban scale, simplified yet valuable methods need to be developed. With the recent technological advancements, computer-based simulation seems the most effective and feasible strategy to investigating the behavior of large complex systems. Virtual case studies are a powerful tool to perform large scale resilience analyses. They allow to

integrate all critical infrastructures within the same model, rather than performing separate analyses. Therefore, complex aspects, such as the interdependency among infrastructures, can be analyzed. For instance, the Center of Excellence for Risk-Based Community Resilience Planning (Ellingwood et al. 2016) used a virtual community called "Centerville" to test an integrated computational framework that includes interdependencies between critical infrastructures. The city was designed based on a typical medium city of Midwestern States including specific characteristics into the built environment.

In this research, network models are used to evaluate the performance of critical physical infrastructures of Ideal City. This is a virtual environment designed to represent a typical European city. It is inspired by the city of Turin in Italy, and its building portfolio includes housing (residential building, hotel, shelter), education (school, university, library), business (shopping centers, retail stores, heavy industries), and public services (hospital, police station, churches, airport, etc.). The critical infrastructures to support the community's demands are: (i) road transportation network, (ii) power network, (iii) telecommunication network, (iv) water distribution network, (v) gas network. Additionally, a socio-technical network is introduced to analyze emergency and rescue procedures, making Ideal City a hybrid multi-layered model. Thanks to its definition, the proposed hybrid model is able to consider interdependencies and possible cascading effects between the building damage and the other networks in the aftermath of a seismic event. The damage suffered by the buildings is often the cause of disruption and losses in all the remaining networks. Similar interdependency relationships can be easily introduced in the model. For instance, the functionality of the water network is partially dependent on the damage to the power network as pumps and electric valves need to be power supplied. Also, the functionality of all the physical networks affects the overall response of the socio-technical network (e.g., efficiency of rescue and evacuation procedures, human behavior, etc.).

The first step in the resilience analysis of Ideal City was the estimation of the damage occurred to the buildings. From there, damage and interdependency effects on the road transportation, power, and telecommunication networks were evaluated.

All the analyses were implemented in a user-friendly computing platform with visualization capabilities. The software was developed in a Python-based environment using also advanced features such as parallel computing to allow for a more efficient workflow. The underlying idea was to create different Python classes, one for each algorithm used to assess building damage states and interdependencies on the other networks. The visualization interface allows to translate numerical results into straightforward maps and charts that can be easily interpreted by any user.

4.2 Building portfolio database

The first step to generating the building database of Ideal City was to collect all available data from public and accessible sources for the city of Turin, Italy. General parameters such as area and height were obtained from OpenStreetMap (Haklay and Weber 2008). Additional information, such as the number of storeys and the year of construction, were found in Geographical Information Systems provided by the Municipality. Census data provided by the national institution (ISTAT 2016), and other technical information provided by real estate agencies and design reports were consulted to increase the level of knowledge. Ideal City's building portfolio consists of about 23,420 residential buildings and it extends for about 120 km^2 with a population of more than 900,000 inhabitants. The portfolio is mainly made of RC buildings (63%), although masonry structures represent a significant share (37%). These are also the oldest buildings, typically concentrated downtown, as in most of European historic cities. Residential buildings, as opposed to strategic facilities that must meet strict structural performances to keep operating even after strong ground motions, are the most vulnerable asset of the built environment. Additionally, since they have a higher daily occupancy, they are responsible for the highest human losses in case of natural disasters.

Some information was estimated by identifying common patterns. For instance, the year of construction can be deducted from construction techniques, which are essential to define the geometrical and mechanical properties of the structural elements. Inevitably this approach leads to differences with the actual data. For this reason, a realistic estimate of the structural behavior needs a probabilistic approach to account for uncertainties. These were accounted considering all input parameters as random variables characterized by a normal distribution. Three categories of input parameters were identified, namely mechanical, geometrical, and construction. Mechanical parameters include the elastic modulus, compressive, and tensile strength of materials (i.e., concrete, bricks, mortar, steel rebars). Geometrical parameters represent the dimensions of the structural components such as span length, cross-section dimensions, percentage of reinforcement. Construction-based parameters are related to variables that influence the design, such as vertical and horizontal loads, type of floor, type of infill walls, etc. Each category is characterized by a different standard deviation based on the building archetype and year of construction. This distinction was done for bot RC and masonry buildings. Larger standard deviation values were chosen for older buildings since in general information about them was approximate. Masonry buildings were also associated with a larger dispersion as the definition of the structural elements and construction details was only fairly accurate. Moreover, correlation between some parameters was evaluated. The correlation between the percentage of reinforcement bars and the characteristic steel yield strength was treated according to the probabilistic model of (Vrouwenvelder and Faber 2001). The correlation between the compressive strength and the concrete elastic modulus was represented with a correlation coefficient of 0.8 (Mirza and MacGregor 1979).

After the data was collected and processed, it was stored in a structured database. Figure 4-1 shows a flowchart describing how the database was generated.
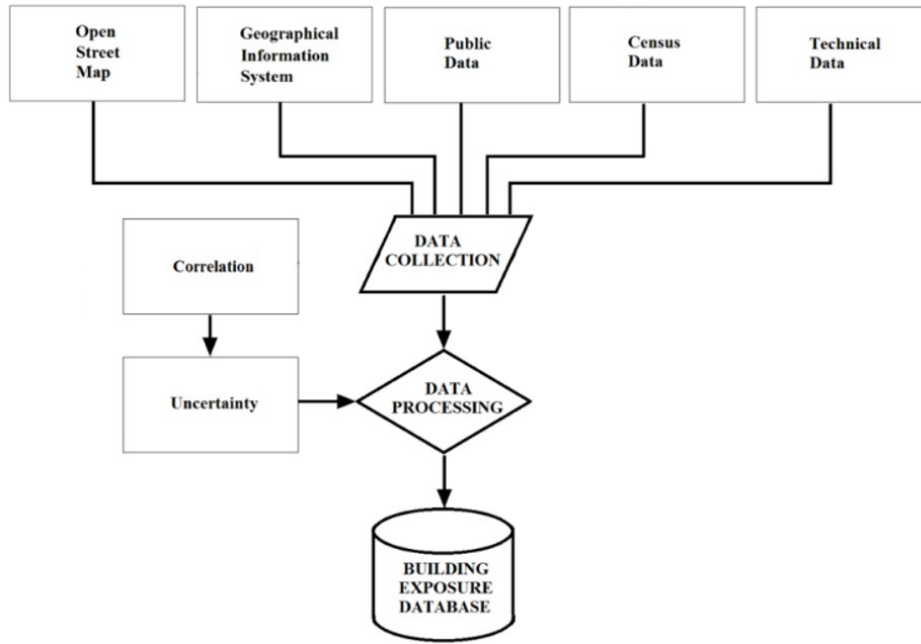
Figure 4-1. Flowchart of the generation of the database.

4.3 Simulation methodology

Due to the large scale of the problem, the evaluation of the seismic response of the building portfolio requires simplified simulation methods. To reduce the computational effort, a surrogate model that describes the relationship between base shear and top horizontal displacement for each building was developed (Marasco et al. 2017). The force vs. displacement relationship is defined through a parametric backbone curve, where the post-elastic field is characterized by decreasing stiffness. Hysteresis is derived from the Takeda model (Takeda et al. 1970). Such surrogate model makes for a significantly faster analysis compared to a finite element model, which is crucial on an urban scale with several thousand structures. A Multi-Degree-Of-Freedom (MDOF) scheme was used to model the buildings. This is loaded through a lateral distribution of forces that is proportional to the principal mode. The elastic behavior is defined by the base shear and top displacement values that induce the yielding of the weakest column. The post-elastic behavior is obtained applying the upper-bound theorem and the equal energy rule (Marasco et al. 2017). Elastic and post-elastic parameters allow to draw a backbone curve. This curve simplifies the analysis since it can be used to describe each building as an equivalent Single-Degree-Of-Freedom (SDOF) oscillator.

The structural behavior of RC buildings was schematized through a four-point backbone curve, while a three-point curve was adopted for masonry buildings.

37

Monte Carlo simulations were performed to compute the curve for each building by varying the input parameters in the range of a standard deviation from the median. The iteration ends when a stable estimate of the median backbone curve is found. Figure 4-2 illustrates an example of a Monte Carlo simulation (MCS) to obtain backbone curves for a 7-storey RC building and a 4-storey masonry building built in 1930 and 1978, respectively.
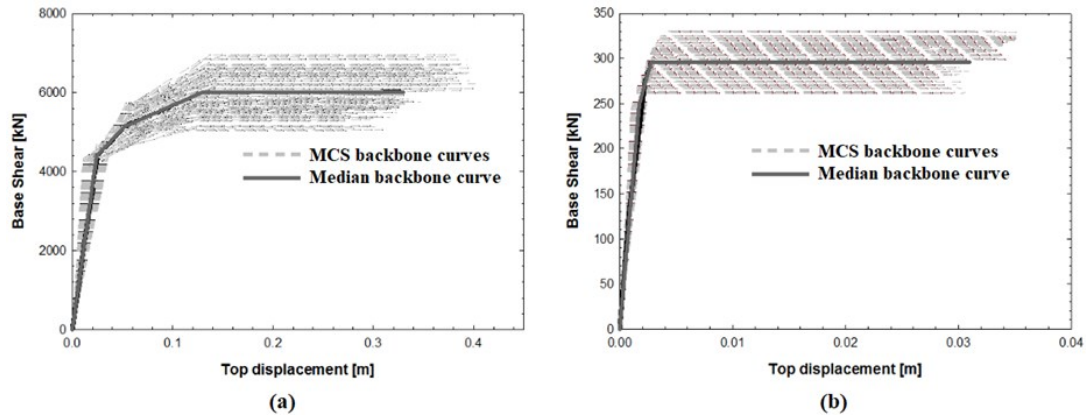
Figure 4-2. Estimation of the median backbone curve for (a) RC and (b) masonry buildings through MCS.

The structural response was evaluated using the finite element code OpenSees (Mazzoni et al. 2006). Each building was modeled as "ZeroLength" element. Stiffness and damping characteristics are assigned to each element along the principal horizontal directions according to the median backbone curve. The force deformation relationship was simulated through the uniaxial "MultiLinear" material. Seismic inputs were applied to each element in both horizontal directions. Then, nonlinear time history analyses were performed, determining the maximum top displacements.

To reduce the overall duration of the analysis, the "OpenSeesPy" Python library combined with multiprocessing were exploited (Zhu et al. 2018). Multiprocessing allows to launch multiple processes to independent memory slots. This avoids errors in case two processors are using the same memory location contemporarily. In this case study, multiprocessing proved to be particularly effective as different memory slots were allocated to run the nonlinear time history analysis of each single building.

4.4 Damage assessment

The building damage assessment is the core element of the entire resilience analysis. Due to interdependency relationships, the damage suffered by buildings induces significant damage and loss of functionality to the other infrastructures.

The Hazus methodology (FEMA 2011) classifies seismic damage to buildings into five levels, namely none, slight, moderate, extensive, and complete. Give that, various indicators can be used to quantify the damage, such as local and global damage indicators. These indicators are called Engineering Demand Parameters (EDPs) and are used to evaluate the Damage State (DS) of structural and nonstructural elements. Typically, deformation-based criteria are more effective to describe the post-elastic seismic response of structures. The maximum inter-storey drift is broadly adopted as EDP, since it gives a direct measure of the dynamic response. Several studies have been conducted to associate the inter-story drift with DSs.

In this application, DSs are determined from the maximum inter-story drift thresholds proposed by (Ghobarah 2004) since they are valid both for RC and masonry buildings. According to this model, the structure is not damaged until concrete starts cracking. Stiffness reduces between concrete cracking and steel yielding point. In this phase the building is still reparable. Past the yielding point, repair costs are high, and the building is irreversibly damaged. The ratio between the collapse displacement and the displacement that causes the global yielding represent the ductility. Obviously, materials and the structural system affect the ductility of the system. Therefore, Ghobarah defined inter-storey drift thresholds for ductile and non-ductile RC Moment Resisting Frame (MRF) structurers, MRFs with ductile walls, and masonry infills (Table 4-1).

Table 4-1. Inter-storey drift thresholds proposed by (Ghobarah 2004).

Damage state	Ductile MRF	Non-ductile MRF	Ductile Walls	Non-ductile Walls
No damage	<0.2%	<0.1%	<0.2%	<0.1%
Slight	0.4%	0.2%	0.4%	0.2%
Moderate	<0.1%	<0.5%	<0.8%	<0.4%
Extensive	1.8%	0.8%	1.8%	0.7%
Complete	>3.0%	>1.0%	>2.5%	>0.8%

The maximum top displacements that were determined through nonlinear time history analyses needed to be converted into maximum inter-storey drifts. To this purpose, a simplified response model was implemented. This is based on a lateral displacement distribution that simulates the response of an MDOF system. The distribution is obtained as a sum of an elastic and a plastic contribution. The elastic displacement distribution is estimated from a pushover analysis. The plastic displacement distribution is assumed to be directly proportional to the displacement distribution corresponding to the collapse mechanism. Once the maximum inter-storey drift is calculated, damage states can be assigned to each building. Figure 4-3 summarizes the entire damage assessment procedure.
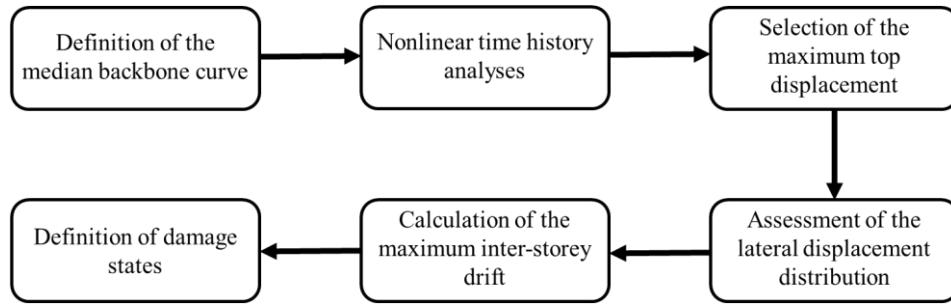
Figure 4-3. Flowchart of the damage assessment procedure.

4.5 Seismic scenarios

The seismic scenario to evaluate the structural response of the building portfolio is simply defined by epicenter location, moment magnitude, and acceleration time history recorded at the site of the epicenter. At each building location, two horizontal orthogonal seismic inputs calculated through Ambraseys ground motion model were applied along the principal directions (Ambraseys et al. 1996). Shear wave velocities (Vs30) were collected from the USGS database (USGS 2013). Thus, the methodology allows the user to change at any time the seismic scenario by selecting (i) epicenter location, (ii) magnitude of the earthquake, (iii) acceleration time history at the epicenter, and (iv) ground motion model. Figure 4-4 shows the epicenter location and an example of the PGAs obtained at each building location.
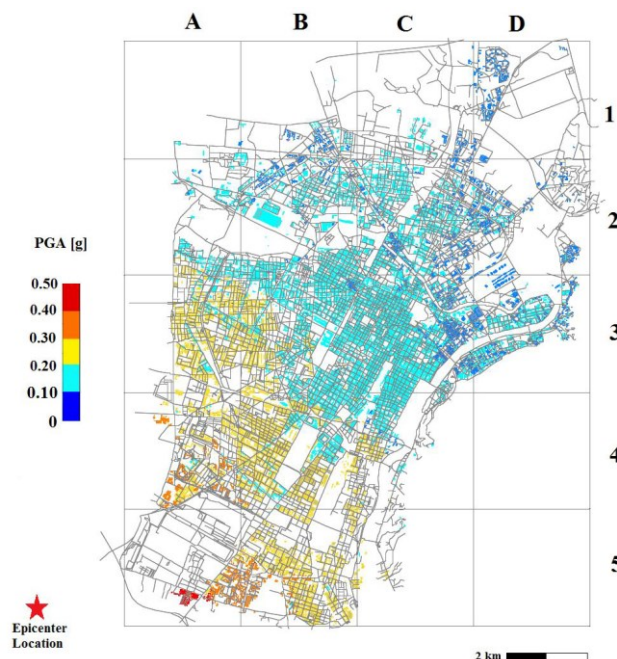
Figure 4-4. Example of a PGA map.

To better analyze the structural response and make comparisons, four notorious seismic scenarios were chosen as benchmarks. The horizontal acceleration time histories were obtained from the software Opensignal (Cimellaro and Marasco 2015). The selected time histories are Northridge (lmar County Hospital parking lot in Sylmar, California, USA), Kobe (Kobe Japanese Meteorological Agency station, Japan), El Centro (Imperial Valley Irrigation District substation, California, USA), and Hachinohe (Hachinohe City, Japan). Northridge and Kobe records represent near-field earthquakes, whereas El Centro and Hachinohe are examples of far-field seismic scenarios. Table 4-2 describes the main seismological characteristics of each event. The epicenter is supposed to be located in a fictional fault located about 9 km to the southwest.

Table 4-2. Characteristics of the four benchmark scenarios.

	El Centro	Kobe	Hachinohe	Northridge
Date	5/18/1940	1/17/1995	5/16/1968	1/17/1994
Region	Imperial Valley	Hyogoken Nanbu	Tokachi-oki	California
M_w	6.9	6.8	8.2	6.7
Depth [km]	16.00	17.60	26.00	11.30
PGA [g]	0.35	0.82	0.23	0.84

4.6 Results

Nonlinear time history analyses were carried out for the four benchmark scenarios and the results in terms of damage state were plotted using different colors on a map. Figure 4-5 shows the damage states of part of Ideal City downtown after each seismic event. The percentage of buildings in each damage category is reported in Table 4-3. Northridge and Kobe scenarios caused severe damage: completely damaged buildings are 86% and 79%, respectively. Less than 1% of the structures was either undamaged or slightly damaged for both scenarios. El Centro mostly caused moderate (40%) and complete damage (27%), while extensive and slight damages accounted for about 14% and 19%, respectively. The less damaging earthquake was Hachinohe, with most of the construction remaining in acceptable conditions: 52% reported slight or no damage. Moderate damage was found in 37% of cases, while only 9% collapsed.
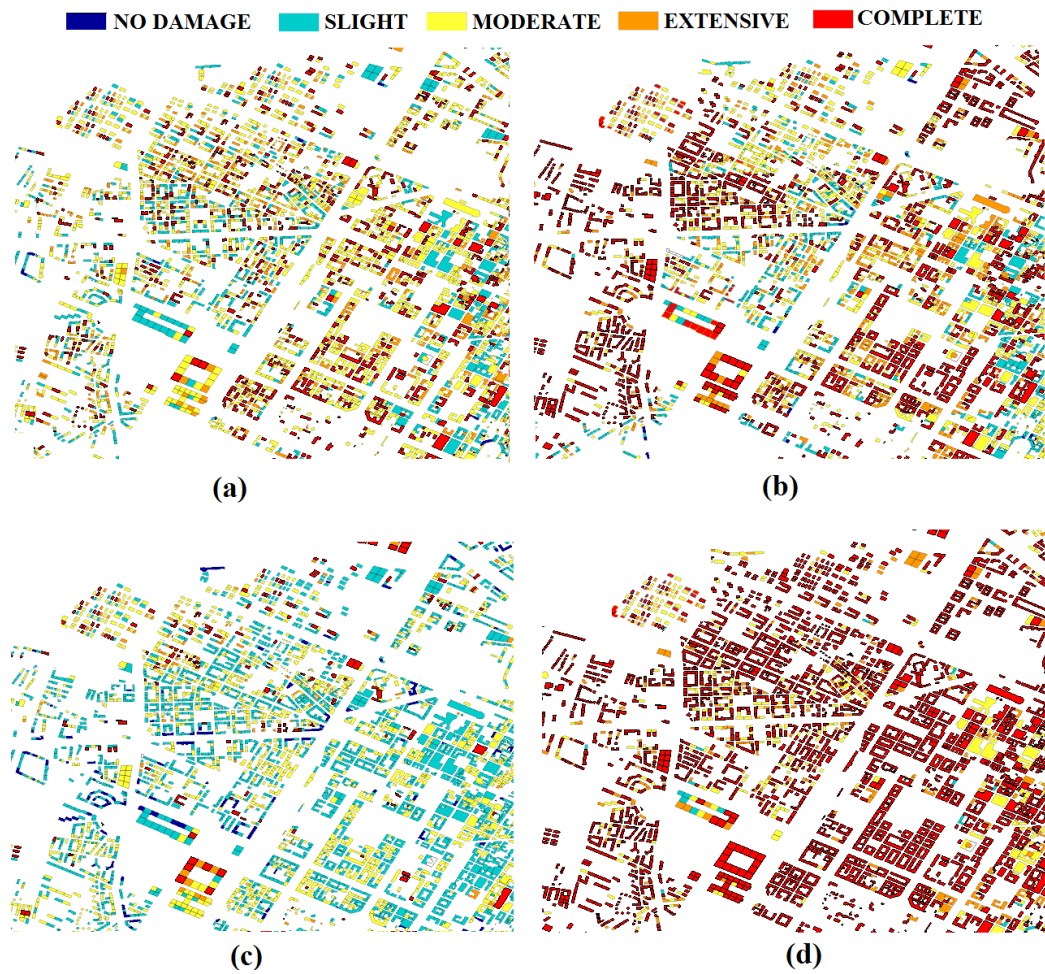
Figure 4-5. Damage state maps of an Ideal City district after (a) El Centro, (b) Kobe, (c) Hachinohe, and (d) Northridge scenarios.

Table 4-3. Percentage of buildings by damage state after each scenario.

Damage States	El Centro	Kobe	Hachinohe	Northridge
No damage	0.62%	0.03%	5.90%	0.03%
Slight	18.75%	0.77%	45.68%	0.77%
Moderate	39.38%	9.53%	36.73%	7.17%
Extensive	14.10%	10.21%	2.22%	5.83%
Complete	27.14%	79.47%	9.47%	86.19%

The two near field earthquakes, Northridge and Kobe, were extremely disruptive due to the high PGA. On the other hand, the significant differences between the two far field earthquakes, Hachinohe and El Centro, are attributable to different seismological characteristics. Hachinohe has the largest magnitude, but its hypocenter depth is also greater than El Centro's. Therefore, Hachinohe's seismic wave propagation is notably reduced by the geometrical attenuation. Indeed,

Hachinohe's PGA is smaller than the PGA of El Centro. In the nonlinear time history analyses, such difference in PGA values causes largely different responses.

It is worth noting that most of the buildings built before 1937 suffered moderate and extensive damage. On the contrary, those built after 1975 were mainly affected by slight damages. This is consistent with the measures introduced with the first seismic design codes. In addition, the downtown and other old neighborhoods were the most damaged since they are primarily composed by historical masonry buildings, which are more vulnerable than modern RC structures.

4.7 Conclusions

In this chapter, a virtual urban environment to be used as a testbed for seismic resilience analyses was introduced. The virtual environment, named Ideal City, is meant to be representative of a typical European urban community. To model the city, a multi-layer approach was followed, where each layer corresponds to a critical infrastructure. This approach allows to perform simulations on the single infrastructure and to model the interdependencies between them. The first element to be modeled was the building portfolio. Several sources were consulted to gather existing information. Missing parameters were estimated through a typological approach and based on past design codes and constructive techniques. To consider uncertainties in these estimates, input parameters were characterized by a different standard deviation based on the building archetype and year of construction. Ideal City's building portfolio consists of about 23,420 residential buildings. RC buildings are the most common (63%), while the remaining part are masonry structures (37%).

The seismic capacity was evaluated through a Monte Carlo simulation process that estimates the median global capacity curve of each structure and the corresponding dispersion. Four-point and three-point backbone curves were obtained for RC and masonry buildings, respectively. Nonlinear time history analyses were performed to assess the seismic response in terms of top displacements. Multiprocessing was exploited to speed up the duration of the analyses. To obtain the maximum inter-storey drifts a simplified response model was implemented. The maximum inter-storey drifts were then converted into damage states.

Four simplified seismic scenarios were defined to test the seismic performance of Ideal City. These are representative of two near-field (Kobe, Northridge) and far-field earthquakes (El Centro, Hachinohe). It was found that the two near-field earthquakes produced the most disruptive damage scenarios. It was also observed that older buildings reported more damage compared to more recent structures, showing that the newer design procedures enhanced the structural performance limiting the damage. In addition, masonry buildings demonstrated to be more vulnerable, and their vulnerability increased with the number of storeys. The intrinsic fragility of this type of structures led to higher levels of damage. The

obtained results can support decision-makers in analyzing how their community responds to a given seismic event, quantifying the performance of the building portfolio, and consequently planning strategies to minimize losses and recovery time.

Chapter 5

5 Road transportation network

5.1 Introduction

Transportation networks are essential for the social and economic growth of communities. The road infrastructure is especially crucial as many other systems and services rely on it. Therefore, it is important to investigate the characteristics of road transportation networks and their resilience towards disruptive events. For example, predicting the availability of roads and changes in the topology would facilitate the decision-making process under emergency. Graph theory is certainly one of the most frequent principle to model transportation networks due to its advantages when solving problems related to routing, traffic, minimum cost flow, etc. Many studies exploited graph theory principles to develop automated tools to study large-scale transportation systems and perform simulations. Examples are Python libraries such as NetworkX (Hagberg et al. 2008) and open-source software like Gephi (Bastian et al. 2009).

In case of strong ground motions, the debris generated from the collapse of buildings might block several roads, hampering medical aid and search and rescue operations. The estimate of debris represents a relevant gap in the literature. The main aspect that limits the number of attempts at tackling this important matter is the large number of input parameters needed for such analyses. Structures and seismic events should be fully characterized for an accurate estimate. Domaneschi et al. (2019) proposed a parametric study on masonry buildings under several collapse scenarios using numerical simulations. The empirical formula for the evaluation of debris extension for masonry buildings is obtained from an interpolation of numerical results and it is mainly based on geometric parameters. Moreover, this work approximates the maximum volume of debris that allows the passage of vehicles. Lu et al. (2019) investigated pedestrian evacuation during a seismic scenario, evaluating the influence of debris on the time needed for

45

evacuation. In this study, a method to calculate debris extension is proposed, performing finite element analysis of a brick wall. The collapse of the wall is characterized by a maximum drift ratio of each storey and the projection of debris is determined from motion laws defined in relation to the velocity of the building. Unfortunately, the applicability of these methodologies is limited to masonry structures of which discrete knowledge is required to perform finite element analyses. Garcia et al. (2016) proposed a methodology to estimate the amount of debris of residential infrastructures based on their vulnerability and construction materials. Several earthquakes have been selected to describe different seismic scenarios, and generalization of the model is proposed to describe the behavior of several housing types.

Machine learning (ML) techniques could be a practical solution to estimate of debris generated after a seismic event. ML is a subcategory of BDA based on the idea that computers can learn from input data and make predictions from recognized patterns. This field has been growing for the past ten years thanks to the advancement in the computer industry. Nowadays, ML has applications in virtually any industrial and research field. ML algorithms have spread in everyday life to help detecting spam, recognize people inside pictures, recommend content and advertisement, automate decision-making processes, etc.

This chapter describes the model of Ideal City's road transportation network and its interdependence with the building portfolio. The network was modelled through graph theory, which allowed to use graph metrics to evaluate its performance. Then a ML procedure to estimate the debris footprint caused by damaged buildings is presented. From the information available in existing collections of post-disaster data, seven parameters have been selected as capable of affecting the debris extension (DE). They are event magnitude, distance from the epicenter, building's year of construction, building's height, number of storeys, construction material, and direction of evaluation (vertical or horizontal). The dataset has been split into a training and test set using three split ratios and eight ML algorithms have been applied: k-Nearest Neighbour (KNR), Ridge Regressor, LASSO model, Elastic Net (EN), Decision Trees (DT), Random Forest (RF), Support Vector Regression (SVR), and multilayer Perceptron Regressor (MLP). The accuracy of each algorithm has been evaluated through Mean Squared Error (MSE) and the R-squared values. After a comparison among models, the most suitable algorithm was selected for the case study. Therefore, according to the structural damage suffered after the four benchmark scenarios, DE was calculated for each building. Comparing DE to the width of the adjacent roads it was possible to determine which roads were blocked and analyze the performance of the new topology of the network. This information would help first responders during the emergency phase to identify the most critical situations and the shortest paths between any origin-destination nodes. Moreover, this type of analysis could be used by policy makers to identify the most efficient evacuation routes.

5.2 Model of the network

The transportation network of Ideal City was modeled using graph theory. This is a simple yet powerful tool to deal with a number of problems concerning network systems. In transportation and logistics related problems, graph theory is widely used to solve routing and traffic flows in the network. In fact, it was with Euler's negative resolution to the Seven Bridges of Königsberg problem that graph theory originated.

A graph *G=(N,E)* consists of a set of nodes *N* (also called vertices) and a set of edges *E* (also called links). The number of elements in the node set is called the order of the graph. The degree of a vertex is the number of edges connecting that vertex to others. Once nodes and edges are defined it is possible to draw the graph. For instance, given three nodes *N=(1, 2, 3)* and *E=[(1,1),(1,2),(2,3)]*, the resulting graph would be somewhat similar to the one shown in Figure 5-1. An edge of the form $(n,n) \in E$ is called a loop. The graph of the previous example has one loop. If *G* has no loops, it is called a simple graph. Any graph can be modified into a simple graph by removing all loops. In simple graphs, edges can be defined as subsets of *N* of size 2.
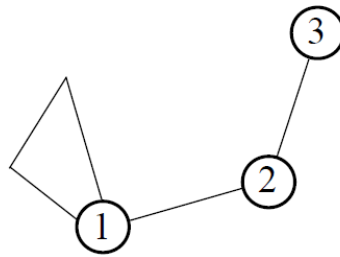
Figure 5-1 - Example of undirected graph presenting a loop.

An important property of graph is directionality. Some are undirected, meaning that edges can be followed in both ways, while others have directed edges. In this case, links can be seen as ordered pairs *(u, v)*. This leads to the following definition: a directed graph, also called digraph, *G=(N,E)* consists of *N* nodes and *E* edges such that $E \subset N \times N$. If $e = (u,v) \in E$ is a directed edge, then *e* goes from node *u* to node *v*, and it is graphically indicated with an arrow. Otherwise, if *(u, v)* and *(v, u)* both belong to *E*, then it is possible to draw either a single line or a double headed arrow that connects *u* and *v*.

Any graph, whether directed or undirected, can be mathematically described by an adjacency matrix. Let *N* be the ordered node set $\{n_1, n_2, \dots, n_n\}$, the adjacency matrix of the graph *G* is defined as the following *n×n* matrix:

$$A = (a_{ij}), \qquad a_{ij} = \begin{cases} 1 & (n_i, n_j) \in E \\ 0 & (n_i, n_j) \notin E \end{cases} \qquad (5\text{-}1)$$

Therefore, the resulting matrix contains 1-elements and 0-elements to describe whether is a connection or not between the nodes identified by the indexes of the selected element. For instance, the adjacency matrix for the graph illustrated in Figure 5-1 is:

$$A = \begin{pmatrix} 1 & 1 & 0 \\ 1 & 0 & 1 \\ 0 & 1 & 0 \end{pmatrix} \tag{5-2}$$

This provides a straightforward tool to check connections among nodes without having to draw the actual graph. By looking at the matrix of Equation (5-2), one can immediately tell that there are links from nodes 1 to 1 (i.e., a loop), 1 to 2 and 2 to 1 (undirected edge), 2 to 3 and 3 to 2 (undirected edge). It can be observed that loops imply having ones on the main diagonal of the adjacency matrix. On the contrary, simple graphs are characterized by all zero elements on the main diagonal. Moreover, a symmetric matrix means that the graph is undirected. This does not depend on the on the order chosen for the nodes in the set N. If the graph is undirected, then $(e_i, e_j) \in E$ is equivalent to $(e_j, e_i) \in E$ for all $1 \le i, j \le n$, which means that value of $a_{ij} = a_{ji}$.

Assuming that two nodes are connected, it is possible to determine the distance between them. If $u, v \in V$ and $\Lambda(u, v)$ is the set of paths from u to v, the distance $d(u, v)$ between u and v is:

$$d(u,v) = \begin{cases} \infty & \text{no path from } u \text{ to } v \\ \min\{length(\gamma) : \gamma \in \Lambda(u,v)\} & \text{otherwise} \end{cases} \tag{5-3}$$

Thus, the distance between two nodes is the least number of links that it takes to get from one to the other. To understand how well connected a graph is, the average distance can be calculated. This metric estimates the distance between a pair of nodes randomly selected. For a directed or undirected graph G, the average distance is defined as:

$$d_{avg}(G) = \frac{1}{n(n-1)} \sum_{u \in V} \sum_{v \in V, v \ne u} d(u,v) \tag{5-4}$$

Furthermore, graphs can be associated with a weighting function $w : E \to \mathbb{R}^+$. In this case the graph is called weighted. The weight coefficients are generally applied to each edge. These coefficients can be useful in multiple ways. For instance, the weight can be seen as the cost of using that specific edge (e.g., a physical distance, a financial cost, a time cost). The adjacency matrix allows to represent weighted graphs easily. Given a vertex set $V = \{1, 2, \ldots, n\}$, $w_{ij} = w(i, j)$

if $(i, j) \in E$ and $w_{ij} = 0$ otherwise. One might define the length of a path as the sum of the weights of the edges within the path. In this case the concept of distance is the minimum cost of a path from a node to another. The lowest cost path might not involve the least number of edges. Thus, the algorithm to compute distances in weighted graphs is different from the one used in unweighted graphs.

The application of graph theory to road networks is quite straightforward: edges represent the middle axis of roads, while nodes represent road intersections. Road transportation networks are usually directed graphs because of one-way streets. However, Ideal City's transportation network was treated as an undirected graph. This choice was made based on the assumption that in emergency conditions the directionality of the streets might be disregarded to prioritize evacuation and rescue operations. The graph was manually drawn in AutoCAD using the Turin's road map taken from OpenStreetMap. Despite OpenStreetMap and other GIS maps available for the city of Turin give the possibility to access a data structure containing the coordinates of the streets, it was impractical to create a graph out of this information. First of all, the road layout was not completely coherent with the building database, which had already been created, with many roads intersecting building footprints. In addition, these sources present huge number of points as each road is fragmented in many segments. Drawing the graph manually was certainly time consuming but led to a much more coherent and computationally efficient graph without oversimplifying the network. Usually, in transportation networks, an edge represents a road in between two intersections. In this application, however, the actual road map was followed as much as possible in order to capture changes of direction and curvy roads. In these cases, the road connecting two intersections is divided into multiple edges and nodes (Figure 5-2).

(a)   (b)
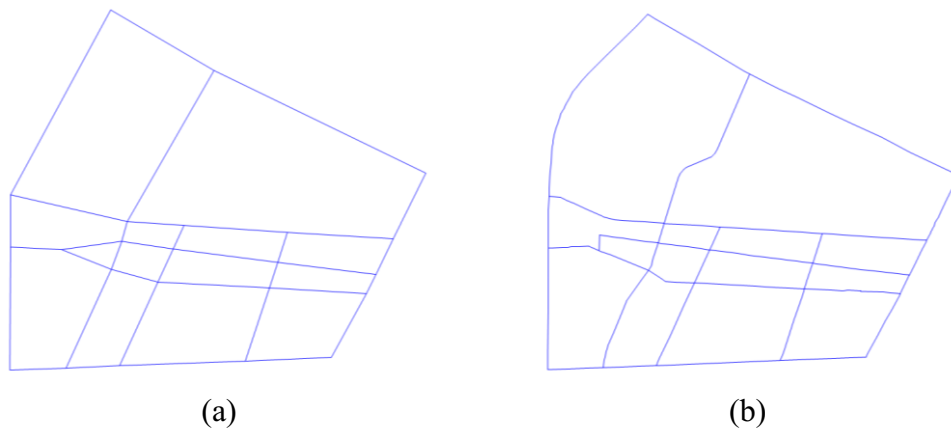
Figure 5-2. (a) Graph obtained considering a single segment between intersections and (b) graph obtained considering multiple segments.

The obtained undirected graph G consists of 14,239 nodes (N) and 18,798 edges (E), described by an $N \times N$ adjacency matrix A. In addition, a weighted adjacency matrix was generated. Whenever there was a connection between nodes, one-

elements were replaced with the width of each road. This information was collected manually from Google Maps (Google 2021) ensuring the compatibility with the existing building database. Figure 5-3 illustrates the entire graph representing the road transportation system of Ideal City.
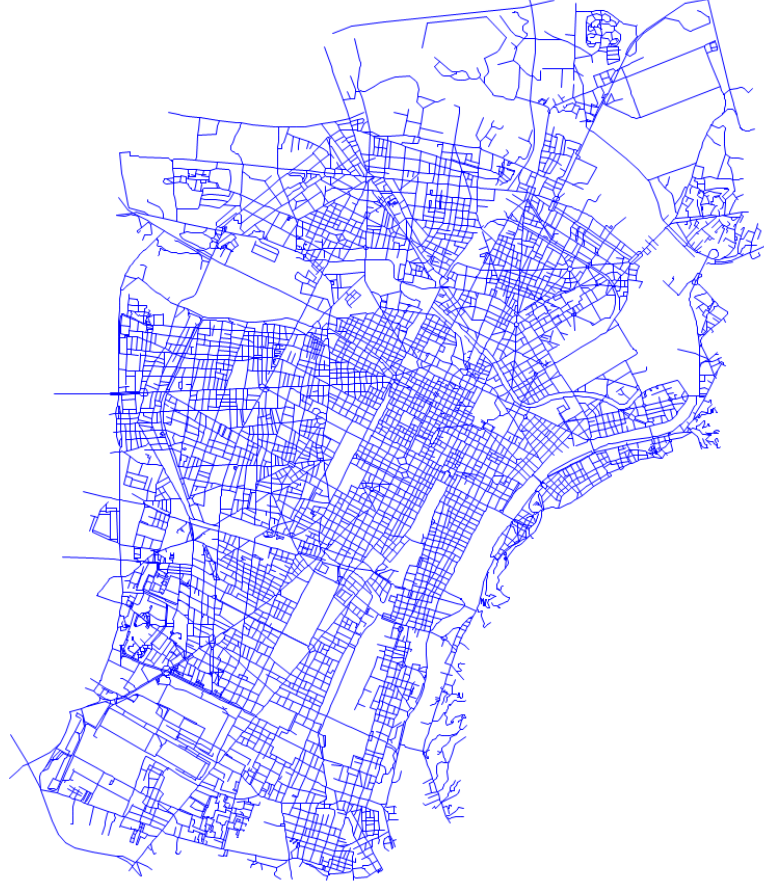
Figure 5-3. Ideal City's road transportation network.

The adjacency matrix allows the calculation of interesting performance parameters and to change the topology of the network in case some edges become unavailable. Another advantage of modeling the system through graph theory is the possibility to use graph indicators to quantify the characteristics and performance of the network. An important metric is the average vertex degree $\langle vd \rangle$ of the graph, which indicates how many edges pass through a given node:

$$\langle vd \rangle = \frac{1}{N} \sum_{i \in N} \sum_{j \in N} a_{ij} \tag{5-5}$$

To apply the formulation to undirected graphs, edges passing through a node should be accounted only once. Hence, the adjacency matrix must be reduced to a triangular matrix. The higher the vertex degree the better the connectivity of the network.

Another graph metric that can be used as a measure of network performance is the global efficiency E_{glob}. This parameter was introduced by (Latora and Marchiori

2001) and it is defined as the average of the number of edges in the shortest path $d_{(i,j)}$ between nodes i and j, as shown in Equation (5-6):

$$E_{glob} = \frac{1}{N(N-1)/2} \cdot \sum_{i \neq j} \frac{1}{d_{(i,j)}}$$

(5-6)

By definition $0 \leq E_{glob} \leq 1$. The optimal condition of $E_{glob} = 1$ can be reached when there is an edge between each pair of nodes. In large networks, like the one of the analyzed case study, the global efficiency tends to assume small values. This is especially true in road networks where the shortest path might consist of several edges.

Table 5-1 summarizes the main characteristics of the generated graph. These values are representative of the undamaged condition and will be used as reference for each seismic scenario.

Table 5-1. Characteristics of the road transportation network in normal conditions.

Graph parameters	Value
No. Edges	18,798
No. Nodes	14,239
Average vertex degree	2.6404
Global efficiency	0.0394

5.3 Debris estimation

5.3.1 Data collection and methodology

In this section the use of ML techniques to estimate debris generated after a seismic event is discussed. Different ML algorithms were tested to forecast the debris extension (DE) in the vertical or horizontal direction. The first part of the work consisted of collecting around 10,000 pictures from four different sources: Earthquake Engineering Research Institute (EERI) Clearinghouse (EERI) and EERI collection of case studies (EERI); Digital Environment for Enabling Data-Driven Science (DEEDS); Geotechnical Extreme Events Reconnaissance (GEER). The first selection criterion was to get pictures in which the area of the debris is clearly visible and distinguishable from other elements. In addition, they had to show at least a portion of the damaged building to analyze its characteristics. After this screening process, a database of 310 pictures from 25 different events was generated. Table 5-2 reports the number of pictures selected for each of the 25 different earthquakes.

The learning phase of ML algorithms begins with an input dataset containing a number of features. After a careful analysis of the information that was deductible from the selected pictures, the following features were identified as capable of influencing the area of debris:

- *Material*: masonry and reinforced concrete buildings are considered.
- *Number of storeys*: the increase of mass and rigidity at each floor level can amplify horizontal seismic forces resulting in more damages and consequently more debris.
- *Year of construction*: construction quality can vary over the years because of different design standards and construction techniques. Generally, recently built structures can better withstand earthquakes.
- *Magnitude*: the stronger the ground motion, the higher the potential damage.
- *Distance from epicenter*: the smaller the epicentral distance, the greater the effects on structures;
- *Building's height*: tallest buildings can potentially produce more debris.
- *Direction*: for each image, DE can be evaluated along the vertical or horizontal direction.

Unfortunately, not all of these features were visible in each picture. Table 5-3 summarizes the number of pictures where each feature could be identified. To compensate for this lack of information, undefined values were estimated according to the details present in the pictures (e.g., materials, construction techniques, information on adjacent buildings, etc.).

Table 5-2. Number of pictures for each seismic event.

Seismic event	Year	No. of Pictures
Central Italy	2009	65
Cephalonia (Greece)	2011	22
Christchurch (New Zealand)	2011	13
Ecuador	2016	54
India	2001	28
Loma Pietra (US)	1989	5
Mexico Central	2017	20
Nepal	2015	34
Northern Iran	2017	1
Northridge (US)	1994	2
North-west Armenia	1988	5
South Napa Valley (US)	2015	6
Southern Taiwan	2016	24
Turkey	1999	10
Alaska	1964	3
Algeria	1980	1
Armenia	1988	1
California	1994	4
Chile	2010	4

Haiti	2010	3
Honduras	2009	1
Indonesia	2005	1
Japan	2012	1
Korea	2017	1
Oklahoma (US)	2016	1

Table 5-3. Number of samples for each feature.

Feature	No. of samples
Material	310
Stories	310
Year of construction	66
Magnitude	310
Distance from epicenter	278
Height	310
Direction of DE	310

To quantify DE in each picture, the amount of rubble was compared to the dimension of other recognizable objects whose size can be precisely determined. This procedure can be done by using any photo editing software, evaluating actual distances from pixel coordinates. An example from the dataset is hereby presented to clarify the procedure. Figure 5-4 shows how the width of a car was used as a reference to evaluate DE.

Figure 5-4. Width of a car used as a reference measure to determine debris extension.

To predict DE along one direction the simple relation shown in Equation (5-7) is used:

$$DE = p \times \frac{P}{d} \qquad (5\text{-}7)$$

where:

- $P = x_{1r} - x_{2r}$ where x_{1r} and x_{2r} are the pixel coordinates of the reference element;

- $p = x_{1d} - x_{2d}$ where x_{1d} and x_{2d} are the pixel coordinates of the debris extension;

- d is the actual value, in meters, of the dimension of the reference element;

The parameters used in the example of Figure 5-4 are summarized in Table 5-4.

Table 5-4. Input and output data for the example of Figure 5-4.

Coefficient	Value
x_{1r}	502
x_{2r}	334
x_{1d}	720
x_{2d}	371
p	349
P	168
d [m]	1.8
DE [m]	3.629

The so obtained results where then normalized to the height of the building. In this way, the training data is less dependent on the size of the considered samples. Also, their log_{10} value is considered to diminish the variance, compare results to other existing models found in the literature, and speed up the convergency of the ML algorithms.

5.3.2 Data visualization

For visualization purposes, data was divided based on input features and plotted. Figure 5-5 shows the DE values for different features: (a) the epicenter distance, (b) the magnitude, (c) the stories of a building, (d) the year of construction, and (e) the building height. Results for masonry and RC buildings are identified in each chart using labels. The information regarding the direction of DE is not represented for a clearer visualization. The values shown in Figure 5-5 come from the initial raw data. As previously discussed, lacking information about the year of construction and distance from the epicenter was estimated. From these chart, no clear correlation patterns are evident. It seems that data follows linear trends, mostly horizontal or sub-horizontal. However, the dispersion is quite significant, and the distribution is not even throughout the samples.
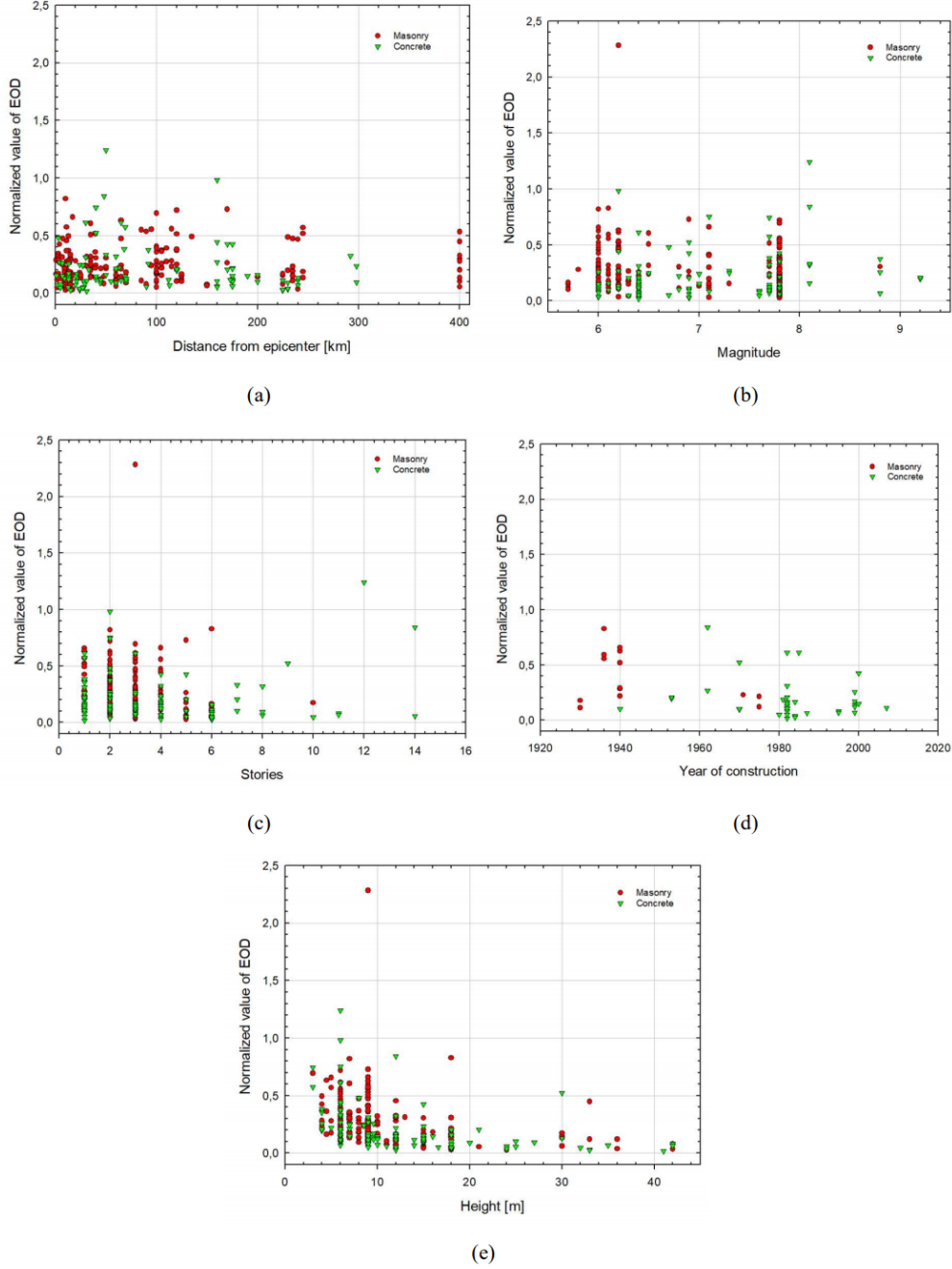
Figure 5-5. Data visualization of (a) epicenter distance, (b) magnitude, (c) number of storeys, (d) year of construction, (e) building height.

The analyzed case study is a multi-features regression in 7 dimensions that cannot be visualized in a traditional way. Nonetheless, the visualization of data distribution is an important step to evaluate density, variety, and other data characteristics. For instance, a various dataset might be able to generate a comprehensive ML model that can be applied to samples with different characteristics.

To avoid this limitation, the t-SNE method was used (van der Maaten and Hinton 2008). It aims at creating a map of the data, where the distance between

points in the *t*-dimensional space are evaluated to create groups of neighbor data. This model utilizes a probability distribution function of distances between points, using Barnes-Hut approximation, and minimizes the Kullback-Leibler divergence using a gradient descent method. Figure 5-6 shows the application of t-SNE to the case study. As it can be seen, the dataset can be divided into five groups of samples. Moreover, since categories are not concentrated in a specific area, the variance of the dataset is likely to be large.
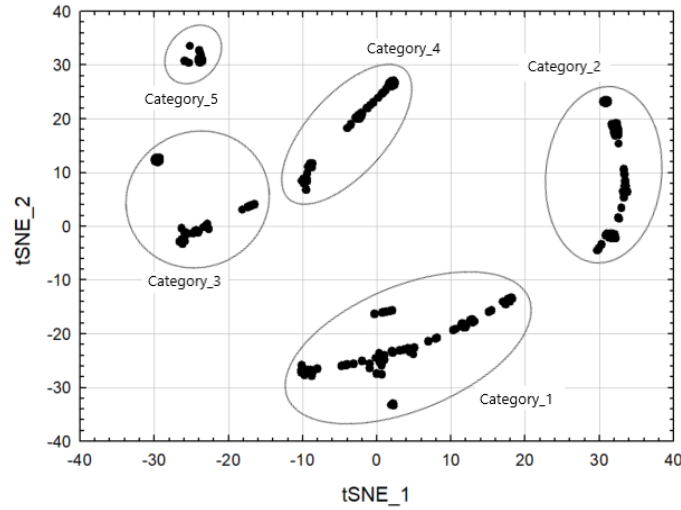
Figure 5-6. t-SNE chart showing the dataset grouped into five categories.

5.3.3 Data testing and preprocessing

To find the best performing ML algorithm for the case study tuning and comparing procedures were defined. For each model, different parameters are needed to tune the algorithm. Further information can be found in the documentation of Scikit-learn (2018). In the implementation of each algorithm, a self-tuning process is used to find the best set of input parameters. The self-tuning process tests a range of values for each parameter on the training set and selects the best configuration comparing the MSE value of prediction on the test set.

The MSE of an estimator measures the average of the squared errors, i.e., the average squared difference between the predicted values and the input values. MSE is typically used to assess the quality of an estimator. MSE is always a positive quantity, and values close to zero mean high accuracy. Being $\hat{y}_i$ the predicted value of the i-th sample and y_i the corresponding actual value, the MSE measured for $n_{samples}$ is calculated as shown in Equation (5-8).

$$MSE\left(y, y\right) = \frac{1}{n_{samples}} \sum_{i=0}^{n_{samples}-1} (y_i - \hat{y}_i)^2 \qquad (5\text{-}8)$$

Three different size-ratio of training and test sets were evaluated, i.e., 85%-15%, 80%-20%, and 70%-30% respectively. Each split dataset was tested with 100 different random states. First, the self-tuning process identified for each random state the best set of parameters and evaluated the MSE of the final configuration. In the next step, the results obtained for each random state were compared in terms of R-squared values to identify the best set of input parameters for each partition of the dataset. The R-squared value can be seen as a measure of the distance between the data and the regression line calculated by the algorithm, providing a measure of the accuracy for new samples. Commonly, R-squared values range between 0 and 1, where 1 represents the best possible score. However, it is worth noting that R-Squared can be negative in some cases. This happens when the model does not follow the trend of the data. In these cases, absolute values are used in the analysis. Being $\hat{y}_i$ the predicted value of the i-th sample and y_i the corresponding actual value, the R-squared (R^2) coefficient of correlation estimated for $n_{samples}$ can be defined as:

$$R^2\left(y,y\right)=1-\frac{\displaystyle\sum_{i=0}^{n_{samples}-1}\left(y_i-\hat{y}_i\right)^2}{\displaystyle\sum_{i=0}^{n_{samples}-1}\left(y_i-\bar{y}\right)^2} \tag{5-9}$$

where:

$$\bar{y}=\frac{1}{n_{samples}}\sum_{i=0}^{n_{samples}-1}y_i \tag{5-10}$$

Finally, some preprocessing strategies were applied to avoid overfitting, which occurs when an algorithm is highly accurate when applied to the train set but a low accuracy for predictions. In this case the algorithm accurately fits the training set but fails to represent new samples. Depending on the algorithm, different pre-processing approaches can be utilized that can help to avoid overfitting. Since the ML algorithm were implemented in Python, the Python library Scikit-learn (2018) was chosen to tackle overfitting issues as it includes the StandardScaler function. This pre-processing tool ensures that the mean of each feature is 0 and the variance is 1, scaling all the features to the same magnitude, to avoid outliers and improve accuracy. This function was used to avoid overfitting before testing the ML algorithms.

5.4 Machine learning algorithms

The dataset of post-disaster pictures is analyzed with a supervised ML learning approach using regressor algorithms. In the literature, many existing algorithms

based on different techniques are available. The choice of the most suitable one depends on the specific case study. Usually, the size of the input dataset and error comparison are the main criteria to choose one algorithm over another. To facilitate the process, a category of suitable algorithms can be detected from the flowchart shown in Figure 5-7, adapted from (Scikit-learn 2018). In the following paragraphs, the algorithms used in this study, are presented.
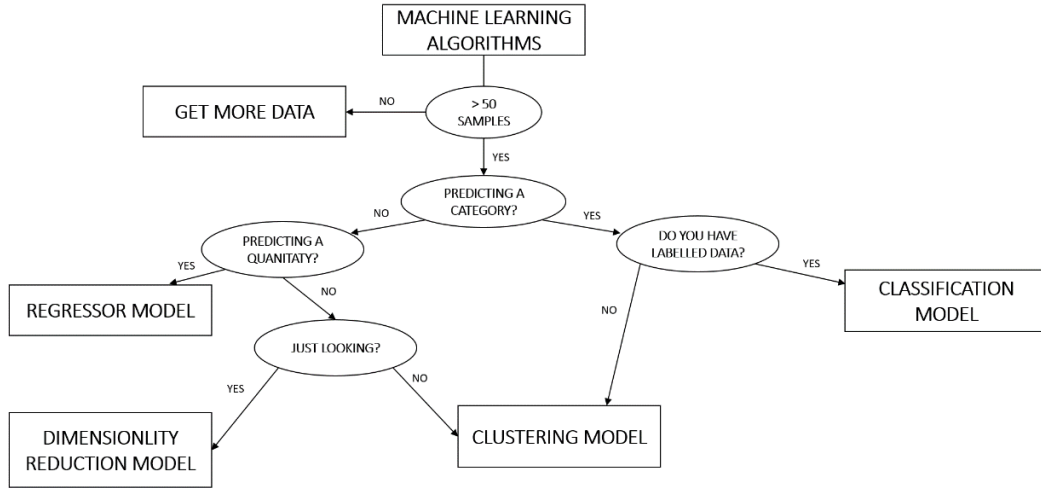
Figure 5-7. ML algorithm categories flowchart.

5.4.1 k-Nearest Neighbors Regressor (KNR)

The k-Nearest Neighbors (k-NN) is a non-parametric algorithm used for regression and classification. When used as a regressor, it is commonly called k-Nearest Regressor (KNR). It predicts an output value starting from the closest points in the training sample, namely its nearest neighbors. The "k" indicates the number of points used to make the prediction (Goldberger et al. 2004). Distances within data can be evaluated using different techniques: (i) Manhattan/city block distance; (ii) Euclidean distance; (iii) Minkowski distance; (iv) Chebychev distance. KNR predicts outputs using the mean value of the selected distance among the k points:

$$y(x_0) = \frac{1}{K} \sum_{i=1}^{k} d_i \qquad (5-11)$$

where d is the selected type of distance. A value of $k \leq 5$ is usually recommended.

Figure 5-8 illustrates a generic application of the KNR algorithm showing the different precision between $k=1$ and $k=3$.
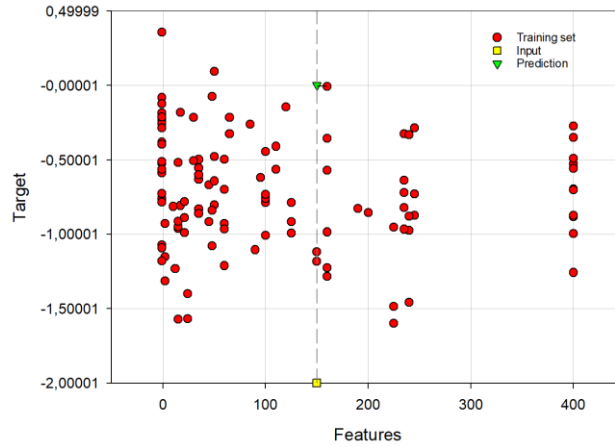
(a)
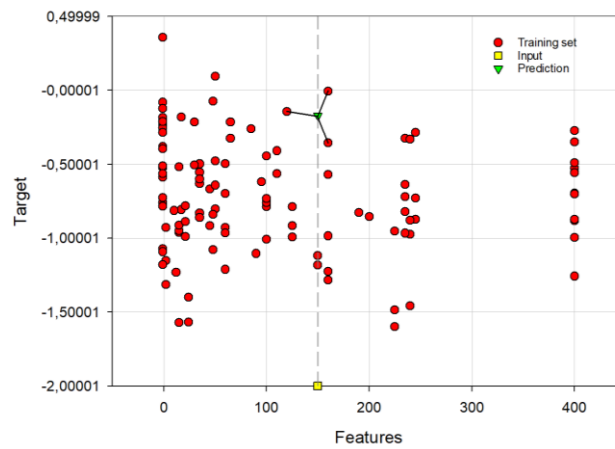
(b)

Figure 5-8. KNR prediction with (a) *k=1* and (b) *k=3*.

For the KNR algorithm, two input parameters are required:
- the *k-value* of considered neighbors, i.e., the number of points taken into account in the prediction for the *X* test;
- the type of *distance*.

It was found that he best set was: size ratio=85%-15%, *k=6*. Manhattan distance was used.

5.4.2 Linear regression models (LRM)

Linear models can be used to fit the input data through regression and use a loss function for predictions. Due to their simplicity and versatility they are broadly adopted. They produce the best results when the number of predictors is large.

The algorithms selected for estimating DE are: (i) Ridge Regression; (ii) LASSO model; (iii) Elastic Net.

Ridge Regression (Faber et al. 2017) uses as loss function the penalty function in Equation (5-12):

$$\sum_{i=1}^{n}\left(y_i - \beta_0 - \sum_{j=1}^{p}\beta_j x_{ij}\right)^2 + \lambda_2\underbrace{\sum_{j=1}^{p}\beta_j^2}_{L_2-penalty} = RSS + \lambda_2\sum_{j=1}^{p}\beta_j^2 \qquad (5\text{-}12)$$

where b_j are predictors, and λ_2 is a tuning parameter. When $\lambda_2=0$, Ridge Regression gives the same results of a 'Root Sum Squared' (RSS) method. This method however cannot remove features in the prediction phase.

The LASSO model (**L**east **A**bsolute **S**hrinkage and **S**election **O**perator), presented by Tibshirani (1996), uses the loss function reported in Equation (5-13):

$$\sum_{i=1}^{n}\left(y_i - \beta_0 - \sum_{j=1}^{p}\beta_j x_{ij}\right)^2 + \lambda_1\underbrace{\sum_{j=1}^{p}|\beta_j|}_{L_1-penalty} = RSS + \lambda_1\sum_{j=1}^{p}|\beta_j| \qquad (5\text{-}13)$$

where a new *L₁-penalty* function is implemented to overcome the limitations of Ridge Regression. The penalty is defined as the sum of the absolute values of the predictor b_j. As for Ridge Regression, when $\lambda_1=0$, the model gives the results of an RSS. When $\lambda_1 \to \infty$, the predictor b_j are null and they can be removed from the evaluation. Thus, the LASSO model is able to perform a variable selection. However, the model has a couple of limitations. In case the number of predictors b_j is larger than the number of observations (*n*), LASSO selects at most *n* variables. In addition, when predictors can be grouped for their high correlation, LASSO tends to select only one variable from the group, regardless of which one is selected.

Elastic Net (EN) is a model presented by Zou and Hastie (2005). Its loss function is a linear combination of the *L₁* and *L₂* penalties, as shown in Equation (5-14):

$$L(\lambda_1, \lambda_2, \beta_j) = |y_i - \beta_j x_{ij}|^2 + \lambda_2\sum_{j=1}^{p}\beta_j^2 + \lambda_1\sum_{j=1}^{p}|\beta_j| \qquad (5\text{-}14)$$

where the *L₂-penalty* function does not have the limitation on the number of selected features and regularizes the *L₁-penalty* that generates a sparse model. EN can be defined as a hybrid model because for $\lambda_1=0$ it is a Ridge Regression model and for $\lambda_2=0$ it is a LASSO model.

For the Ridge Regression and LASSO model, the only one variable to set (i.e., regularization of *L₂-penalty* and *L₁-penalty* coefficients). In Elastic Net, there is also the *l1_ratio* parameter, which is equal to the ratio between λ_1 and λ_2. The best set for each algorithm was obtained from a size ratio of 85%-15% and the following parameters:

- Ridge Regression: α=10

60

- LASSO: α=0,001
- ElasticNet: α= 0,01 and *l1_ratio*=0,5

5.4.3 Decision Trees (DT)

Decision Tree (DT) (Quinlan 1986) is a supervised learning method that can be used both as a regressor and a classifier. When the target variables can take continuous values, the model is a regressor and it is called Regression Tree (RT). DT model is based on a tree graph obtained from if/else tests that divide the dataset into different subsets with high correlation. Each subset is called 'node'. The tree structure is composed of a first 'root' node that includes the entire input dataset from which 'branches', i.e., tests, start the division process. The last nodes are called 'leaves' and they express the prediction of the tree. Figure 5-9, inspired by Qi et al. (2018), shows the general structure of a tree.
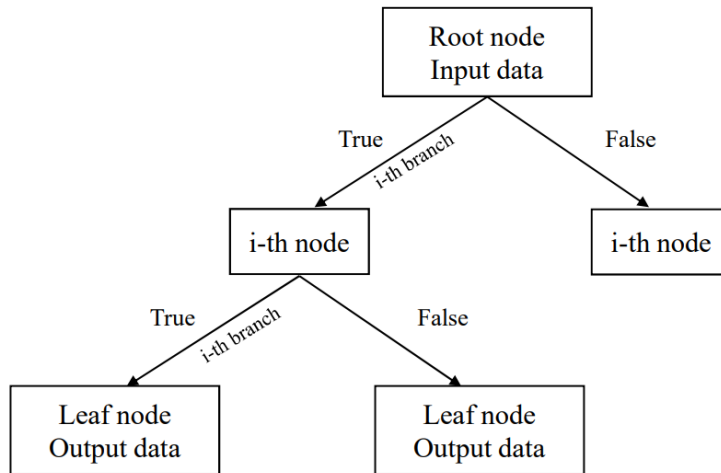
Figure 5-9. DT algorithm flowchart.

A pruning process can be added to the algorithm to control the growth of the tree, choosing from a 'pre-pruning' or a 'post-pruning'. The former stops growth at a fixed point, while the latter deletes nodes that carry little information. Pruning is required to avoid overfitting, but a wrong setup can reduce the accuracy of the predictions. Both processes can be applied to the same model. DT is widely used for its effectiveness and its independence from the scale of the data. The main limitation remains the high probability of overfitting despite the pruning process.

The coefficients used for DT are four:
- *min_samples_split*: minimum number of samples required to split an internal node;
- *min_samples_leaf*: minimum number of samples required to be at a leaf node;
- *max_depth:* maximum depth of a tree;

61

- *max_features:* maximum number of features to consider when looking for the best split.

It was found that the optimal parameters were: size ratio=80%-20%, *min_samples_split*=20, *min_samples_leaf*=2, *max_depth*=5, and *max_features*=2.

5.4.4 Random Forests (RF)

Random Forest (RF) is a variation of the DT model, as presented by Breiman (2001). It works with several DT predictors, associated with a random root node contained in a random vector. Each random tree gives a prediction *h*, and the result is the most voted prediction in the forest. Theorem 11.2 in Breiman (2001) demonstrated that the accuracy of a forest is higher than the accuracy of a single tree. Equation (5-15) expresses this theorem by comparing the average precision error (*PE**) of both models.

$$PE*(forest) \leq \overline{\rho} PE*(tree) \tag{5-15}$$

where $\overline{\rho}$ is the weighted correlation between the residual of tree and forest predictions.

The coefficients used for RF are 4:
- *min_samples_split*: minimum number of samples required to split an internal node;
- *min_samples_leaf*: minimum number of samples required to be at a leaf node;
- *max_depth:* maximum depth of a tree;
- *max_features:* maximum number of features to consider when looking for the best split.

It was found that the optimal parameters were: size ratio=85%-15%, *min_samples_split*=5, *min_samples_leaf*=2, *max_depth*=6, and *max_features*=2.

Support Vector Regression (SVR)

SVR is a regression technique obtained from the Support Vector Machine proposed by Vapnik (1995), (1998). The technique relies on the definition of a hyperplane fitted to the input data. The distances between input points and the plane are then evaluated. A typical formulation to define a hyperplane is reported in Equation (5-16):

$$f(x, \alpha) = (w \cdot x) + b \tag{5-16}$$

where *w* and *b* are coefficients coming from the training set and α is the Lagrange multiplier used for the optimization of *w* and *b*. SVR predicts output data

finding a regression function from the minimization of the empirical risk in Equation (5-17):

$$\Phi(w, \xi^*, \xi) = \frac{\|w\|^2}{2} + C\left(\sum_{i=1}^{j} \xi_i^* + \sum_{i=1}^{j} \xi_i\right) \tag{5-17}$$

where C represents the strength of the regularization, and ξ^*, ξ are slack variables indicating the upper and lower constraints of the j outputs.

The required parameters for SVR are four:

- C: the strength of the regularization;
- ε: the epsilon-tube within which no penalty is associated with the loss function;
- *kernel*: specifies the kernel type used in the algorithm;
- *gamma*: kernel coefficient;
- *degree:* specifies the degree of the polynomial kernel function only with a 'poly' kernel;

It was found that the optimal parameters were: size ratio=85%-15%, C=1000, ε=0,1, *kernel*=linear, *gamma*='scale', and *degree*=2.

5.4.5 Multilayer Perceptron Regressor (MLP)

A multilayer perceptron (MLP) is a subcategory of Artificial Neural Networks (ANN) where perceptrons are the equivalent of neurons. Its formulation is reported in Equation (5-18):

$$f(x) = w_2 \cdot g(w_1^T x + b_1) + b_2 \tag{5-18}$$

where w_1 and w_2 are weighting factors, b_1 and b_2 are the bias, and $g(x)$ is the activation function (Khadem and Hossein-Zadeh 2014). The structure is composed of an input layer, two hidden layers, and an output layer as reported in Figure 5-10.
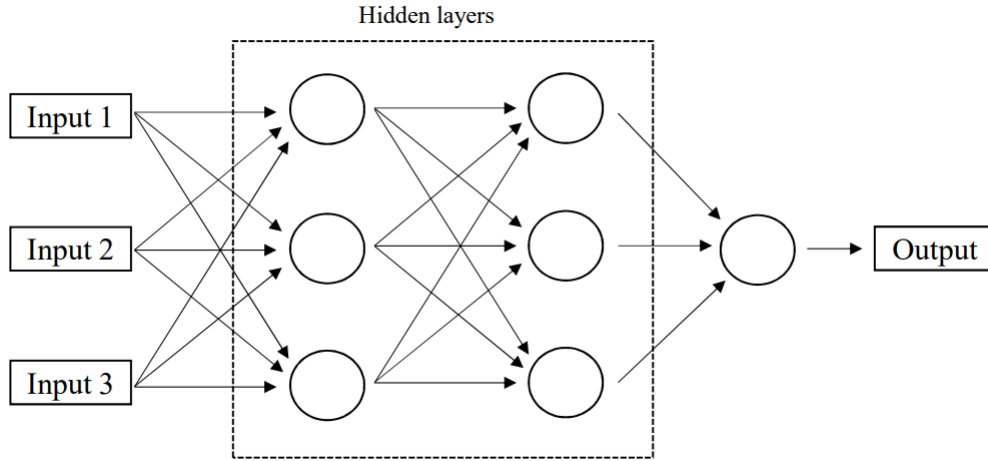
Figure 5-10. MLP structure.

Weights of input features are updated through an iterative process based on the minimization of the error by a backward transmission in the hidden layers. The process ends after a fixed number of iteration or by specifying a cutting point.

MLP requires several parameters to tune due to its multilayer connective framework. In this study, five inputs were considered:

- *alpha*: regularization parameter;
- *hidden_layer_sizes*: number of neurons in the i-th hidden layer;
- *activation*: activation function for the hidden layer;
- *solver:* solver for weight optimization;
- *max_iter:* maximum number of iterations.

It was found that the optimal parameters were: size ratio=80%-20%, *alpha*=0,001, *hidden_layer_sizes*=10, *activation*='relu', *solver*='lbfgs', and *max_iter*=350.

5.5 Comparison of the machine learning algorithms

After the training phase, the ML algorithms were applied to the test set, and both MSE and R-squared were evaluated. MSE was used to compare the algorithms and define the most accurate. On the other hand, R-squared was used to detect possible overfitting and choose the best split between training and test datasets.

Figure 5-11 and Figure 5-12 show the results in terms of MSE for the training and the test set, respectively. The different grayscale colors identify different test sizes: (i) black bars represent a test size of 15% of the dataset; (ii) grey bars indicate a test size of 20% of the dataset; (iii) white bars illustrate a test size of 30% of the dataset.
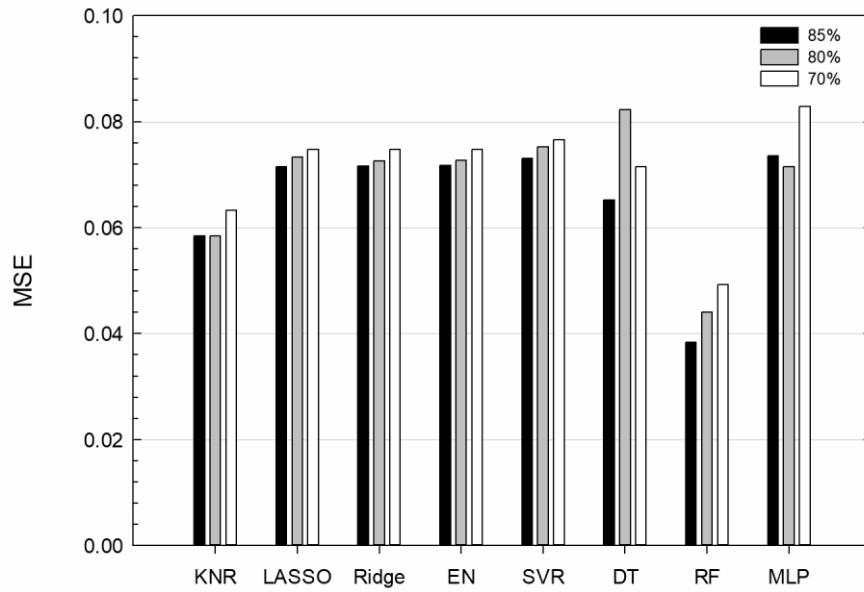
Figure 5-11. MSE comparison of the training set.
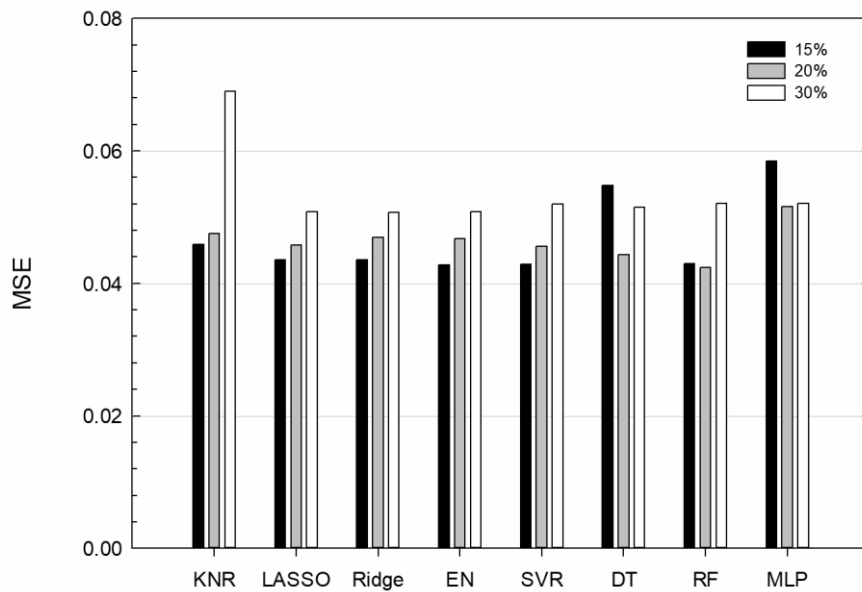
Figure 5-12. MSE comparison of the test set.

From the training set results (Figure 5-11), it is noticeable that the three linear regression models (LASSO, Ridge Regression, and EN) and SVR produced extremely similar results, with better accuracy in the 85-15% split size. In addition, for KNR, linear models, SVR, RF, and MLP a lower size of the training set, implies a larger MSE value. The only exception is DT, which showed the largest MSE when the size of the training set is 80% of the original dataset. From this first comparison, it is possible to conclude that RF has by far the lowest MSE value for every dataset partition.

As far as the test set is concerned (Figure 5-12), the obtained MSE values were similar, being comprised in the range between 0.04 and 0.06 for all algorithms and data sizes. The only exception is KNR when using a 30% test size, which returned an MSE value of about 0.07. For most of the algorithms, the 30% split size produced the largest MSE value. DT and MLP do not follow this trend as the 15% split gave the largest MSE value.

Since RF is the only method that had similar MSE values for both training and test set, it was identified as the most accurate algorithm for this case study. On the contrary, MLP could probably be regarded as the less accurate. This might be explained by the fact that the size of the original dataset (310 samples) is too small to fully exploit its potential.

The R-squared values for the RF algorithm are shown in Figure 5-13. It can be observed that the test set has always a lower R-squared value compared to the training set for each partition of the dataset. The difference between the two is around 30%. This means there are no overfitting issues in this model. Moreover, since the 85-15% subdivision has the largest R-squared and the lowest MSE values, it is safe to say that this is the best split between training and test sets.
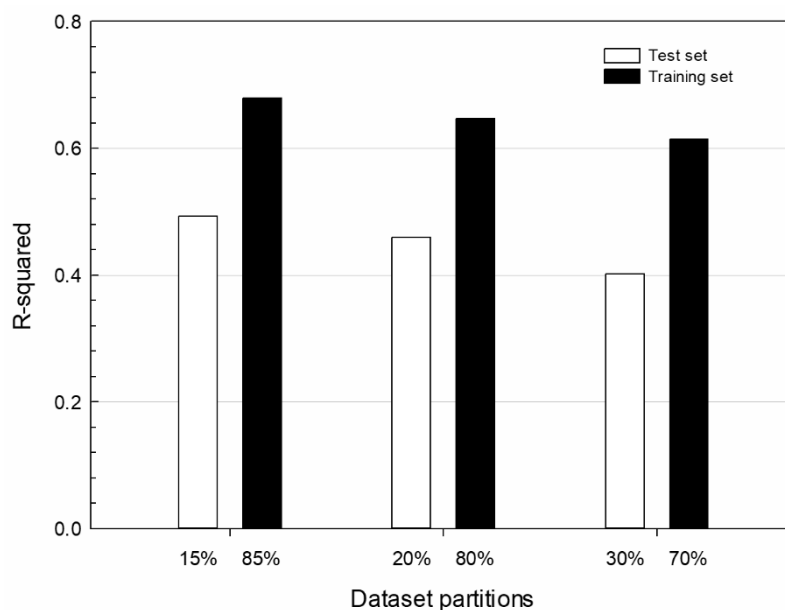
Figure 5-13. R-squared values of RF algorithm.

For the sake of completeness, Table 5-5 reports the numeric evaluation of R-squared and MSE for all algorithms and data sizes.

Table 5-5. Results of the R-squared and MSE evaluation for each algorithm.

Algorithm	Indicator	Training set			Test set		
		85%	80%	70%	15%	20%	30%
KNR	R^2	0.525	0.531	0.427	0.382	0.395	0.453
	MSE	0.058	0058	0.063	0.046	0.048	0.069
LASSO	R^2	0.410	0.412	0.398	0.487	0.417	0.461
	MSE	0.072	0.073	0.075	0.044	0.046	0.051
Elastic Net	R^2	0.408	0.417	0.398	0.497	0.405	0.460
	MSE	0.072	0.073	0.075	0.043	0.047	0.051
Ridge Regression	R^2	0.409	0.417	0.398	0.487	0.403	0.462
	MSE	0.072	0.073	0.075	0.044	0.047	0.051
Decision Trees	R^2	0.445	0.355	0.391	0.475	0.357	0.529
	MSE	0.065	0.082	0.072	0.055	0.044	0.052
Random Forest	R^2	0.679	0.647	0.614	0.493	0.459	0.402
	MSE	0.038	0.044	0.049	0.043	0.042	0.052
SVR	R^2	0.398	0.395	0.384	0.495	0.419	0.448
	MSE	0.073	0.075	0.077	0.043	0.046	0.052
MLP	R^2	0.357	0.394	0.372	0.514	0.518	0.309
	MSE	0074	0.072	0.083	0.059	0.052	0.052

Overall, the main outcomes can be condensed as it follows:

- RF provides the best MSE value on both training and test set and the best R-squared value; the difference between the R-squared value of training and test set show that RF is not subject to overfitting. For these reasons, it was deemed as the most accurate algorithm for estimating debris extension for the given input dataset.
- Linear models and SVR give very similar results in terms of error evaluation, but they are less accurate than RF.
- KNR produces a better fit of dataset than linear models but significantly decreases its precision as the size of the test set increases.
- MLP is the least accurate algorithm for this application, probably because the original dataset does not contain enough samples.

5.6 Results

Debris extension was calculated using the RF algorithm described in the previous section for each of the four benchmark scenarios based on the results of the structural damage analysis. Therefore, for each building it was possible to estimate and visualize its debris footprint. This information is then used to determine whether roads were blocked or available by comparing debris extensions and road widths. It was assumed that whenever there is a debris footprint that covers more than 80% of its width, that road cannot be travelled. This value was set a

compromise between narrow and wide streets of the city to allow the transit of a car or a rescue vehicle.

Figure 5-14 shows the results in terms of blocked roads (in red) and available roads (in grey) in a part of Ideal City downtown after each of the four seismic scenarios. Northridge earthquake caused the largest number of unavailable roads (30.48%) followed by Kobe (21.29%) and El Centro (14.49%), while Hachinohe was the least severe with only 4.47% of blocked streets. Interestingly, it was observed that some clusters of blocked roads formed in some parts of the urban area. Some neighborhoods were more affected than others and some parts were completely isolated because of the collapses and heavily damaged buildings. This highlights the relevance of this analysis to plan in advance efficient evacuation routes and rescue operations. The *average vertex degree* and *global efficiency* were computed for each scenario (Table 5-6). For comparison purposes, they were normalized to the undamaged values. Results are illustrated in Figure 5-15, where it is possible to immediately observe the two parameters decreasing as the intensity of the seismic event increases.

Figure 5-14. Visualization of blocked roads under the (a) El Centro, (b) Kobe, (c) Hachinohe, and (d) Northridge earthquake scenarios.

Table 5-6. Average vertex degree and global efficiency metrics of Ideal City's RTN for the considered scenarios.

Scenario	Average vertex degree	Global efficiency
No damage	2.6404	0.0394
El Centro	2.2576	0.0286
Kobe	2.0780	0.0214
Hachinohe	2.5222	0.0366
Northridge	1.8351	0.0142
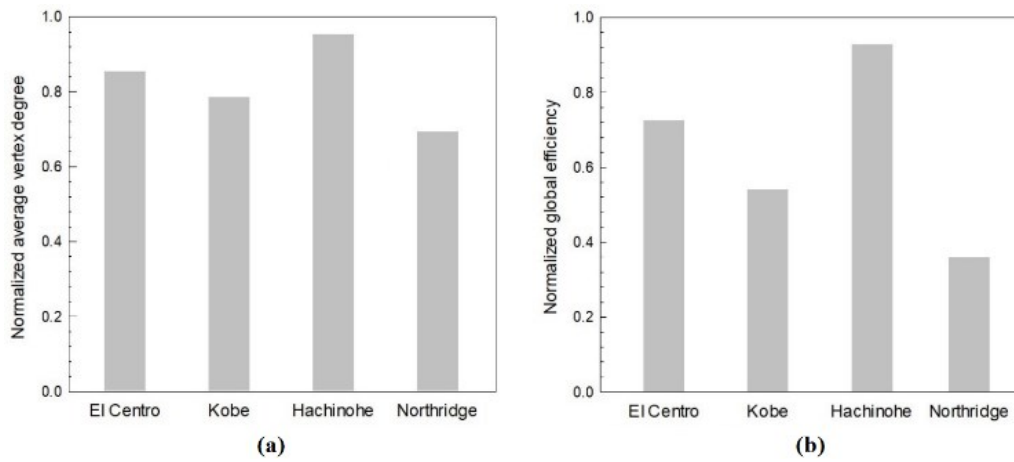
Figure 5-15. Variation of the normalized average vertex degree (a) and normalized global efficiency (b) under different seismic scenarios.

5.7 Conclusions

In this chapter, the modeling and seismic analysis of a road transportation network on an urban scale was discussed. The infrastructure was modeled as an undirected graph consisting of 14,239 nodes and 18,798 edges. Average vertex degree and global efficiency were used to quantify the connectivity and performance of the network. The analysis under a seismic scenario was aimed at determining available roads and roads blocked by debris caused by the collapse of buildings. This type of analysis highlights the interdependence between the building portfolio and the transportation system. High levels of structural damage result in large debris extensions which are likely to make it impossible for vehicles to travel the adjacent roads.

Since debris extension depends on several structural and event parameters that are often not available, ML algorithms were applied to propose a solution based on reconnaissance data collected from previous earthquakes. After a screening process, 310 pictures taken from 25 international seismic reports were analyzed. From each picture debris extension was evaluated through a photo-editing software,

comparing it with other recognizable objects. Seven features were identified to characterize the prediction and eight ML algorithms were tested. The dataset was split into a training and a test set using three different size ratios. A self-tuning process was utilized to define for each algorithm the best input parameters. Finally, the trained algorithms were applied to the test sets and an error evaluation in terms of mean squared error and R-squared values was performed to identify the most accurate algorithm and the best partition size. It was found that the random forest algorithm performed better both in terms of mean squared error and R-squared. Therefore, this algorithm was implemented to estimate the debris extension for each building of Ideal City's virtual environment.

Under each of the four selected seismic scenarios, the debris extension of each building was compared the width of adjacent roads. Consequently, it was possible to determine which roads were blocked and update the topology of the network considering only the available roads. It was found that the percentage of unavailable roads varies greatly as under the Northridge scenario 30.48% of roads were blocked while only 4.47% was blocked after the Hachinohe scenario. It was also observed that even in less disruptive events some neighborhoods were completely isolated due to collapsed and heavily damaged buildings. The average vertex degree and global efficiency metrics were found to be useful to compare the performance of the network after the earthquakes to the undamaged condition.

The proposed procedure is intended to provide critical information for the emergency management phase. It could be used as a predictive tool to identify serviceability of roads in an urban area after an earthquake of a given intensity. Critical areas could be identified, allowing first responders to plan and prioritize their rescue operations. Future work is geared towards improving the accuracy of the debris extension prediction by adding new input data as they are collected in future events. In addition, it would be beneficial to include information about other building archetypes such as wood structures.

Chapter 6

6 Power network

6.1 Introduction

Power networks play a key role in modern communities. Technological advancements have led many other infrastructures and essential services to rely on electricity. Hence, power outages may result in huge economic and social losses. Past seismic events proved the vulnerability of power networks. In the 2011 Christchurch earthquake, both the distribution and the sub-transmission systems failed, leaving almost 80% of the population without electricity (Giovinazzi et al. 2011). The main infrastructure was recovered in five days, but for some areas it took more than a month to restore the service. That event was also analyzed by (Kongar et al. 2017) and compared to the 2009 L'Aquila earthquake (Italy) to highlight functional impacts, resilience characteristics and interdependencies observed during the emergency management and recovery. (Krishnamurthy et al. 2016) took the 2012 Maule and 2011 Tohoku earthquakes to discuss failure mechanisms and restoration processes. Results showed that there was a strong relation between the recovery of power and telecommunication systems in both events. This underlines the importance of considering interdependencies among infrastructures when performing seismic and resilience analyses. Research on past destructive events has brought attention on various aspects that should be taken into account and led to new tools and technologies such as microgrids (Marnay et al. 2015), retrofit strategies (Romero et al. 2015) and decision support systems (Giovinazzi et al. 2017).

In this chapter, the model and the resilience analysis of Ideal City's power network are discussed. Since little information about existing networks was found, a design method was proposed to generate the urban grid. The method allows to specifically design the infrastructure based on the population density and power demand of each neighborhood. In the literature, most of the works focus on the

vulnerability of electric components. (Cavalieri et al. 2014) reported a comprehensive review on fragility functions developed for electric system components. The fragility is generally expressed in terms of peak ground acceleration. The weak point of grids is at the substation level and transformers are the non-structural elements that are expected to fail most frequently (Eidinger 2018). However, the electrical components in a substation can usually withstand the seismic excitation itself. On the contrary, the building where they are located suffer severe damages. The partial or complete collapse of buildings compromise the functionality of the substations. For this reason, in this work the power network's vulnerability was related to the damage which the buildings hosting substations are subject to. Substations located in extensively damaged and collapsed buildings were assumed to fail, resulting in power outages in the buildings that were supplied by them. This approach allowed to intrinsically consider the interdependence with the building portfolio. A new resilience index was introduced and compared to other indexes. The proposed index accounts for important characteristics of resilience such as redundancy and resourcefulness and can be used to compare the performances of different networks, regardless of their scale and number of customers. Moreover, the network was tested under the four benchmark scenarios, highlighting the network damage and the number of customers affected by a power outage.

6.2 Modeling the network

Urban power networks are typically composed of a high voltage transmission system that covers long distances, and a distribution system, which distributes electric power at medium and low voltages. The low voltage line (230 V single-phase, 400 V three-phase in Europe) supplies residential housing and small commercial customers. Usually, at the urban level, power networks run both overhead and underground, following the main streets.

The main challenge to face when modeling an urban power network is data collection. Usually information about number, type and location of electrical components are hold by private stakeholders or local authorities and cannot be shared due to security policies, privacy issues, or conflict of interest. For this reason, two approaches were considered, namely the Similarity Design Method (SDM) and the Density Design Method (DDM).

The SDM is based on the idea that typical power grid schemes can be applied to neighborhoods of the city and adapted according to the specific needs and characteristics of that area. The adaptation process consists in adding or removing some electrical substation and checking the load flow according to the covered area. As reference for typical grid schemes, the technical report issued by the Distribution System Operators Observatory of the Joint Research Centre (JRC) was used (Prettico 2016). They collected data from 79 European Distribution System Operators responsible of the 70% of the electric power supplied by all operators

serving over 100,000 customers. They used this information to define several indicators about the characteristics of a network, which helped to build typical power grids. The so called "urban" network from the JRC database can be used for densely populated areas, while the "semi-urban" can be used for less populated areas. These models give information about high voltage (HV), medium voltage (MV) and low voltage (LV) buses such as position, electric parameters, protection devices, etc. LV data is actually used only to determine the number of customers. If the number of customers is known or van be estimated from the number of buildings, the position of LV buses is not relevant. Thus, the network topology can be described just by the position of HV and MV substations. The position depends on the number of buildings and customers. Typically, it is assumed they are barycentric with respect to a cluster of buildings. The number of HV and MV substations is defined through an iterative process. Once a compatible grid scheme has been selected, a tentative number of substations is chosen (slightly modifying the original scheme to fit the case study). Then a load flow analysis is performed. This can be done, for example, using Matpower 6.0, a MATLAB tool (MATLAB 2018) developed by the Power Systems Engineering Research Centre at Cornell University (Zimmerman 2011). This tool uses the Newton-Raphson algorithm to solve the nonlinear problem of computing the load flow on the entire grid. At each iteration, modifying the number of substations, the tolerance should decrease, and the algorithm converge. When the tolerance is lower than a prefixed threshold and the algorithm converges in few steps, the network is properly designed.

In the DDM the network is designed according to the actual population density and power demand. Unlike typical grid schemes, which are quite rigid, this method allows for a specific design of the system while being timesaving. The load flow analysis required by the SDM might demand a prolonged running time to complete. Three design aspects are considered in the DDM: (i) population density and number of customers, (ii) power load density, (iii) engineering constraints (e.g., length of the distribution lines, load types, redundancy of the components, etc.). The first step consists in dividing the urban area into neighborhoods to locate primary substations. Electric loads can be defined following guidelines such as the procedure described by the European technical report (Prettico 2016). Then distribution substations that supply clusters of buildings can be located. Primary and distribution substations are evenly located according to number and position of the buildings. The main criterion is to try to minimize the length of the distribution lines by placing the substation in a central position with respect to the buildings they supply.

The SDM and the DDM are not mutually exclusive, meaning that they can be used to complement each other depending on the available information. For instance, existing schemes might suit some neighborhoods almost perfectly while others might need a peculiar design.

6.3 Application of the design method

Ideal City's power network was modeled using the DDM. Since information regarding the building portfolio and population was complete and already known, this method allowed to build a more detailed model, without relying on predefined schemes. First, the 10 administrative neighborhoods in which the city of Turin is divided (Geoportale 2018) were considered as shown in (Figure 6-1). This allows to better adapt the network to the characteristics of each area. The software used to build the power grid was QGIS (QGIS 2019) as it allows to draw the network as a georeferenced graph and store data about each component in a structured database.
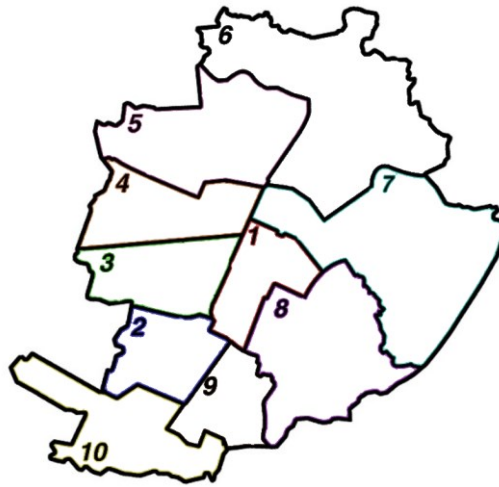
Figure 6-1. Map of Ideal City neighborhoods.

According to the guidelines provided in (Prettico 2016), the design load density is equal to 8 MVA/km^2 for each neighborhood. This input data is necessary to establish the size of each substation. Each neighborhood has one or two HV primary substations, depending on its number of customers. MV distribution substations are then positioned in the area considering the estimated power demand. As a result, each substation supplies a different number of buildings. Three types of transformers were considered in this study, based on their nominal power: 0.40 MVA, 0.63 MVA, and 1.00 MVA. The chosen proportions for each category were 60%, 30%, and 10%, respectively, accordingly to current best design practices. Each type of transformer defines a different type of distribution substation, influencing its supply capacity.

As an example, the application of the Density Design Method to neighborhood 1 is herein described. Design input parameters are listed in Table 6-1. Table 6-2 reports the outputs of the analysis. Figure 6-2 illustrates the position of HV primary and MV distribution substations in neighborhood 1.

Table 6-1. Input parameters for neighborhood no. 1.

Input parameters	Values
Area	6.88 km^2
Population density	11,650 inhabitants/km^2
Population	80,152
Design load	8 MVA/km^2
Estimated MVA	55
Estimated number of substations	104

Table 6-2. Design output data for neighborhood no. 1.

Output parameters	Values
Number of substations	108
Number of 0.4 MVA substations	65
Number of 0.63 MVA substations	33
Number of 1 MVA substations	10

Figure 6-2. Primary and distribution substations of neighborhood no. 1.

Repeating this procedure for all the neighborhoods, it was possible to model the entire network. Overall, Ideal City's PG consists of 15 primary substations and 1,274 distribution substations. Table 6-3 summarizes the number of distribution substations for each power category. Figure 6-3 depicts the final map of the power distribution network of Ideal City.

Table 6-3. Ideal City's distribution substations.

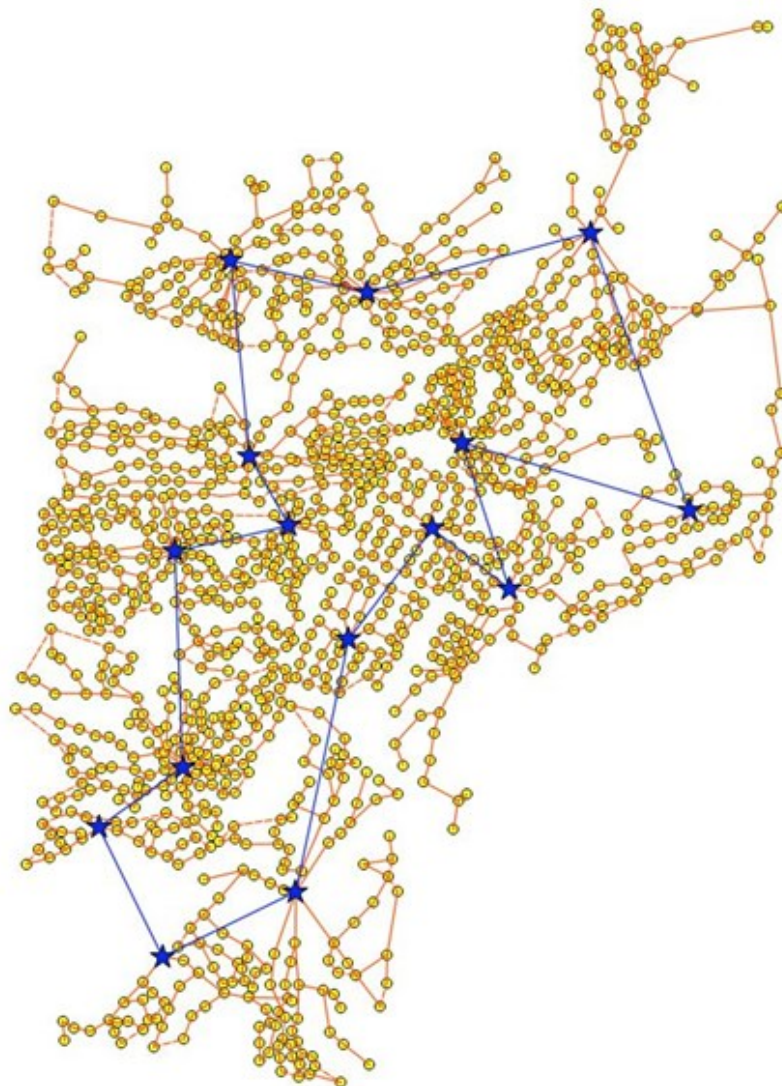| Distribution substation type	Values
Number of 0.4 MVA	766
Number of 0.63 MVA	382
Number of 1 MVA	126
Total	1,274

Figure 6-3. Power grid of Ideal City.

A comparison between the designed network and some real data obtained from one of the Turin's electricity suppliers has been performed. Table 6-4 reports the results of the comparison. The MV/LV data have been provided by the Turin Electric Company (IRETI 2016). It can be seen that real data and the results of the Density Design Method are similar, which validates the effectiveness of the procedure. It is however worth noting that the generated network may be notably different compared to the real one in terms of substations' location.

Table 6-4. Comparison between real data and simulation outputs.

Substation type	Real data	Simulation
Number of HV substations	9	10
Number of MV residential substations	1,190	1,274

6.4 Vulnerability and interdependency with the building portfolio

In the literature there have been many attempts at assessing the seismic damage suffered by the power infrastructure (Cavalieri et al. 2014). However, those methodologies require a lot of data regarding network components, which is usually confidential and kept private by stakeholders and public authorities. Furthermore, most of them refer to the inherent fragility of electrical components to assess the resilience the network. While this might seem appropriate, in several past events, electrical components were able to withstand strong ground motions, while the buildings where they are installed suffered severe damages. The debris caused by partial or complete collapses is responsible for damages to electrical components, which compromises the serviceability of the network A situation where hosting buildings withstand the earthquake while the components of electrical substations fail, is unlikely to happen. In most cases, electrical components fail because the buildings where they are installed collapse over them. Plenty of examples can be found in picture taken in the reconnaissance phase. For instance, Figure 6-4 shows a medium-to-low voltage substation that would have remained functional if it had not been hit by the debris of the partially collapsed hosting building due to the 2016 Central Italy earthquake.

Figure 6-4. MV/LV substation damaged after the 2016 Central Italy earthquake (Rieti, Italy).

The weak element of electric power systems is at the distribution substation level and transformers are expected to be the non-structural elements to fail most frequently, as discussed in (Fujisaki et al. 2014). Failure depends on different constructive factors, which are mainly related to the voltage level: the higher the substation voltage, the higher its vulnerability. Moreover, the fragility of substations depends on the presence and type of anchorages of their components. International codes and guidelines suggest different types of solutions to properly anchor electrical components to limit damages. Most of these solutions were proposed after notorious events, such as the 2014 South Napa and La Habra earthquakes, which led to significant improvements in power grids' performances (Eidinger 2018).

Cavalieri et al. reported a complete overview of the main recent works on fragility functions of electric power system components, with the indication of the methodology used to evaluate the curves, the components considered and the damage states and indices (Cavalieri et al. 2014). The fragility of main power grid components towards earthquakes is generally expressed in terms of peak ground acceleration (PGA). Considering the HAZUS methodology (FEMA 2003), fragility functions are presented for different damage states (e.g., slight, moderate, extensive, complete). To have extensive level of damage (substation operational after repairs), the median PGA should reach 0.34g for low voltage substations with unanchored components and 0.45g in case of anchored components. Using a wider approach, Dueñas-Osorio et al. presented fragility functions of the entire power network (Dueñas-Osorio et al. 2007). A median value of 0.45g was again found to generate extensive damage to low voltage substations. Such values of PGAs are certainly likely to cause severe damage to the buildings given the characteristics of the typical built environment of European cities.

Assuming that the vulnerability of the power network is related to the damage reported by the buildings where substations are located, it is possible to implicitly

account for the interdependency between the power network and the building portfolio. If the building where a substation is installed collapses or is extensively damaged, the electrical components are no longer capable of supplying power. Consequently, the electric load drops to zero, and all the buildings that were supplied by that substation are left without electricity. Moreover, since distribution substations are connected in a tree structure, if a substation fails then all the downstream substations will also fail. The 15 primary substations are supposed to maintain their functional state even after strong ground motions since they are typically located in robust technical facilities. Once all the failed substations are identified, the number of buildings and users not supplied after each seismic scenario can be determined.

As far as distribution lines are concerned, their fragility was not taken into account because on a city scale they are more robust than distribution substations. As previously mentioned, distribution systems can run both overhead and underground, despite in modern cities underground systems are prevalent as they are safer and more efficient. In the virtual city model, it was not distinguished between overhead and underground lines, although many distribution lines are meant to be underground as they follow the roads. However, in both cases substations are more vulnerable to earthquakes. Commonly, underground lines failure happens only in case of strong ground motions that cause significant ground deformations, and most likely serious building damage. Instead, overhead distribution lines are mainly vulnerable to strong winds, while their vulnerability to seismic events is limited due to the slenderness and small size of urban utility poles.

6.5 Resilience indexes

Methods to evaluate the resilience of power networks have been discussed also at the political level. For instance, the Italian Regulatory Authority for Power, Gas, Water and Wastes suggested to relate resilience to the risk of having customers without electricity in case of extreme natural events and weather conditions [24]. The risk index that was proposed is the *IRI*, which is calculated as shown in Equation (6-1):

$$IRI = NUD \cdot PD \tag{6-1}$$

where *NUD* is the number of users with no power and *PD* is the probability of disservice. *PD* is calculated as the inverse of the return period of the event T_R, which is obtained from the European standard CEI EN 50341 [25].

The resilience index derived from the *IRI* is the energy not supplied (*ENS*) as shown in Equation (6-2):

$$ENS = NUD \cdot P_{N,U} \cdot t_U \tag{6-2}$$

where $P_{N,U}$ is the nominal power, expressed in kW, to satisfy the demand of each customer, and t_U is the duration of the power interruption. This index includes a time component, giving an immediate representation of the earthquake effects on the network.

These indices focus mainly on the failure aspect, without taking into account the essential characteristics of resilience, which are: (i) rapidity, the system capability to quickly react and achieve results to limit the human and economic losses; (ii) robustness, the ability of elements, systems or other units to withstand a certain level of stress without suffering degradation or loss of functionality; (iii) redundancy, the possibility for a system to be fed through alternative paths, while the usual ones are under restoration; (iv) resourcefulness, the system managers capability to identify weaknesses and mobilize resources to reduce the effects of a likely damage (Cimellaro 2010).

To include these aspects, the Power Resilience Index (*PRI*) was introduced (Equation (6-3)):

$$PRI = \int_{t_1}^{t_2} T_{rr} \cdot n_{nodam} \cdot \gamma_{path} \cdot PG \cdot dt \qquad (6-3)$$

where:
- T_{rr} is the Transformer Restoration Rapidity that can be equal to 1 when there are only 0.4 MVA transformers; 0.67 for 0.4 and 0.63 MVA transformers; 0.57 when there are 0.4, 0.63 and 1 MVA transformers. Those values were taken from the transformer restoration guidelines provided by FEMA (FEMA 2016). The different types of transformers that form the network influence the rapidity of the restoration process. For example, a network with only 0.4 MVA transformers would have a faster restoration phase. The higher T_{rr}, the higher the *PRI*, and the more resilient the network.
- n_{nodam} is the percentage ratio between the number of undamaged substations that remain functional after the event and the total number of substations. It represents the robustness of the network.
- γ_{path} is related to the presence of additional power lines that can be used from adjacent neighborhoods. This parameter ranges between 0 and 1, where 0 means there are no alternative lines and 1 indicates complete connection among neighborhoods. The value assumed by γ_{path} refers to independent paths available for a node. If a node can be supplied by two independent paths, and one of them fails, then γ_{path} is equal to 0.5. If it can be supplied by three lines, and one of the paths fails, γ_{path} would be 2/3, and so on.
- *PG* depends on the availability of temporary backup systems to be used in the first hours of the emergency. This parameter ranges between 0, meaning no backup systems are available, and 1, when every area can be promptly supplied with temporary solutions. The estimate of *PG* can be done based on the

experience gained by the Distribution System Operator (DSO) from past events. For instance, if the DSO can always guarantee to provide a mobile backup station in about 30 minutes, *PG* can be assumed equal to 1. As the expected time to have backup systems in place increases, *PG* decreases linearly (e.g., for an estimated 1h intervention time, *PG* would be 0.5).

- t_1 and t_2 define the start and end time of the analysis. *PRI* is not a static measure of resilience, but it evolves as the described parameters change over time.

Equation (6-3) was inspired by the definition of resilience given in (Cimellaro 2010). The novelty of the *PRI* is to include dimensionless coefficients describing the redundancy (γ_{path}) and resourcefulness (*PG*) aspects of power networks.

6.6 Case study

The presented resilience indexes were tested on Ideal City's power network under a seismic scenario. For this application, the 6.5 M_w Central Italy earthquake that occurred on October 30, 2016 was simulated. The epicenter and the ground motion model are the same as those used for the definition of the other four scenarios.

Once the structural damage was estimated and the buildings in "complete" and "extensive" damage states detected, the failed substations could be identified. Overall, 240 over 1,274 substations failed after the applied scenario (Figure 6-5). Consequently, it was estimated that 4,815 buildings, corresponding to the 20.6% of the total, were no longer supplied.
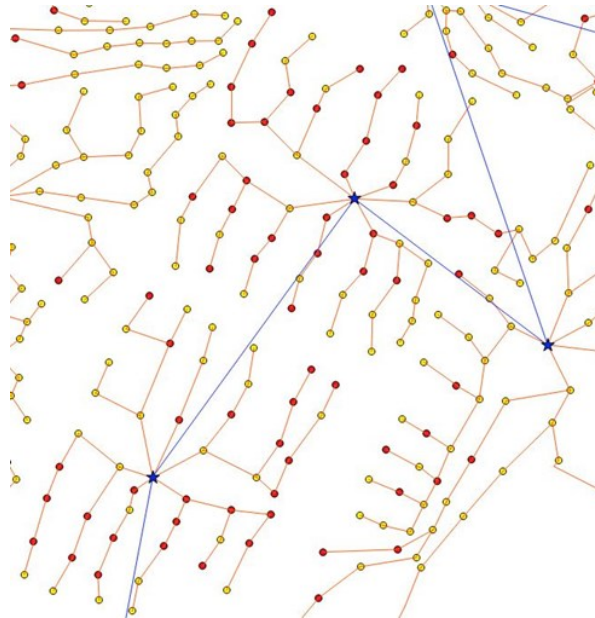

Figure 6-5. Damaged substations (in red) in neighborhood no. 1 after the earthquake simulation.

The recovery time was determined based on the transformers' recovery time indicated by (FEMA 2016), and a linear recovery function was assumed. Under these conditions, the *IRI* was calculated using a return period (T_R) of 50 years. Figure 6-6 shows the variation of the *IRI* over 10 days. The initial condition, meaning complete functionality, corresponds to *IRI*=0. The event is supposed to take place on day 1. On day 2 repair interventions can start. From the *IRI* curve it is possible to notice the long time needed to restore all the substations. Six days after the event, almost 50% of the damaged network was back on working. However, the *IRI* does not give an idea of the actual dimension of the loss of power.
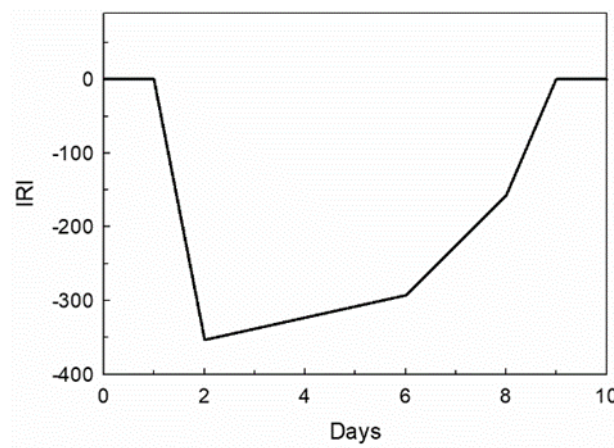
Figure 6-6. Risk Index (*IRI*).

After the *IRI* the *ENS* was calculated (Figure 6-7). Results show that the power loss was relatively limited. This means that the network had a good robustness toward this particular event. Nonetheless, the overall performance could be improved by increasing redundancy and resourcefulness. As previously discussed, *IRI* and *ENS* do not consider such resilience components, and they are not capable of representing the initial resilience of the network. On the contrary, the resilience assessment with the proposed *PRI* (Figure 6-8) highlighted, at the initial condition, the overall resilience. This was found to be around 0.6 which is quite far from the optimal condition of *PRI*=1. In this case study, T_{rr} was equal to 0.57 since all three classes of transformers are used, γ_{path} and *PG* were both assumed equal to 1, given the connectivity between neighborhoods and a fast response from the DSO. The small drop immediately after the seismic event indicates a good resilience performance of the network. The repair phase could be shortened intervening on the rapidity of the restoration (T_{rr}) by improving preparedness and operators' training.
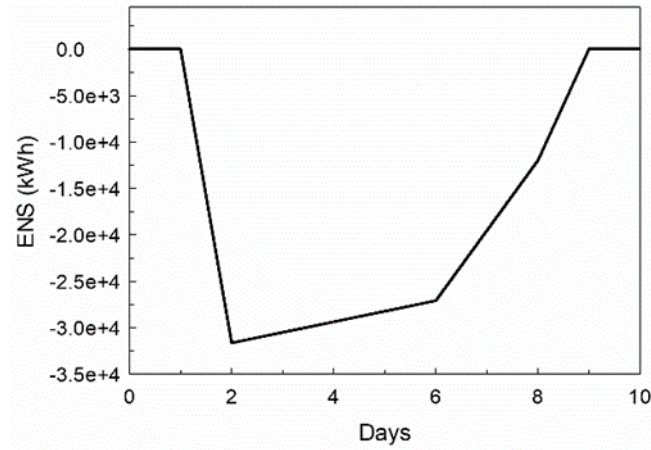
Figure 6-7. Energy Not Supplied (*ENS*).
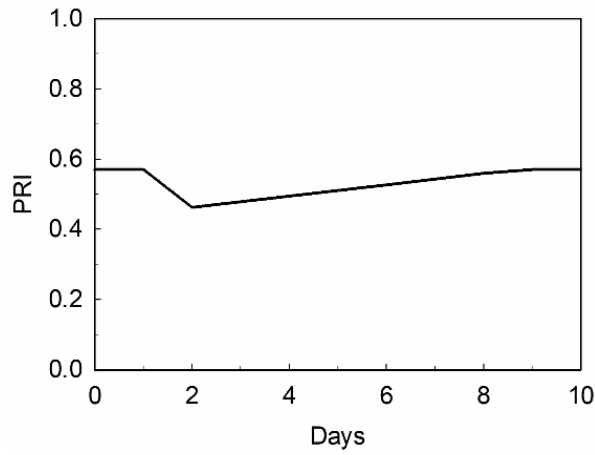
Figure 6-8. Proposed Power Resilience Index (*PRI*).

6.7 Results

Once the physical damage to the buildings was assessed for the four seismic scenarios used as benchmark, the damage to the power network could be evaluated. Whenever a distribution substation is located in a building that suffered extensive damage or collapsed, the substation fails. In addition, any other downstream substation of the tree structure fails because it is no longer supplied with power. The failed distribution substations for the four seismic events are shown in Figure 6-9.
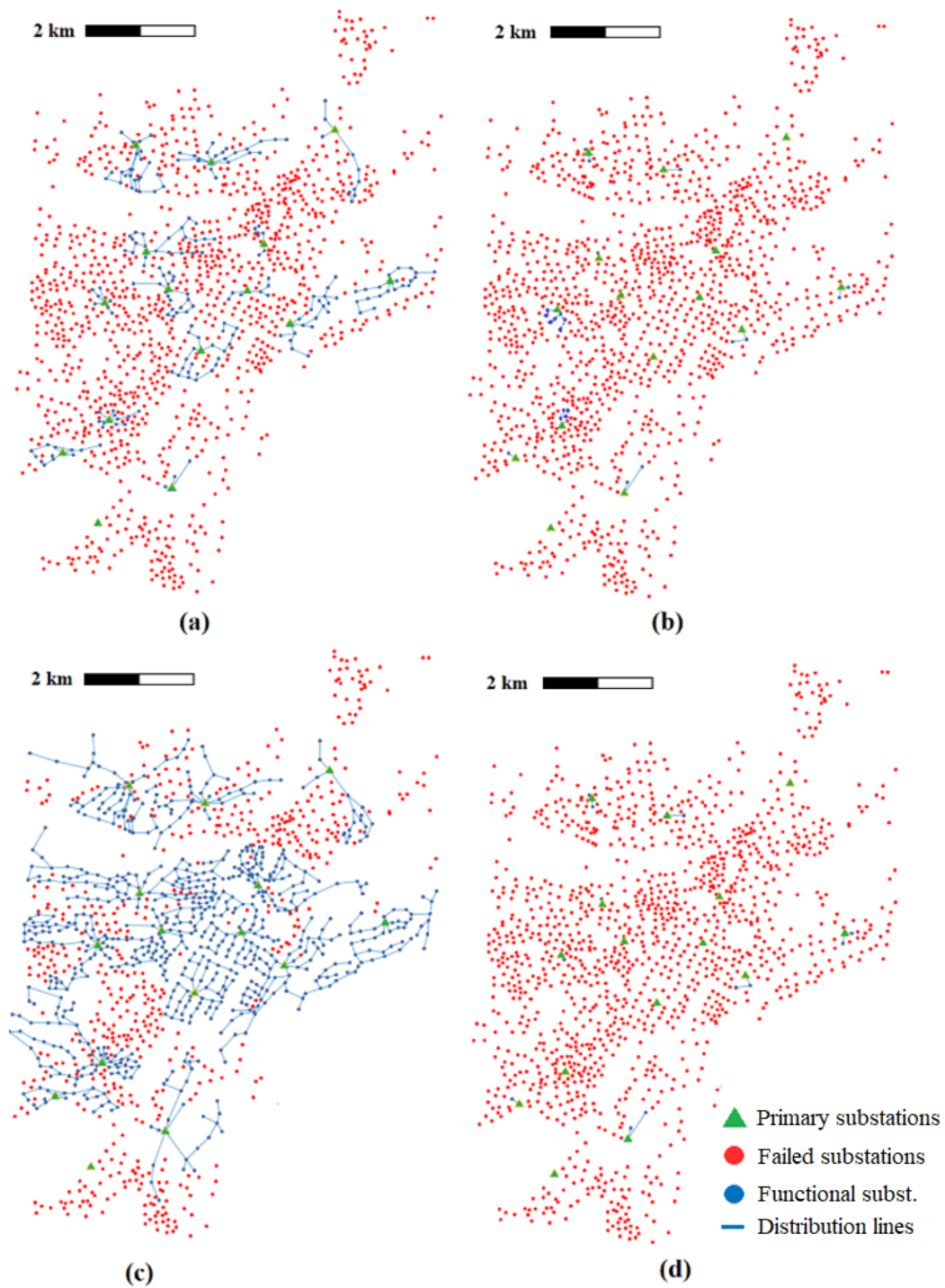
Figure 6-9. Failed substations under (a) El Centro, (b) Kobe, (c) Hachinohe, and (d) Northridge earthquake scenarios.

The substations that remain functional after Northridge are 12, after Kobe are 25, while for El Centro are 220, and for Hachinohe are 747 out of a total of 1274 substations (Table 6-5). For this particular case study, results indicate that the near-field earthquakes (i.e., Northridge and Kobe) are more disruptive than the far-field ones.

Table 6-5. Failed substations under the four benchmark scenarios.

Seismic scenario	Failed substations	Percentage of failed substations
El Centro	1,054	83%
Kobe	1,249	98%
Hachinohe	747	41%
Northridge	1,262	99%

From the information of failed substations, it was possible to individuate the buildings, hence the customers, that are no longer supplied with electricity after each event. Figure 6-10 shows the impact of the network's disruption in one part of Ideal City. Buildings in red are those without power, whereas blue indicates buildings that are still supplied. As far as the number of customers is concerned, 98.5% of the population does not have access to power after Northridge and Kobe scenarios, while after the El Centro earthquake the percentage decreases to about 80%. On the other hand, Hachinohe is the less disruptive, causing a power outage for about 40% of the customers. The ratio between the number of users who are still supplied with electricity and the total population of Ideal City could be used as a straightforward resilience index. Table 6-6 reports the values of this resilience index ($R_{SUPPLIED}$) for the four scenarios.

Table 6-6. $R_{SUPPLIED}$ for the considered scenarios.

Seismic scenario	$R_{SUPPLIED}$
Northridge	0.015
El Centro	0.206
Kobe	0.015
Hachinohe	0.604
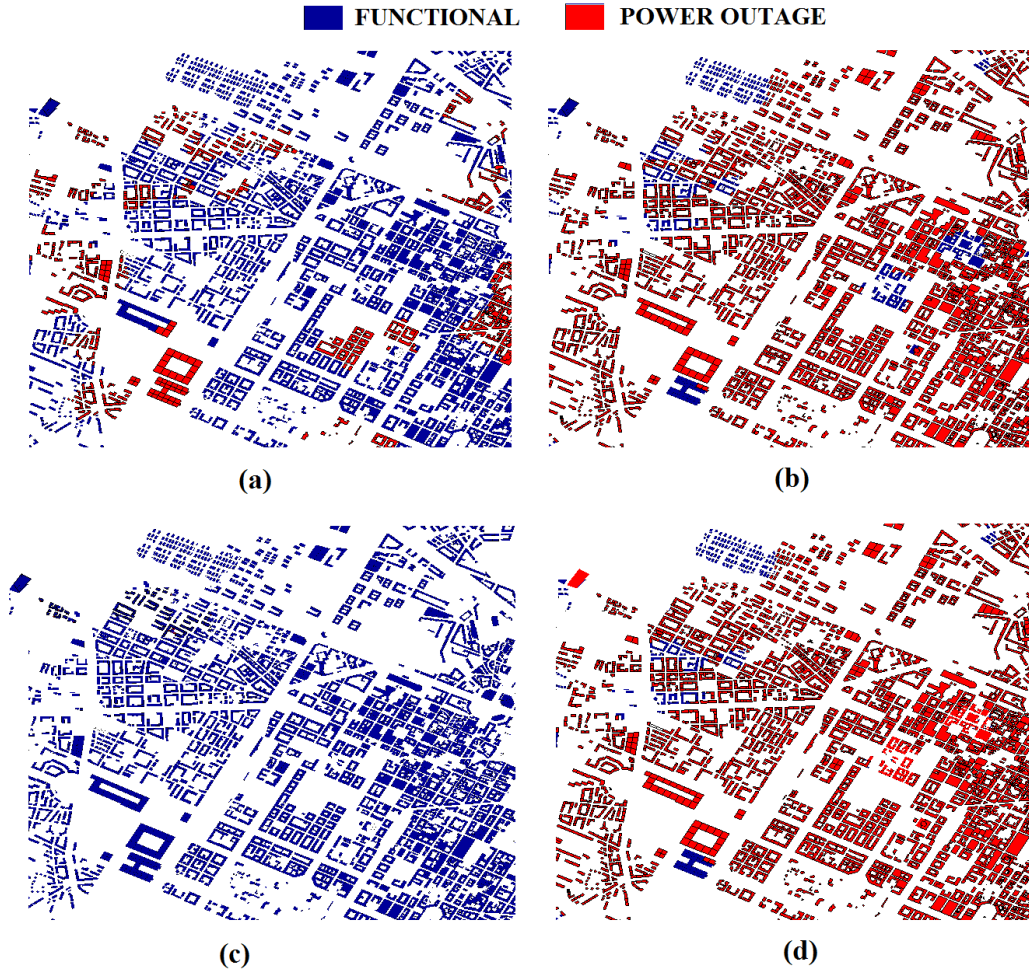
Figure 6-10. Visualization of the buildings with and without power under (a) El Centro, (b) Kobe, (c) Hachinohe, and (d) Northridge earthquake scenarios.

6.8 Conclusions

The model and resilience analysis of Ideal City's power network were presented in this chapter. The proposed Density Design Method allowed to model a network specific to the characteristic of the urban area, based on the actual population density and demand of each neighborhood instead of using predefined typical grid schemes. The obtained network consists of 15 primary substations and 1,274 distribution substations connected in a tree-like structure. The seismic vulnerability of substations was set to be dependent on the building damage state. Therefore, after a given earthquake, failed substations are those located inside extensively damaged or collapsed buildings. This approach allows to directly model the interdependency between the infrastructure and the building portfolio.

A new resilience index (*PRI*) was proposed and compared to the *IRI* and *ENS* indexes. Results showed how the *ENS* expresses economic losses in terms of power loss, while the *IRI* focuses on the impact on the customers. On the other hand, the *PRI* considers all important aspects of resilience, including redundancy and

resourcefulness. It highlighted the importance of timely and effective repair interventions to avoid downtime economical losses. In addition, the *PRI* estimates the initial resilience level, which depends on the type of electrical components. Future work is aimed at introducing temporary backup systems in the model and quantifying economic losses.

The power network was tested under the four benchmark seismic scenarios. It was found that the impact was catastrophic. Even the least severe event caused more than 40% of substations to fail. This outcome underlines the importance of having the key components of the infrastructure located inside robust buildings. Moreover, the tree-like structure of the network amplified the damage as once a substation fails, all the downstream substation of that branch are disconnected. Secondary and redundant connections among substations would improve the robustness of the network. Finally, a straightforward resilience index was introduced to discuss the results in terms of percentage of population still supplied with power.

Chapter 7

7 Telecommunication network

7.1 Introduction

Over the past few decades, telecommunication networks have become one of the most important lifelines. The demand for new infrastructure has been increasing thanks to the digitalization and global expansion of the markets. The purpose of a telecommunication network is to allow the exchange of information between two end users located in geographically distinct positions. This is achieved through the conversion of information into a signal and the subsequent transport of this signal from one user to another using the network resources. They have a key role in everyday life, not only because they allow to stay in contact with people in a simple and immediate way, but also to get information quickly, operate businesses, manage first responders during emergencies. After a natural or manmade disaster, having a functioning communication network is essential for maintaining the coordination of rescue activities efficient. Therefore, it is essential that densely populated urban areas are provided with a resilient network that can be back in operation in a short time even after catastrophic events.

There are different types of communication networks. The main categories are landline, wireless, and satellite networks. These are connected to each other via cables or wireless. Several components are involved in the transmission of a signal (e.g., technical buildings, steel tower, antennas, fiber optic cables, etc.), which are designed for routing, switching, transmitting and receiving voice calls, texts, images, sounds or data of any kind (Adachi and Obata 1990).

A landline telephone network is a telecommunications network that connects telephones through cables that are wired into a telephone exchange switch. This is the oldest telecommunication system. The Public Switched Telephone Network is the largest existing telephone network, which connects a number of circuit-switched telephone networks worldwide.

Wireless networks represent the natural evolution of traditional landlines, where mobile devices can communicate with a ground-based infrastructure through radio waves, guaranteeing signal coverage for large areas even while the user is moving. Thanks to technology advancements and new communication protocols, wireless networks nave become the primary lifelines in sensitive operations related to economics, safety, and emergency management. The main components of wireless telecommunication networks are:

- Mobile switching center (MSC): a robust telecommunication facility managing a large area at a regional/state level. It is mainly used to enable the communication between the wireless and the telephone and internet networks.
- Base station controller (BSC): a technical building managing the communication on an urban scale.
- Base transceiver station (BTS): the last element of the physical infrastructure. Typically, it consists of a steel structure where antennas are mounted, and a series of electronic devices hosted in a structure at the base.
- User equipment (UE): mobile devices with wireless connectivity.

BTSs and towers supporting antennas are the most vulnerable elements in case of disasters. The purpose of towers is to rise the antennas to an elevation adequate enough to avoid obstacles in the transmission of the signal. Towers can be standalone elements, such as posts, lattice structures, and masts, or located on top of other structures, such as buildings, bridges, streetlights, water towers, etc. Cables connect the antennas mounted on towers to base station equipment, which is located in special outdoor shelters at ground level or in some indoor technical compartment.

The design and seismic performance of telecommunication infrastructure have improved after the investigation of the effects of past earthquakes. Few decades ago, the Federal Emergency Management Agency (FEMA) started reporting guidelines on the measures to be taken to build seismic resistant power and telecommunication facilities (Yokel 1990). These measures were improved and in the HAZUS methodology, where FEMA proposed fragility curves to assess the seismic vulnerability of telecommunication buildings for different damage states (FEMA 2003). On the other hand, many researchers studied risk mitigation strategies and methods to improve seismic resilience. (Dikbiyik et al. 2012) developed a probabilistic risk model for optical networks to analyze loss in terms of penalty paid by the provider to the customers. Their model allows to consider the probability of damage, disaster probability, and the number of possible events. Based on the results they also proposed a mathematical model that reduces the risk and loss in case of a disaster. Looking at the events of the 2011 Great East Japan earthquake, (Nemoto and Hamaguchi 2014) discussed strategies to improve the robustness of wireless networks after a disaster. These include prompt recovery operation using mobile equipment, an information distribution platform to collect data and facilitate decision-making, a rapidly deployable mesh network that bridges

communication through satellites and unmanned aerial vehicles. A mesh network system was also proposed by (Owada et al. 2018) as an alternative to the conventional tree topology. Tree-like architectures are popular because cost-effective but weak against disaster because in case of link or node failure, all downstream nodes would be disconnected. The mesh network enhances connectivity through a platform of distributed servers that are not dependent on an Internet connection. (Gomes et al. 2016) provided an overview of approaches to improve robustness and resilience of communication systems against natural disasters. Several methods can be applied to intervene on existing networks and to enhance post-disaster recovery. Nevertheless, they pointed out that the number of failures is still relatively high compared to other critical infrastructures, mainly because of poor design choices. This becomes evident after severe seismic scenarios. For instance, (Giovinazzi et al. 2017) described the impacts of the 2016 Kaikoura earthquake in New Zealand highlighting how physical damage to several components of the network caused a loss of service in large areas for several days.

In this chapter, the model and resilience analysis of the urban telecommunication network of Ideal City are presented. Three infrastructures, managed by as many providers, were characterized through a crowdsourced database and satellite imagery inspection. To define the connectivity among the base station controllers (BSCs) a three-layer topology was used, while base station transceivers (BTSs) were connected to BSCs according to a star scheme. The performance of the network was evaluated through the signal-to-interference-plus-noise-ratio (SINR). The population was divided into clusters distributed according to the location and characteristics of the buildings. For each user cluster the SINR was calculated and then converted into a throughput value using different modulation coding schemes (MCSs). The largest throughput obtained was deemed to determine to which BTS each cluster connects to.

Given the limited information available and the number of hypotheses that would be required to perform a thorough damage simulation, the vulnerability of the network was associated with the collapse of the buildings on top of which telecommunication towers are mounted. Three indexes were proposed to evaluate the vulnerability and performance of the networks. The first is based on the physical damage to the towers, the second on the quality of service in terms of throughput, and the last one is aimed at highlighting overloads considering the average number of users that would possibly connect to a BTS. The networks were tested under the four benchmark scenarios and the performance metrics for resilience discussed. As a measure to improve resilience it was proposed that in the post-disaster phase the three providers would share their resources to create one large infrastructure.

7.2 Ideal City's wireless network model

7.2.1 Data collection

Telecommunication networks are mostly privately own by providers. Typically, each provider has its own infrastructure, although smaller providers rely on others' infrastructure under specific economic contracts. However, it is common that the structures where telecommunication components are installed are shared. For instance, the same tower can be used to mount the antennas of different providers. Since they are privately owned, information about telecommunication infrastructures is hardly shared. To model Ideal City's network a hybrid approach was followed. When possible, existing data was used, whereas missing information was supposed based on design procedures and best practices from reliable sources. One of the most useful sources was the web site CellMapper which is crowdsourced and provides cellular tower and coverage mapping information (CellMapper 2021). The same approach has been used by many researchers. For example, (Malandrino et al. 2017) used crowdsourced cellular network traces to characterize the LTE network of San Francisco, California. First, the available data for the city of Turin was consulted. From there it was possible to collect information about antennas such as geographic coordinates, frequency bands, bandwidth, etc. The three largest providers in Italy were considered. For the purpose of this application, they are referenced to as P1, P2, and P3. Following the available data at national level, the customers of each providers are 35.4%, 32.9%, 31.7% of the total population, respectively. Thus, three different networks were modeled and analyzed. The so obtained information was verified and completed using the GIS tool offered by the municipality of Turin (Geoportale 2021) and satellite imagery provided by Google Maps (Google 2021).

Visual investigation through satellite imagery was particularly useful to find out geometric parameters of the telecommunication towers supporting antennas. It was indeed possible to identify the type of structure, section, and estimate the height. Since no information about the materials of those structures could be found, the design codes and reports were utilized to define the mechanical characteristics of the materials and common connection schemes (EN1993-3-1 2006). Visual investigation was also fundamental to identify BSCs. It was observed that some of the previously localized BTSs were located on top or in close proximity to telecommunication buildings. It was then assumed those buildings were BSCs. Overall, it was possible to locate 18 BSCs, which is a reasonable figure since each BSC usually manages between 10 and 20 BTSs (Giovinazzi et al. 2017). It was also assumed these facilities are shared among the three considered providers. Thus, each of the three networks has 18 BSCs in the same locations. On the other hand, the number of BTSs slightly varies among the providers. Some of these also share the same location given that on the same tower there are antennas from different providers or multiple antennas of the same provider working at different frequencies. The MSC was not included in the network as they operate at the

regional level. In addition, MSCs are robust facilities that are designed to withstand strong ground motions to guarantee functionality even after catastrophic events.

The collected information was organized in a database where each row identifies an antenna characterized by the following features:

- Coordinates: the geographical coordinates were converted into geometrical ones to fit in the virtual environment. Rooftop towers were assigned with the coordinates of the center of gravity of the buildings in order to have an exact correspondence between antennas and buildings.
- Band: the radio bands assigned to the providers were 3 and 20.
- Frequency: the frequencies corresponding to bands 3 and 20 are 800MHz and 1,800MHz, respectively.
- Type of antenna: omni-directional and tri-directional antennas were identified.
- Type of cell served: based on the frequency antennas can serve macro or micro cells.
- Tower type: this parameter discerns between raw land and rooftop towers.
- Tower structure: the identified structures were posts and masts.
- Tower section: posts were found to have polygonal-circular pipe sections, while masts are made of L-shaped profiles connected to form lattice structures.
- Tower height: this estimated through satellite imagery. For rooftop towers the estimated measure was added to the height of the buildings contained in the building database.
- Tower material: all towers are made of steel; S235 was associated with posts while S275 with masts.

Figure 7-1 illustrates the location of BSCs and BTSs for the three providers, while Table 7-1 reports some characteristics of the database. The number of BTSs indicates all antennas serving macro and micro cells. The number of towers is lower because in some cases multiple antennas are mounted on the same tower.
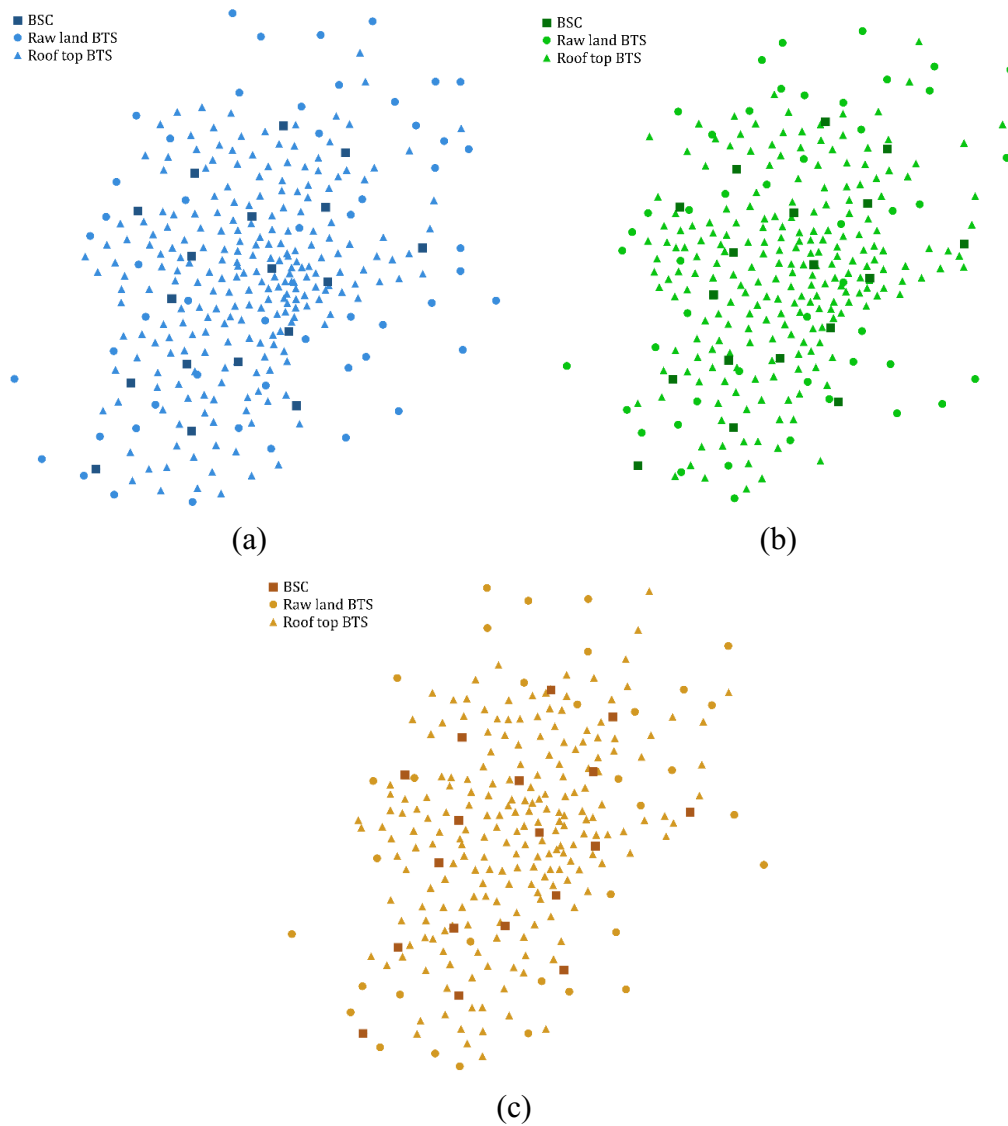
Figure 7-1. BSC and BTS locations for (a) P1, (b) P2, (c) P3.

Table 7-1. Characteristics of the networks.

	P1	**P2**	**P3**
No. of BTS	387	359	359
No. of Towers	304	286	260
No. of Raw land towers	57	53	38
No. of Rooftop towers	247	233	222
No. of Raw land macro cells	33	25	22
No. of Raw land micro cells	50	46	37
No. of Rooftop macro cells	70	83	95
No. of Rooftop micro cells	234	205	205
Raw land towers height	25 – 45m	25 – 45m	25 – 45m
Rooftop towers height	2.5 – 7m	2.5 – 7m	2.5 – 7m

No. of Raw land posts	35	33	21
No. of Raw land masts	22	20	17
No. of Rooftop posts	186	170	157
No. of Rooftop masts	61	63	65

7.2.2 Network topology

The network was modeled using the principles of graph theory, especially to define its topology. MSCs, BSCs, BTSs, UE are all nodes of the telecommunication graph. In wireless networks, the edges do not always represent physical connections. Some of them are just logical but equally important to define data transmission. Examples of physical connection are coaxial cables, which are the old standard cables consisting of shielded copper or aluminium wires, ribbon cables, which have many conducting wires running parallel to each other, and optical fiber cables, which are the new standard since they offer many advantages such as transmission over long distances at high bandwidths with minimal signal loss and no electromagnetic interference issues. Physical links do exist between MSCs, BSCs and in most BSC to BTS connections. On the other hand, UE connects to BTSs wirelessly. Standard wireless technologies are radio waves and microwaves.

The actual topology of existing networks is sensitive information, which is not shared by network owners for obvious security reasons. However, communication systems are usually connected in tree-like structures (de Souza Couto et al. 2016). Their robustness is strictly related to the chosen architecture. However, robust architectures come with high end components and prohibitive costs. For this reason, a number of alternative topologies have been proposed to improve cost efficiency and scalability. For instance, the fat tree is one of the most common for using low-cost components. The fat tree topology, introduced by (Leiserson 1985), has three layers representing core switches, aggregation switches and edge switches. Aggregation and edge switches are group together in what are called pods. Each core is connected to all the pods through an aggregation switch. Within a pod, each aggregation switch is connected to all edge switches, which are then used to connect different sets of servers (Figure 7-2). Despite its practical application, fat trees have a rigid structure which is difficult to scale and adapt to telecommunication networks.
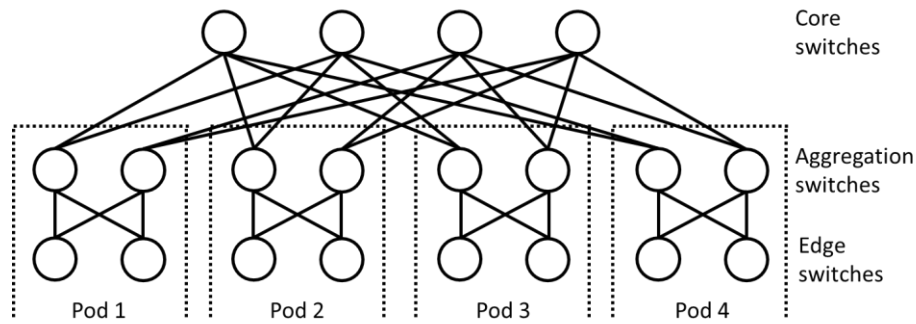
Figure 7-2. Example of a fat tree with four port switches.

Therefore, a hybrid topology was implemented to model Ideal City's network. BTSs were connected to BSCs using a star topology so that each BSC is connected to about the same number of BTSs. The main criterion for deciding the connections was based on the shortest distance. It was supposed that all connections are made through fiber optic cables running underground. The star topology has many advantages: (i) when a BTS node fails the rest of the network is still able to operate; (ii) the system can be easily expanded adding more nodes and connecting them to the central BSC; (iii) it can handle heavy data traffic. Nonetheless, this topology comes with some disadvantages since it can be quite expensive to build due to the length of the connections. Also, the failure of a BSC implies that all BTSs linked to it would fail as well, leaving a large area unserved.

As far as the BSCs are concerned, they were arranged in a hierarchical topology following a three-layer approach where the layers are core, aggregation, and edge like in a fat tree. In the literature there is no unique definition of typical three-layer topologies as they are specifically designed based on the components and requests of infrastructure managers. The proposed three-layer topology consists of two core nodes which are both connected to four aggregation nodes. Each aggregation node has six connections to the edge nodes so that each edge node is linked to two different aggregation nodes. The topology scheme is illustrated in Figure 7-3.
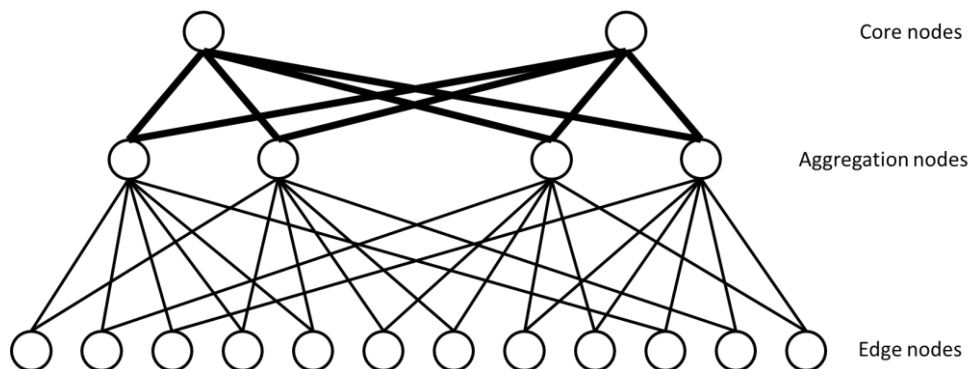
Figure 7-3. Proposed topology scheme.

The classification of BSCs amongst core, aggregation, edge nodes was determined mainly by their geographic location and size of the facilities. The most barycentric BSCs were selected as core nodes, then the closest and biggest ones were assumed as aggregation nodes. The remaining peripheral stations are the edge nodes. Figure 7-4 shows the connection and the classification of the BSCs.

(a)

(b)

(c)
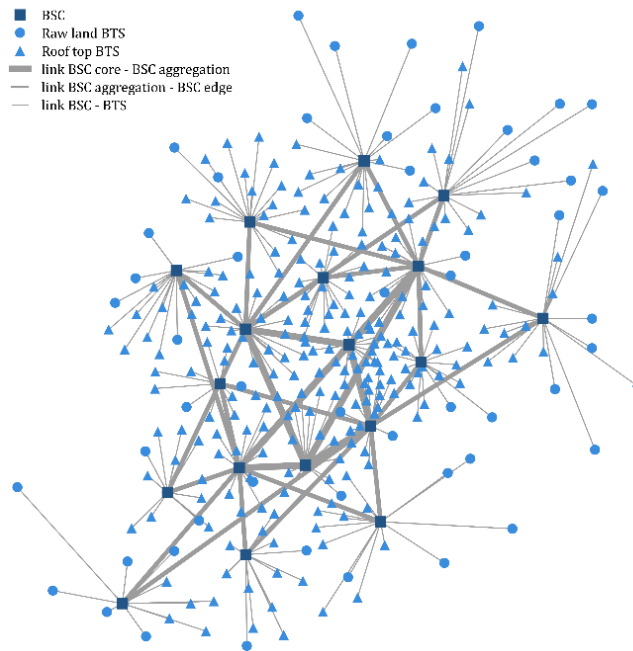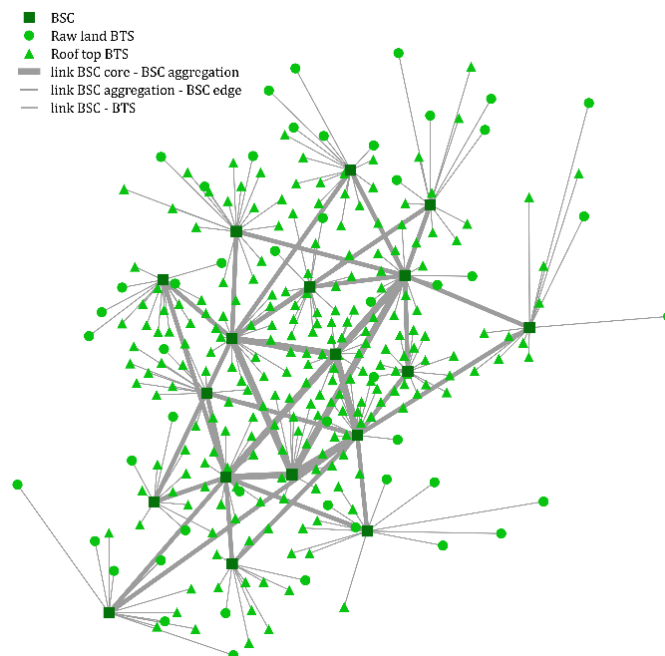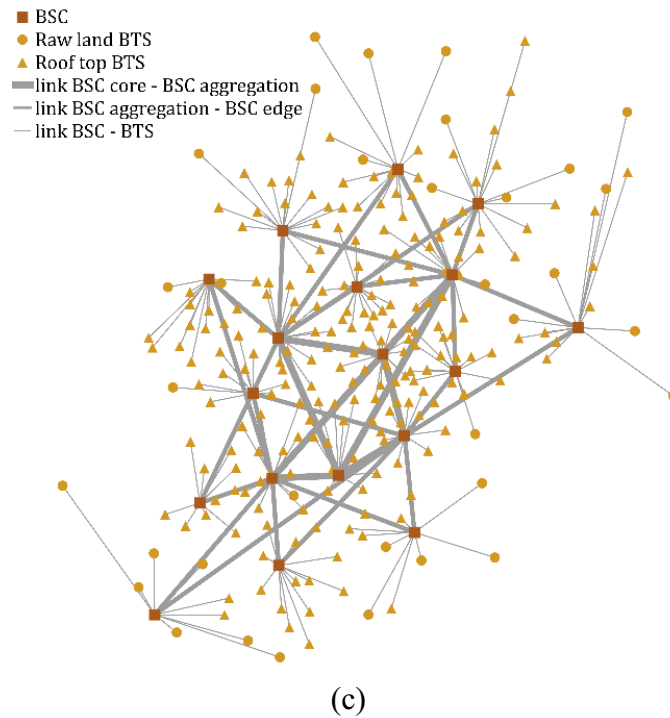
Figure 7-4. Network components and topology of (a) P1, (b) P2, (c) P3.

Each tower with an antenna enables a coverage area called cell. Usually, hex patterns are used to design wireless networks and pinpoint tower locations. Ideally, locations are chosen to ensure that the demand is met without having holes or excessive overlaps. Other factors influencing the location are the proximity to roads for easy access, the availability of power, the lack of electromagnetic interference. Most importantly, the choice is influenced by demographic and traffic data. When the potential utilization is near the capacity of the network, additional antennas should be deployed. To get the best performance out of the network, providers set adjacent cells to use different frequencies (Figure 7-5). In this way mobile devices can connect to a specific antenna avoiding possible interference.

Figure 7-5. Typical hex cell frequency pattern.

Since there is a limited amount of data that each antenna operating at a given frequency can handle, in highly populated areas additional antennas operating at different frequencies are added within a large cell. This process is called segmentation and allows to reuse frequencies, squeezing more customers in the same spectrum (Figure 7-6a). Furthermore,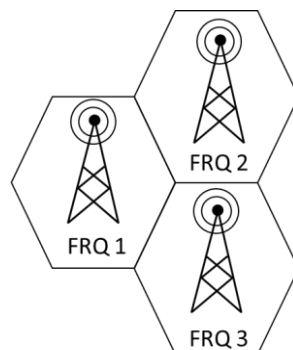 instead of omnidirectional antennas, bi- or tri-directional antennas can be exploited to enable the reuse of additional frequencies. (Figure 7-6b) shows an example where three antennas mounted on the same tower and operating at different frequencies allow to create three sectors within each cell, essentially tripling the overall capacity.

(a)   (b)
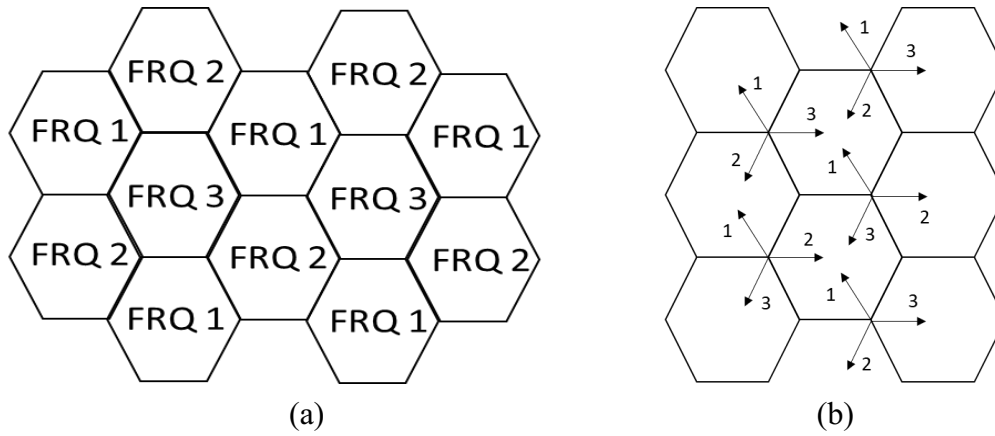
Figure 7-6. Example of (a) segmentation and (b) frequency reuse with tri-directional antennas.

Cells are categorized as macro or micro depending on their coverage area. Macro cells use low frequencies (from 700 to 900 MHz), which are able to carry the signal for longer distances, while micro cells use high frequencies (over 1 GHz). Based on the collected information, it was possible to distinguish between BTSs that serve macro cells from those serving micro cells. Consequently, it was deemed that micro cells can cover an area up to 2km of maximum radius, while macro cells can reach further distances. This threshold was defined according to the common practice as described in (Peric and Callahan 2013; Zhang et al. 2014).

7.3 Network performance

7.3.1 SINR

The performance of the network was evaluated through the signal-to-interference-plus-noise-ratio (SINR). This quantity is widely used in telecommunication engineering to define the capacity of the system and the rate of data transfer. It is defined as shown in Equation (7-1):

$$SINR = \frac{P}{I + N} \qquad (7\text{-}1)$$

where:

- P is the power of the received signal calculated as the difference between the transmission power (PT) and the reduction in power density called path loss (PL).
- I is the interference coming from other signals.
- N is the background noise in the signal.

The larger the SINR the better the signal strength. Table 7-2 indicates how SINR values expressed in decibels translate in terms of signal quality.

Table 7-2. SINR and quality of the signal.

SINR	Signal strength	Description
≥ 20 dB	Excellent	Strong signal with maximum data speeds.
10 dB to 20 dB	Good	Strong signal with good speeds.
0 dB to 10 dB	Fair	Fair but useful, fast and reliable data speeds may be attained, but marginal data with dropouts is possible.
-15 dB to 0 dB	Poor	Performance will drop drastically.
≤ -15 dB	No signal	Disconnection.

In accordance with (Series 2015; Wannstrom 2013), it was assumed a transmission power PT of 43dBm and 30dBm for macro and micro cells, respectively. The power contained in the transmitted signal attenuates as it propagates through space. This path loss is due to many reasons such as free-space loss, refraction, reflection, diffraction, etc. Depending on the surrounding environment it could be more or less significant. For instance, urban areas tend to have greater path loss because of the dense built environment which represents an obstacle for the propagation of signals. The simplest path loss model is the free space (Balanis and Polycarpou 2003). Its formulation involves only the distance between BTS and UE and the frequency of the signal. It is then assumed that BTS and UE are in line of sight, meaning that no obstacles are considered. This model can be useful for a raw estimate of the path loss, although is not adequate for applications in urban areas. A more refined model is the one proposed by (Hata 1980). This empirical model has two formulations that can be used to calculate the

attenuation in both urban and rural areas, and it is based on data collected in Tokyo, Japan. Additional parameters of the formulation are the height of BTS and the height of UE. The Hata model comes with some limitations: it is valid for frequencies between 150 and 1,500 MHz, BTS heights up to 200m, and maximum BTS-UE distance of 20 km. Since in modern infrastructures frequencies reach beyond 1,500 MHz, an extension of the Hata model was proposed by the European Co-operative for Science and Technical research (Mogensen and Wigard 1999).

For a more accurate application, macro and micro cells were considered separately in the analysis of the signal propagation. This was possible choosing the model developed by the International Telecom Union (ITU) (Series 2009), which is based on the results found in (Dong et al. 2007; Zhang et al. 2008). In addition, the method differentiates between a line of sight (LoS) and a not line of sight (NLoS) condition. If the distance between BTS and UE is small, then they can be considered in LoS, meaning the signal travels in a direct path from the source to the receiver without being diffracted, refracted, reflected, or absorbed. LoS is a desirable condition but not essential to get good performance since modern error correction protocols are able to compensate for indirect signals. The no line of sight condition happens when the UE is shielded by buildings, trees, hills, and other obstacles. To determine the probability for a pair BTS-UE to be in LoS, the ITU proposed two empirical formulas, one for macro ($P_{LoS,ma}$) and one for micro cells ($P_{LoS,mi}$).

$$P_{LoS,ma} = \min\left(1, \frac{18}{d}\right)\left(1 - \exp\left(-\frac{d}{63}\right)\right) + \exp\left(-\frac{d}{63}\right) \qquad (7\text{-}2)$$

$$P_{LoS,mi} = \min\left(1, \frac{18}{d}\right)\left(1 - \exp\left(-\frac{d}{36}\right)\right) + \exp\left(-\frac{d}{36}\right) \qquad (7\text{-}3)$$

Both Equation (7-2) and (7-3) depend only on the distance d between the BTS and UE expressed in meters. The lower thresholds for UE to be in LoS are 0.20 for macro and 0.23 for micro cells. In conclusion, for an urban environment, the ITU model consists of four possible equations to calculate PL: (i) LoS micro cell ($PL_{mi,LoS}$); (ii) NLoS micro cell ($PL_{mi,NLoS}$); (iii) LoS macro cell ($PL_{ma,LoS}$); (iv) NLoS macro cell ($PL_{ma,NLoS}$). These are detailed in the following Equations:

$$PL_{mi,LoS} = 22\log d + 28 + 20\log f \qquad (7\text{-}4)$$

$$PL_{mi,NLoS} = 36.7\log d + 22.7 + 26\log f \qquad (7\text{-}5)$$

$$PL_{ma,LoS} = 22\log d + 28 + 20\log f \qquad (7\text{-}6)$$

$$PL_{ma,NLoS} = 161.04 - 7.1\log_{10} W_m + 7.5\log_{10}\frac{h_m}{h_{BTS}} +$$

$$-\left(24.37 - 3.7\left(\frac{h_m}{h_{BTS}}\right)^2\right)\log_{10} h_{BTS} +$$

$$+\left(43.42 - 3.1\log_{10} h_{BTS}\right)\left(\log_{10} d - 3\right) +$$

$$+20\log_{10} f - \left(3.2\left(\log_{10} 11.75 h_{FU}\right)^2 - 4.97\right)$$

(7-7)

where:

- d = distance between BTS and UE expressed in [km];
- f = frequency of the signal expressed in [MHz];
- h_{BTS} = height of Base station expressed in [m];
- h_{FU} = height of users, set to 1.5m by default;
- W_m = average width of the roads expressed in [m];
- h_m = average height of buildings expressed in [m];

To extend the calculation to the urban area, the population was dived in user clusters located in the same coordinates of the buildings. Each cluster consists of a different number of users who represent the occupants of each building. As an example, Figure 7-7 shows the PL from a user cluster location towards all the BTSs of P1. As it can be seen, PL is strongly influenced by the distance, although some distant BTSs might experience a smaller loss than closer ones because of the height difference. Once the PL between each user cluster and all the BTSs is obtained, the numerator P of the SINR can be computed. Table 7-3 reports a generic correspondence between P values and signal strength.
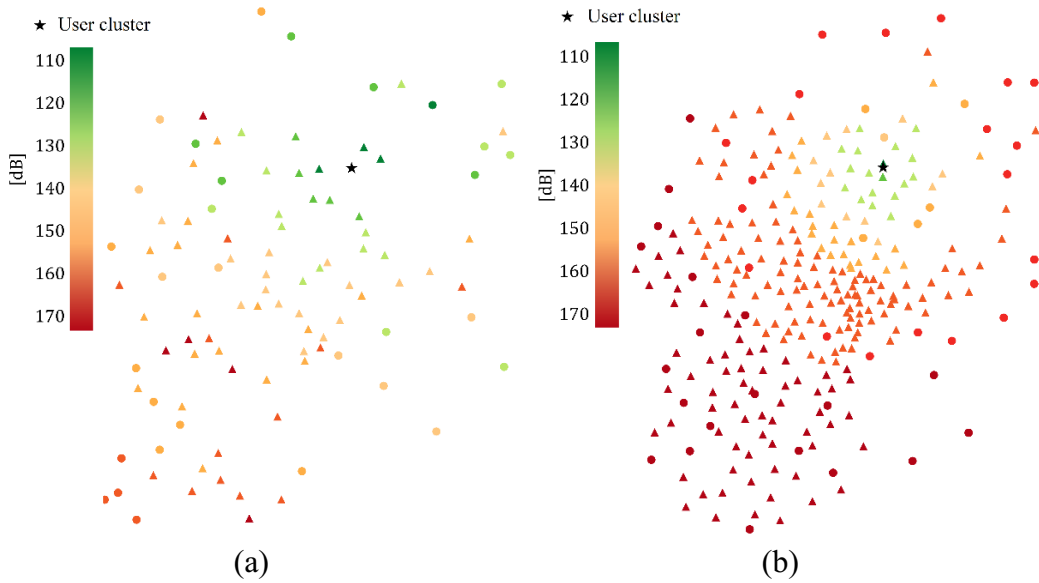

(a)　　　　　(b)

Figure 7-7. Path loss example for (a) macro and (b) micro cells of P1's network.

Table 7-3. Power and quality of the received signal.

P	Signal strength	Description
$\geq$ -75dBm	Excellent	Strong signal with maximum data speeds.
-75dBm to -85dBm	Good	Strong signal with good speeds.
-85dBm to -95dBm	Fair	Fair but useful, fast and reliable data speeds may be attained, but marginal data with dropouts is possible.
-95dBm to -110dBm	Poor	Performance will drop drastically.
$\leq$ -110dBm	No signal	Disconnection.

The interference I depends on the configuration of the cells as previously described. In Ideal City, since it was impossible to replicate the exact cell segmentation and frequency scheme, a frequency reuse factor equal to 1 was assumed. This implies that BTSs can use all the frequencies available to the provider, which is a cautious scenario. Therefore, all BTSs are able to transmit a signal to a given user cluster, generating a high level of interference. Under this assumption, the interference was defined as the difference between the sum of the received power P of all BTSs and the P of the BTS for which the SINR is being calculated. If n is the total number of BTSs, the interference between a user UE and the *i-th* BTS would be given by Equation (7-8):

$$I_{UE-BTSi} = \sum_{j=1}^{n} P_j - P_i \qquad (7-8)$$

The noise N can be seen as an additional interference caused by the surrounding environment. Nonetheless, because a frequency reuse factor equal to 1 was chosen, the interference generated by the other BTSs is so high that it would not make any difference to include the calculation of the noise. Hence, this term was neglected.

Figure 7-8 shows an example of the SINR experienced by a user cluster with respect to all BTSs serving macro and micro cells. As it can be seen, SINR values are quite small due to high interference generated by assuming a frequency reuse factor equal to 1.
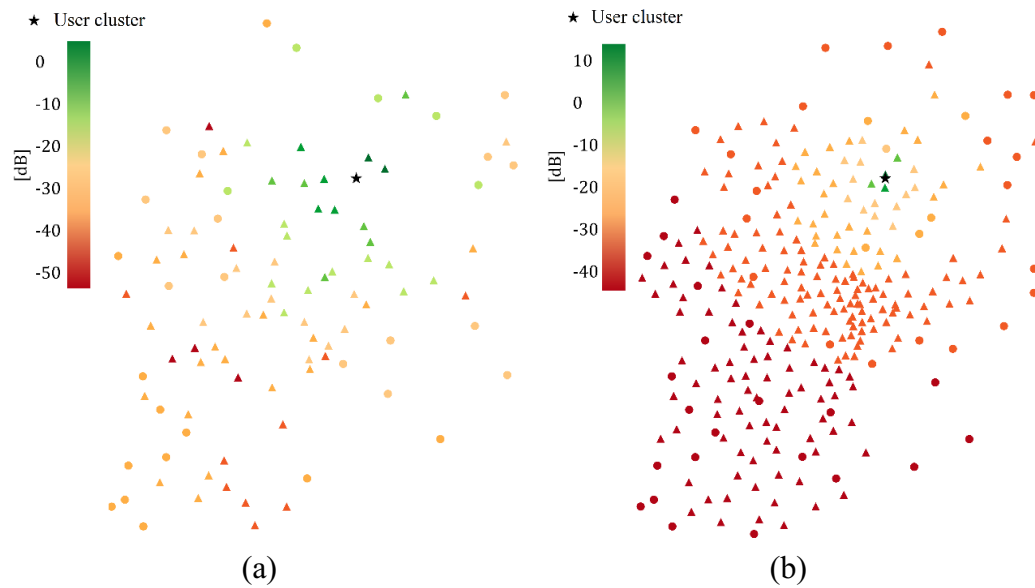
Figure 7-8. Visualization of the SINR experienced by a user cluster for (a) macro and (b) micro cells of P1's network.

7.3.2 Throughput

The performance of the network was measured in terms of throughput, which represents the rate of successfully delivered data per time unit (Miao et al. 2016). Commonly, design procedures are aimed at maximizing the throughput to increase capacity and service quality. The throughput can be calculated from the SINR through a mapping procedure. To this purpose, a number of parameters should be defined. These are:

- Channel Bandwidth
- Resource Block
- Duplex Mode
- Channel Quality indicator
- Modulation Coding Scheme
- Transport block size
- Antenna Configuration

The bandwidth (BW) indicates how many resources are available to transmit data over the selected channel. Different BW means a different number of resource blocks (RBs). An RB represents resource block (RB) is the smallest unit of resources that can be allocated to a UE. In 3G and 4G technology, six bandwidths are available, and each is associated with a maximum number of RBs as shown in Table 7-4 (3GPP 2010).

Table 7-4. Resource blocks per channel bandwidth.

Channel bandwidth [MHz]	1.4	3	5	10	15	20
Resource blocks	6	15	25	50	75	100

Depending on the BTS operating band, different BWs are available. Table 7-5 summarizes the BWs and main characteristics of bands 3 and 20, which are those of Ideal City's BTSs. This information was extracted from the "E-UTRA Operating Bands" and "E-UTRA Channel Bandwidth" tables presented in (3GPP 2010).

Table 7-5. Characteristics of the selected frequency bands.

Band	Duplex mode	Frequency [MHz]	Uplink [MHz]	Downlink [MHz]	Channel bandwidths [MHz]
3	FDD	1,800	1,710 - 1,785	1,805 - 1,880	1.4, 3, 5, 10, 15, 20
20	FDD	800	832 - 862	791 - 821	5, 10, 15, 20

In the absence of data from the providers, it was assumed a BW of 10 MHz for both bands and all providers. This was a somewhat cautious assumption as modern networks aim at higher BWs. As a consequence, for each BW, 50 RBs are available. As described in Table 7-5, the adopted duplex mode was the frequency division duplex (FDD). Duplex modes are spectrum usage techniques to guarantee that the signal is transmitted in both directions downlink and uplink at the same time. Possible modes are FDD and time division duplex (TDD). TDD uses a single frequency band for transmitting and receiving, which means the actual bandwidth capacity is split in half between transmit and receive. On the contrary, FDD needs two separate channels for the transmitter and the receiver, ensuring the full bandwidth capacity in uplink and downlink.

The channel quality indicator (CQI) carries information about the received signal quality. It is usually calculated from the SINR directly by the UE. In LTE (3G and 4G) CQI has 15 levels. To each level corresponds a modulation coding scheme (MCS) (Fan et al. 2011). MCS defined how much data can be transferred per resource element. Obviously the better the quality the higher the MCS and the faster the data flow. Once the UE sends information about the CQI to the BTS, the BTS defines the MCS. Supported modulation schemes in LTE are QPSK, 16QAM, 64QAM. These can theoretically transmit up to 2, 4, and 6 bits respectively. Actual transfer rates depend on the coding rate, i.e., the efficiency of a given modulation scheme. For instance, a 16QAM scheme with a code rate of 0.6504 can carry only

2.6016 bits of successful data. The combination of modulation scheme and coding rate results in the MSC parameter, which is constantly updated during the time of data transfer.

After determining the MCS, the BTS selects the transport block size (TBS). Given the TBS and the number of RBs, the number of bits that can be transmitted in 1ms can be determined (Rathi et al. 2014). The data transmitted can be increased by using multiple antennas. In modern networks, it is common for the receiver, the transmitter, or both to use a multiple-input-multiple-output (MIMO) scheme to improve performances (Lee et al. 2009). In the analyzed case study, the 2x2MIMO technique was used. With this configuration, BTS and UE use two antennas to exchange information increasing the throughput by 1.7 times (Martín-Sacristán et al. 2009).

The relation between SINR and throughput is modulation specific, as discussed by Olmos et al. (2010). Mühleisen et al. (2011) mapped the SINR to a subset of 13 MCSs with different coding rate for a bandwidth of 20MHz. In this study, a subset of 14 MCSs with different coding rate for a bandwidth of 10MHz defined by the LTE standard were used to build the functions. Then, out of the obtained functions, a linear envelop curve was generated by taking the maximums of the functions as illustrated in Figure 7-9. Therefore, it was possible to assign a throughput to each UE-BTS pair based on the previously calculated SINR. It is worth noting that this represents an ideal situation since each UE gets the best modulation available, which is not always the case. The actual modulation selected by the BTS is influenced by many factors such as distance, interference and number of UE already connected. This hypothesis had to be introduced in absence of information about the performance and the data traffic of the existing networks. On the other hand, the assumption of a frequency reuse factor equal to 1 introduced a substantial interference which decreased the SINR for all UE.
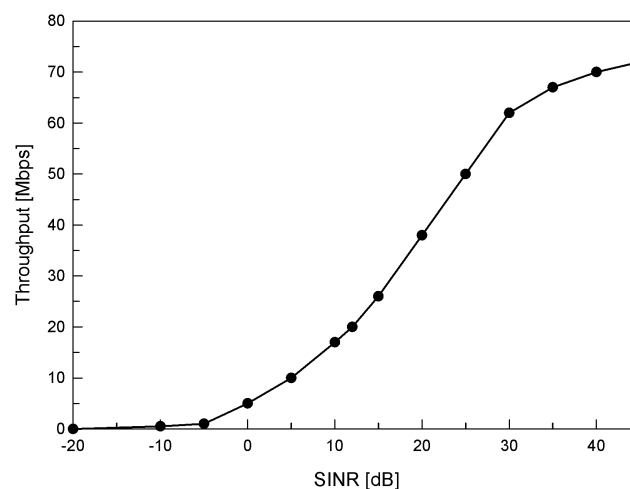

Figure 7-9. SINR-throughput curve.

7.4 Vulnerability and interdependence with the building portfolio

Defining the vulnerability of telecommunication networks is a challenging task due to the large number of components and structures involved. In the literature, few studies can be found related to this endeavor, mainly because networks are privately managed. The only evidence of failure come clear after natural disasters. In many cases, the main reason for failures is due to design errors (Travanca et al. 2013). Masts and monopoles are the most common structures used to install antennas. If not designed correctly, their slenderness and high flexibility can lead to collapse or large displacements which ultimately cause damage to cables and electric components. While (FEMA 2003) provided fragility curves only for telecommunication buildings, little research has been done on the seismic vulnerability of towers. Typically, only peculiar designs and high-rise raw land towers have been analyzed.

The evaluation of vulnerability of towers mounted on rooftops is even more complex as it involves the dynamic response of the building. Assi and McClure (2007) proposed a simplified method to estimate the maximum base shear and overturning moment at the tower-building interface. The analysis serves as a design check. If the seismic loads are predominant, a dynamic analysis of the tower-building system is recommended. Despite being a simplified static method, it requires specific input parameters such as the seismic acceleration at the base of the tower, mass distribution, and horizontal acceleration profile along the height of the tower.

Given the available information, performing a seismic damage simulation on the entire network of the case study would require many assumptions. First, although the section type was identified, the dimensions and the elements of the sections are unknown. Then, information about the type of connections should be speculated to verify them, introducing several uncertainties in the model.

In this study, for a preliminary analysis, the vulnerability of the network was attributed only to the vulnerability of the building portfolio. It is safe to assume that a tower and the corresponding BTS installed on top of a building would fail if the damage state of that building were "complete" (i.e., collapsed). In addition, due to the topology of the network, in case a building hosting a BSCs collapsed, all BTSs connected to that BSC would be out of service. This relationship defines the interdependency between these two systems.

Telecommunication systems are also dependent on the power network. However, most of them have backup systems running on batteries or fuel that can keep them working for few hours, waiting for repairing interventions. Since the analysis is aimed at the evaluation of performance in the aftermath of a seismic

event, the interdependency between power and telecommunication network was not accounted at this stage.

7.5 Performance metrics for resilience

The first proposed metric (R_{TOW}) that can be defined is the ratio between the number of functional towers ($N_{T,f}$) and the total number of towers (N_T):

$$R_{TOW} = \frac{N_{T,f}}{N_T} \qquad (7\text{-}9)$$

R_{TOW} is a performance index related to the physical damage of the network. A value close to 1 indicates that the network is robust, while low values mean that strategic measures should be taken to increase robustness. This metric could be associated with an economic loss due to repair, replacement, and downtime costs. Typically, the more redundant the network the higher the probability to obtain a large R_{TOW} value. However, in large-scale networks, if many towers collapse the economic loss might still be substantial and should be considered.

The second proposed metric (R_{THR}) is related to the quality of the service. It is calculated as the ratio between the post and pre-disaster weighted mean throughput (<THR>):

$$R_{THR} = \frac{\langle THR \rangle_{post-disaster}}{\langle THR \rangle_{pre-disaster}} \qquad (7\text{-}10)$$

Throughput is defined for each pair user cluster-BTS. To get a general measure of the quality of the service for the entire network, for each user cluster the highest throughput was considered. To avoid any bias due to the variance of the throughput, the obtained values were weighted by the number of users in each cluster as shown in Equation (7-11):

$$\langle THR \rangle = \frac{\sum_{i=1}^{c} N_{UE,i} \cdot THR_i}{N_{UE}} \qquad (7\text{-}11)$$

where: $N_{UE,i}$ is the number of users in each cluster, c is the number of clusters, THR_i is the highest throughput for the *i-th* cluster, N_{UE} is the total number of users served by the considered provider. By definition, low values of R_{THR} imply that the event causes a significant loss in the quality of the service, meaning several users experiencing slow data transfer.

Considering the best throughput value obtained for each user cluster, it is possible to calculate the number of users per BTS. This is only a theoretical

representation since depending on the actual demand and traffic, users might connect to other BTSs and have lower throughput. However, the number of users served by each BTS could be used as an indicator of critical conditions. As towers fail because of the earthquake, a smaller number of BTSs would have to serve a larger number of customers. During an emergency, such situation is likely to result in network overloads, compromising the possibility for users to connect. Consequently, the R_{BTS} index was introduced. It is defined as the ratio between the post and pre-disaster average number of users per BTS (<UExBTS>), as shown in Equation (7-12):

$$R_{BTS} = \frac{\langle UE \times BTS \rangle_{post-disaster}}{\langle UE \times BTS \rangle_{pre-disaster}} \qquad (7\text{-}12)$$

By its definition, $R_{BTS} > 1$ indicates that the load on the infrastructure has increased. In case of extreme events, R_{BTS} can assume values greater than 1.

7.6 Results

The proposed procedure was applied to Ideal City under the same four benchmark scenarios for all the providers. Form the building damage assessment, failed BTSs and BSCs could be determined as previously discussed. Figure 7-10, Figure 7-11, Figure 7-12 show the damage maps of the network's towers under all seismic events for P1, P2, and P3, respectively. The maps allow a preliminary and straightforward understanding of the impact of each event on the network. Northridge scenario was the most disruptive, followed by El Centro and Kobe, while Hachinohe was the one that caused the least damage for all the providers. The failure maps take already into account the topology of the networks. Therefore, in case a BSC fails, the connected BTSs are automatically excluded and considered as failed, even though some of them might not have suffered any damage. The actual number of collapsed towers is reported in Table 7-6 for each provider and event. From the number of failed towers, it was then possible to calculate the first of the proposed metric R_{TOW}, which is also reported in Table 7-6. Overall, R_{TOW} values are very similar for all networks. P3, which is also the provider with the least number of towers, turned out to be slightly more robust, with the exception of the Northridge scenario. The collapse of BSCs seemed to be a key factor as it can drastically change the conditions of the network. For instance, under the El Centro event, the collapsed towers are only about 30, but since 8 out of 18 BSCs collapsed, the total number of failed towers increased more than four times. The Northridge scenario caused the collapse of 15 BSCs, which reflects in R_{TOW} values smaller than 0.10.

Figure 7-10. P1 network damage after (a) El Centro, (b) Kobe, (c) Hachinohe, (d) Northridge scenarios.

(c)

(d)

Figure 7-11. P2 network damage after (a) El Centro, (b) Kobe, (c) Hachinohe, (d) Northridge scenarios.
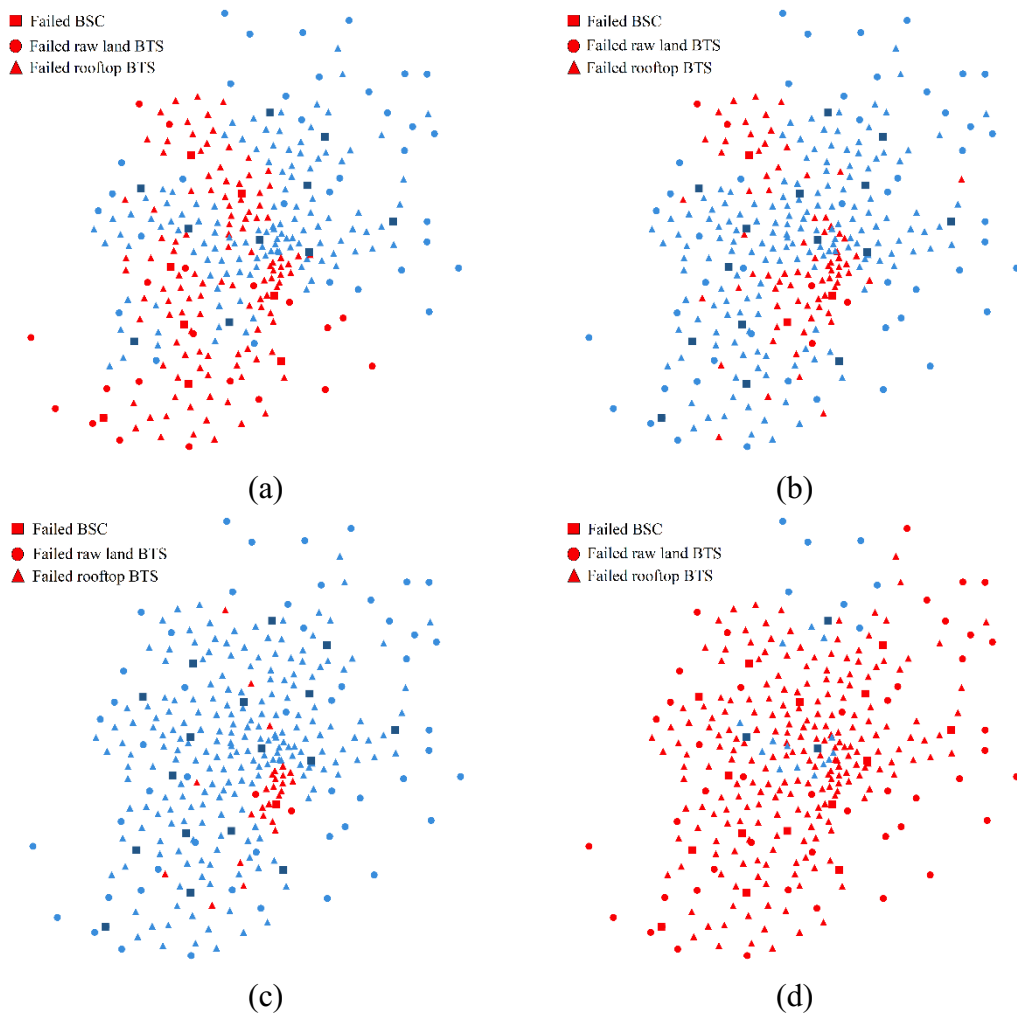

(a)

(b)

(c)
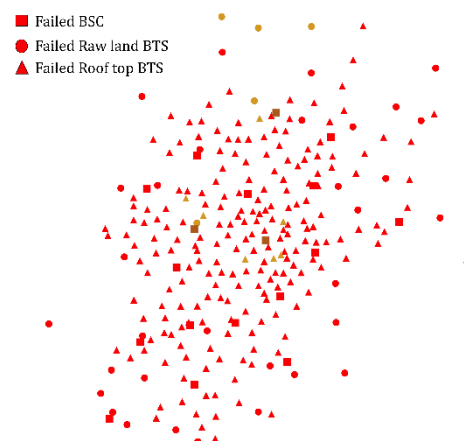
(d)
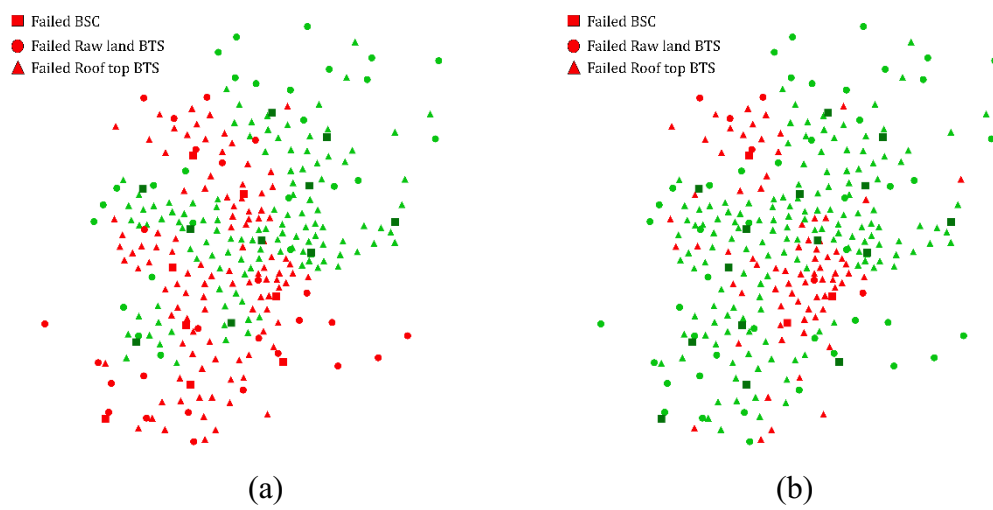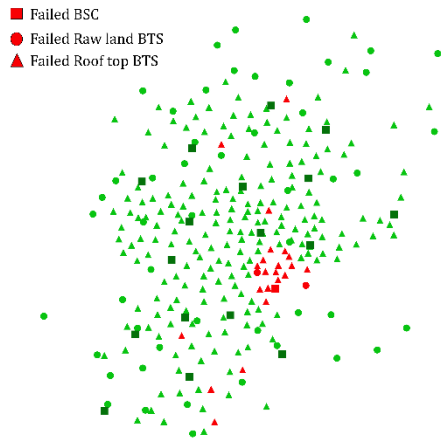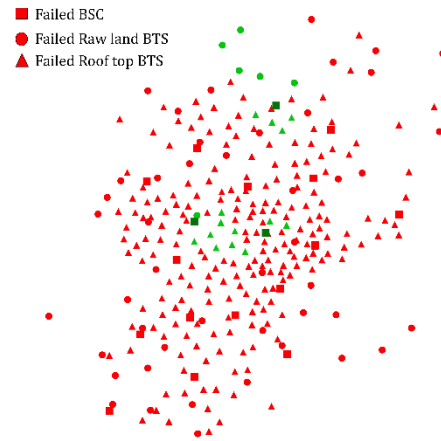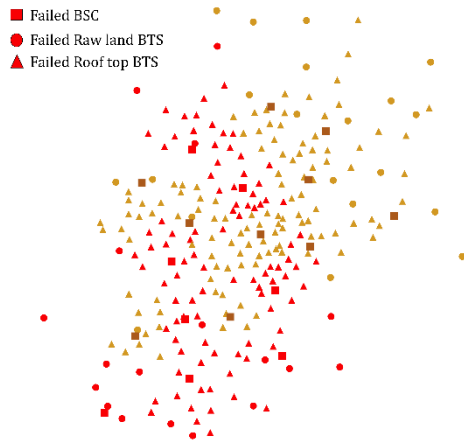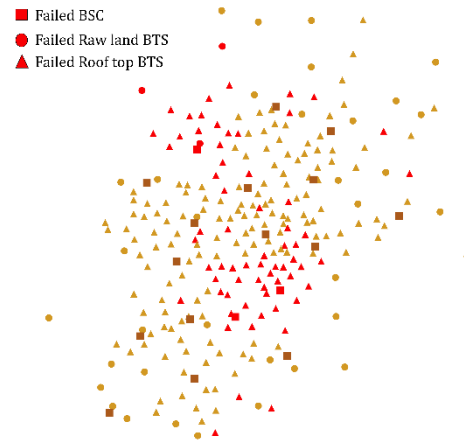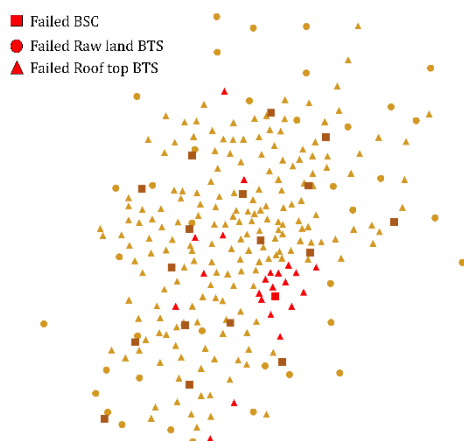
Figure 7-12. P3 network damage after (a) El Centro, (b) Kobe, (c) Hachinohe, (d) Northridge scenarios.

Table 7-6. Damaged components and R_{TOW} values.

		El Centro	Kobe	Hachinohe	Northridge
P1	No. of collapsed BSCs	8	1	3	15
	No. of collapsed towers	31	33	10	162
	No. of failed towers	141	82	29	280
	R_{TOW}	0.54	0.73	0.90	0.08
P2	No. of collapsed BSCs	8	1	3	15
	No. of collapsed towers	33	41	8	158
	No. of failed towers	136	82	25	264
	R_{TOW}	0.52	0.71	0.91	0.08
P3	No. of collapsed BSCs	8	1	3	15
	No. of collapsed towers	27	34	11	137
	No. of failed towers	116	70	23	246
	R_{TOW}	0.55	0.73	0.91	0.05

Failed towers were removed from the model, and the new network topologies were used to perform the rest of the analyses. First, a post disaster throughput was calculated for each user cluster. Figure 7-13 shows part of the throughput map in normal conditions (Figure 7-13a) and after the El Centro scenario for P1 (Figure 7-13b). Overall, it was observed that the throughput tends to decrease as expected. However, some users who are close to functional BTSs might experience a better connection because of the reduced interference. The mean weighted throughput in normal conditions and the index R_{THR} are listed in Table 7-7. The performance of the three networks was fairly similar, with only exceptions being P2 having an R_{THR} of 0.71 after the El Centro scenario against the 0.65 of the other providers, and P1 showing the worst performance after the Northridge scenario with an $R_{THR} = 0.41$.
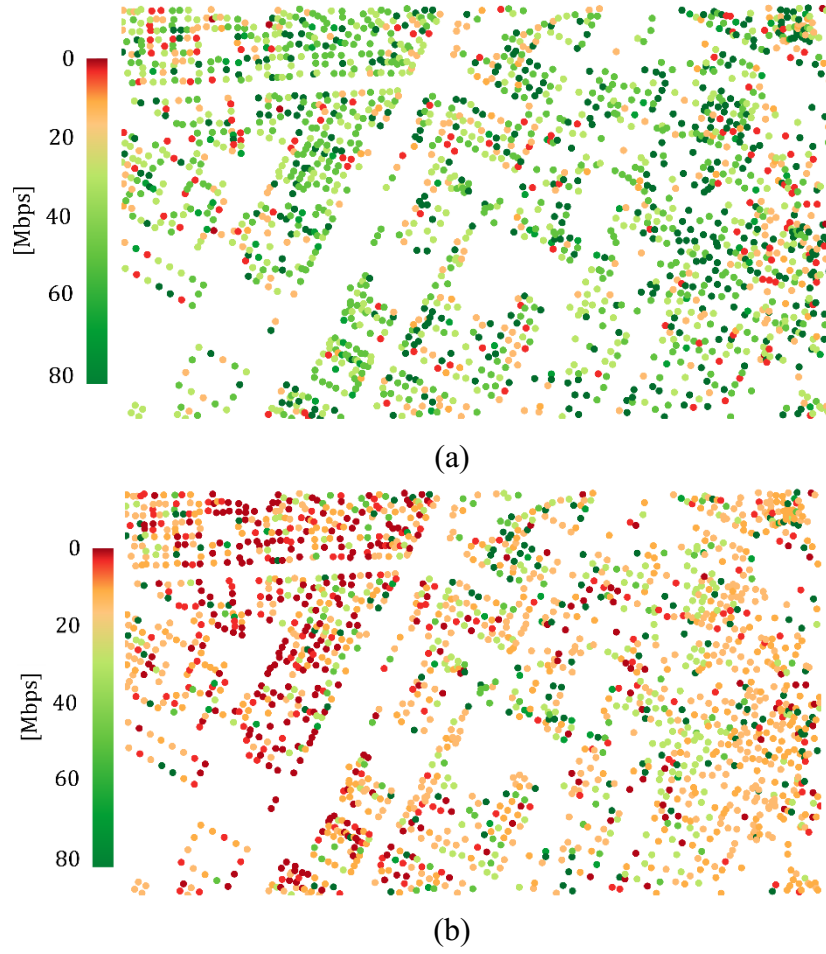
Figure 7-13. Example of throughput map for P1 (a) in normal conditions and (b) after El Centro scenario.

Table 7-7. R_{THR} values.

				El Centro	**Kobe**	**Hachinohe**	**Northridge**
P1	**<THR> [Mbps]**	19.89	**R$_{THR}$**	0.65	0.82	0.91	0.41
P2	**<THR> [Mbps]**	20.14	**R$_{THR}$**	0.71	0.83	0.92	0.45
P3	**<THR> [Mbps]**	19.65	**R$_{THR}$**	0.65	0.82	0.92	0.45

The average number of users served by each BTS in normal conditions and the R_{BTS} indexes after the four benchmark scenarios are reported in Table 7-8. Interestingly, it was found that under Kobe and Hachinohe scenarios, the average number of users decreased. In this case, especially in densely populated areas, the failure of some BTSs is beneficial as it reduces interference and leads to a more even distribution of the customers among BTSs. However, since this is an average

indicator, it is worth checking the actual number of users for each BTS. As shown by R_{BTS} values, under the El Centro scenario, <UExBTS> increased by 11% and 31% for the network managed by P1 and P2, respectively. This suggests that network overload phenomena might happen. On the other hand, overloads are almost certain after the Northridge case study as the calculated R_{BTS} ranges from 6.85 to 10.53.

Table 7-8. R_{BTS} values.

				El Centro	Kobe	Hachinohe	Northridge
P1	<UExBTS>	935.76	**R**BTS	1.11	0.82	0.68	6.85
P2	<UExBTS>	915.53	**R**BTS	1.31	0.92	0.74	9.39
P3	<UExBTS>	702.64	**R**BTS	0.97	0.76	0.63	10.53

To improve the performance in the post-disaster phase, it was proposed that the three providers would work cooperatively and share their resources to have one large network. This solution is often recommended as a strategic measure while the networks are being repaired. For example, after the 2016 Kaikoura earthquake, the providers put in place a temporary solution repurposing a piece of infrastructure, patching connections and sharing equipment (Giovinazzi et al. 2017). Therefore, assuming all BTSs and BSCs that remained functional could serve any user, the mean weighted throughput and the average number of UE per BTS were recalculated for the new shared network (Table 7-9). Overall, the positive effects gained with this strategy were considerable. The mean throughput was always greater than the single networks in all scenarios. Under the Kobe and Hachinohe events it was almost equal to the undamaged conditions. As far as the average number of users per base station is concerned, it significantly reduced in all scenarios, although it was still high for Northridge event indicating that overloads are likely.

Table 7-9. Average throughput and number of used per BTS after the provided measure.

	El Centro	Kobe	Hachinohe	Northridge
<THR> [Mbps]	14.83	18.96	19.20	9.72
<UExBTS>	606.81	444.69	363.12	3,877.55

7.7 Conclusions

The resilience analysis of urban telecommunication networks subject to earthquakes was discussed in this chapter. Three physical infrastructures owned and managed by different providers were modelled using information collected from a crowdsourced service and visual satellite inspections. A topology scheme inspired by typical three-layer hierarchy approach was adopted to define the connectivity. Given the limited information available, the vulnerability of the physical nodes of the network was associated with the vulnerability of the buildings where BSCs and BTSs are located. Considering collapsed buildings and disconnections due to the topology scheme, failed BSCs and BTSs were identified.

Three indexes were proposed to evaluate the performance of the three providers' networks under the four benchmark scenarios. The first represents the damage to the towers, which could also be interpreted as an economic loss. The second metric for resilience aims at evaluating the quality of the service in terms of throughput. This tends to be lower as the intensity of the event increases. However, in a damaged network with less antennas, some users might experience a better connection due to the reduced interference. Finally, an index was proposed to highlight possible overloads due to the increased number of users that BTSs must serve as a consequence of fewer functional BTSs. It was found that topology and vulnerability of BSCs are key aspects that have a huge impact on the results. Without redundant connections, the collapse of BSCs cause failure of large parts of the network.

To improve resilience in the post-disaster phase, it was simulated that the providers would cooperate to put in place one large network out of all the BSCs and BTSs that remained functional after each seismic scenario. The measure turned out to be effective as the mean throughput increased and the average number of users per BTS decreased significantly.

Chapter 8

8 Conclusions

8.1 Summary and concluding remarks

In this dissertation tools and methods to evaluate the resilience of communities and infrastructure systems were presented. After a review on current resilience frameworks and applications highlighting their limitations, a practical indicator-based approach to quantify resilience of regional communities was proposed. As a case study, the method was applied to the Italian regions. Only publicly available statistical records were used as input data. The selected indicators were combined through a weighting factors that consider their importance and interdependence. The importance and interdependence coefficient were obtained from questionnaires and differentiated based on three circumstances, i.e., normal condition, emergency, and restoration phase. In each of these circumstances, a resilience index was calculated for all regions. Results allowed to compare the performance among regions and can be used to identify which indicators need to be improved to increase the overall resilience. The results obtained for the most recent year were also compared to the average over the previous ten years. It was found that in most cases resilience decreased. The method proved to be effective as a preliminary analysis that could be used by decision makers to allocate available resources and national funds for the improvement of resilience.

The resilience of infrastructure systems was assessed by developing a virtual case study representative of a typical medium size European city. The virtual environment, named Ideal City, was modeled following a multi-layer approach that allows to perform analyses on the single infrastructures and to model the interdependencies between them. The vulnerability and seismic analyses of the building assets are a key element of the methodology. Ideal City's building portfolio consists of about 23,420 RC and masonry residential buildings. A simplified yet accurate simulation model was implemented to perform nonlinear dynamic

analyses while limiting the computational effort. Four simplified seismic scenarios were defined to test the seismic performance and resilience of the building portfolio and all the infrastructures of the urban area. The damage reported by the buildings revealed the greater fragility of masonry and old structures.

The road transportation, power, and telecommunication networks were analyzed next. The transportation system was modeled through graph theory. Average vertex degree and global efficiency were used to quantify the connectivity and performance of the graph, which consists of 14,239 nodes and 18,798 edges. To study the interdependency with the building damage, a machine learning approach was proposed. After a data collection and screening process, 310 pictures taken from 25 international seismic reports were used to measure debris extension and define 7 features to be used as inputs to 8 machine learning algorithms. The comparison among the obtained results showed that a random forest algorithm was the most accurate for this application. The debris extension of each building was compared the width of adjacent roads. Therefore, it was possible to determine which roads were blocked after the four benchmark scenarios. It was found that the percentage of blocked roads varies greatly, and even in less disruptive events some neighborhoods were completely isolated due to collapsed and heavily damaged buildings. Thanks to this tool, critical areas could be identified, allowing first responders to plan and prioritize rescue operations.

The Density Design Method was proposed to model Ideal City's power network. Instead of using pre-defined schemes, the method is based on the actual population density and demand of each neighborhood. The obtained network consists of 15 primary substations and 1,274 distribution substations connected in a tree-like structure. Failed substations were identified based on the damage suffered by the buildings where they are installed. The resilience of the network was assessed through a new resilience index and in terms of users without power. The proposed index includes all aspects of resilience, including redundancy and resourcefulness and highlights the importance of timely and effective repair interventions to reduce economical losses caused by outages. Results of the simulations showed that due to the vulnerability of the building portfolio and the tree structure of the network, even the event with the lowest intensity caused the failure of more than 40% of the substations. Locating substations inside of more robust buildings and redundant connections among them would greatly improve the resilience of the network.

Finally, the telecommunication infrastructure was modeled and analyzed. Three separate networks managed by as many providers were designed out of information gathered from a crowdsourced database and visual satellite inspections. Similarly, to the power network case, the interdependence with the built environment was taken into account by associating the failure of BSCs and BTSs with the collapse of the buildings hosting them. Failed telecommunication towers, throughput, and number of users per BTS were calculated for each scenario and used to defined three performance metrics for resilience. It was observed that in a damaged network with less antennas, some users might experience a better

connection due to the reduced interference. However, depending on the intensity of the event, some BTSs might be extremely overloaded. It was found that topology and vulnerability of BSCs are key aspects that have a huge impact on the results. A resilience improvement strategy was also explored by assuming that users could have access to all the BSCs and BTSs that remained functional after each scenario. Results showed the measure was effective as the mean throughput increased and the average number of users per BTS decreased significantly.

The proposed solutions are improvements to existing works and can benefit decision-makers before, during and after a seismic disaster. The research covered in this dissertation has met its main objectives stated in the introduction. The main contributions of this thesis are summarized as follows:

- Straightforward method to quantify the resilience of regional communities using public census data.
- Modeling techniques for complex and large-scale infrastructure systems of an urban community.
- Strategies to consider the interdependencies between the building portfolio and road transportation, power, and telecommunication networks.
- Machine learning approach to estimate the extension of the debris caused by building damages and collapses.
- New seismic vulnerability and performance metrics for the resilience analysis of critical infrastructure systems.

8.2 Future work

The research presented in this dissertation covers many aspects related to the resilience assessment for regional and urban communities. However, the proposed methods could benefit from further investigations to overcome limitations and extend their potential.

Some recommendations for future work are:

- Update the results of the regional resilience methodology as new data becomes available.
- Extend the regional resilience methodology introducing additional weighting factors that consider the social and geomorphological characteristics. In this way, indicators would have different weights for regions predominantly composed by rural communities compared to those mainly composed of large cities.
- Study the effects of specific seismic scenarios that could cause permanent ground deformations. This would allow to consider additional unavailable roads, and to include the vulnerability of the buried distribution lines and fiber optic cables of power and telecommunication networks, respectively.

- Improve the accuracy of the machine learning algorithm for the estimation of the debris extension as more data about previous events are available.
- Include the interdependence between power and telecommunication network by performing analyses over an extended period of time after the seismic event.
- Study the vulnerability of telecommunication towers based on different heights, geometric properties, and types of connection. A probabilistic approach could be followed to explore the seismic response of different categories of towers and develop fragility curves for each category.

References

3GPP (2010). "Further advancements for E-UTRA physical layer aspects." *3GPP TR 36.814, Tech. Rep*.

Abeling, T., Huq, N., Chang-Seng, D., Birkmann, J., Wolfertz, J., Renaud, F., and Garschagen, M. (2019). "Understanding Disaster Resilience." *Framing Community Disaster Resilience*, John Wiley & Sons Hoboken NJ and Chichester, West Sussex, 9-25.

Adachi, Y., and Obata, H. (1990). "Disaster prevention measures of NTT for telecommunications network systems." *IEEE Communications Magazine*, 28(6), 18-24.

Allenby, B., and Fink, J. (2005). "Toward inherently secure and resilient societies." *Science*, 309(5737), 1034-1036.

Ambraseys, N. N., Simpson, K. u., and Bommer, J. J. (1996). "Prediction of horizontal response spectra in Europe." *Earthquake Engineering & Structural Dynamics*, 25(4), 371-400.

Assi, R., and McClure, G. (2007). "A simplified method for seismic analysis of rooftop telecommunication towers." *Canadian Journal of Civil Engineering*, 34(10), 1352-1363.

Ayyub, B. M. (2015). "Practical resilience metrics for planning, design, and decision making." *ASCE-ASME Journal of Risk and Uncertainty in Engineering Systems, Part A: Civil Engineering*, 1(3), 04015008.

Balanis, C. A., and Polycarpou, A. C. (2003). "Antennas." *Wiley Encyclopedia of Telecommunications*.

Bastian, M., Heymann, S., and Jacomy, M. "Gephi: an open source software for exploring and manipulating networks." *Proc., Third international AAAI conference on weblogs and social media*.

Breiman, L. (2001). "Random forests." *Machine Learning*, 45(1), 5-32.

Bruneau, M., Chang, S. E., Eguchi, R. T., Lee, G. C., O'Rourke, T. D., Reinhorn, A. M., Shinozuka, M., Tierney, K., Wallace, W. A., and Winterfeldt, D. v. (2003). "A Framework to Quantitatively Assess and Enhance the Seismic Resilience of Communities." *Earthquake Spectra*, 19(4), 733-752.

Cavalieri, F., Franchin, P., and Pinto, P. E. (2014). "Fragility functions of electric power stations." *SYNER-G: typology definition and fragility functions for physical elements at seismic risk*, Springer, 157-185.

CellMapper (2021). "Cellular Coverage and Tower Map." Accessed, 2021 https://www.cellmapper.net/.

Chang, S. E., and Shinozuka, M. (2004). "Measuring improvements in the disaster resilience of communities." *Earthquake spectra*, 20(3), 739-755.

Cimellaro, and Marasco, S. (2015). "A computer-based environment for processing and selection of seismic ground motion records: OPENSIGNAL." *Frontiers in Built Environment*, 1, 17.

Cimellaro, G., Zamani-Noori, A., Kammouh, O., Terzic, V., and Mahin, S. (2016). "Resilience of critical structures, infrastructure, and communities." *Berkeley, California: Pacific Earthquake Engineering Research Center (PEER)*, 318.

Cimellaro, G. P., Ozzello, F., Vallero, A., Mahin, S., and Shao, B. (2017). "Simulating earthquake evacuation using human behavior models." *Earthquake Engineering & Structural Dynamics*, 46(6), 985-1002.

Cimellaro, G. P., ReinHorn, A.M., Bruneau, M. (2010). "Framework for analytical quantification of disaster resilience." *Engineering Structures*, 32, 3639-3649.

Cimellaro, G. P., Renschler, C., Reinhorn, A. M., and Arendt, L. (2016). "PEOPLES: A Framework for Evaluating Resilience." *Journal of Structural Engineering*, 04016063.

Cimellaro, G. P., Tinebra, A., Renschler, C., and Fragiadakis, M. (2016). "New Resilience Index for Urban Water Distribution Networks." *Journal of Structural Engineering*, 142(8), C4015014.

Cohen, O., Leykin, D., Lahad, M., Goldberg, A., and Aharonson-Daniel, L. (2013). "The conjoint community resiliency assessment measure as a baseline for profiling and predicting community resilience for emergencies." *Technological Forecasting and Social Change*, 80(9), 1732-1741.

Crowder, J. A., Carbone, J. N., and Demijohn, R. (2016). "Multidisciplinary Systems Engineering." *Multidisciplinary Systems Engineering*, Springer, 27-64.

Cutter, S. L. (2016). "The landscape of disaster resilience indicators in the USA." *Natural hazards*, 80(2), 741-758.

Cutter, S. L., Ash, K. D., and Emrich, C. T. (2014). "The geographies of community disaster resilience." *Global Environmental Change*, 29, 65-77.

Cutter, S. L., Burton, C. G., and Emrich, C. T. (2010). "Disaster resilience indicators for benchmarking baseline conditions." *Journal of Homeland Security and Emergency Management*, 7(1).

de Souza Couto, R., Secci, S., Campista, M. E. M., and Costa, L. H. M. K. (2016). "Reliability and survivability analysis of data center network topologies." *Journal of Network and Systems Management*, 24(2), 346-392.

DEEDS (n.d.). "Digital Environment for Enabling Data-Driven Science." Accessed March 13, 2020 https://datacenterhub.org/.

Dikbiyik, F., Reaz, A. S., De Leenheer, M., and Mukherjee, B. "Minimizing the disaster risk in optical telecom networks." *Proc., Optical Fiber Communication Conference*, Optical Society of America, OTh4B. 2.

Domaneschi, M., Cimellaro, G. P., and Scutiero, G. (2019). "A simplified method to assess generation of seismic debris for masonry structures." *Engineering Structures*, 186, 306-320.

Dong, W., Zhang, J., Gao, X., Zhang, P., and Wu, Y. "Cluster identification and properties of outdoor wideband MIMO channel." *Proc., 2007 IEEE 66th Vehicular Technology Conference*, IEEE, 829-833.

Dueñas-Osorio, L., Craig, J. I., and Goodno, B. J. (2007). "Seismic response of critical interdependent networks." *Earthquake engineering & structural dynamics*, 36(2), 285-306.

EERI (n.d.). "The Earthquake Engineering Research Institute collection of case studies." Accessed March 13, 2020 http://db.concretecoalition.org/.

EERI (n.d.). "The Earthquake Engineering Research Institute Earthquake Clearinghouse." Accessed March 13, 2020 http://www.eqclearinghouse.org/.

Eidinger, J. (2018). "Fragility of the Electric Power Grid." *11th U.S. National Conference on Earthquake Engineering*Los Angeles, California.

Ellingwood, B. R., Cutler, H., Gardoni, P., Peacock, W. G., van de Lindt, J. W., and Wang, N. (2016). "The centerville virtual community: A fully integrated decision model of interacting physical and social infrastructure systems." *Sustainable and Resilient Infrastructure*, 1(3-4), 95-107.

EN1993-3-1 (2006). "Eurocode 3: Design of steel structures - Part 3-1: Towers, masts and chimneys - Towers and masts."

Faber, F. A., Hutchison, L., Huang, B., Gilmer, J., Schoenholz, S. S., Dahl, G. E., Vinyals, O., Kearnes, S., Riley, P. F., and von Lilienfeld, O. A. (2017). "Prediction Errors of Molecular Machine Learning Models Lower than Hybrid DFT Error." *J. Chem. Theory Comput.*, 13(11), 5255-5264.

Fan, J., Yin, Q., Li, G. Y., Peng, B., and Zhu, X. "MCS selection for throughput improvement in downlink LTE systems." *Proc., 2011 Proceedings of 20th international conference on computer communications and networks (ICCCN)*, IEEE, 1-5.

FEMA (2003). "Multi-hazard loss estimation methodology, earthquake model." *Washington, DC, USA: Federal Emergency Management Agency*.

FEMA (2011). "Hazus: FEMA's methodology for estimating potential losses from disasters."

FEMA (2016). "Provided Fragility Data." *Seismic Performance Assessment of Buildings, Volume 3 - Supporting Electronic Materials and Background Docu-mentation*, F. E. M. Agency, ed.Washington.

Folke, C., Carpenter, S., Elmqvist, T., Gunderson, L., Holling, C. S., and Walker, B. (2002). "Resilience and sustainable development: building adaptive capacity in a world of transformations." *AMBIO: A journal of the human environment*, 31(5), 437-440.

Fujisaki, E., Takhirov, S., Xie, Q., and Mosalam, K. M. "Seismic vulnerability of power supply: lessons learned from recent earthquakes and future horizons

of research." *Proc., Proceedings of 9th international conference on structural dynamics (EURODYN 2014). European Association for Structural Dynamics, Porto, Portugal*, 345-350.

Garcia, S., Kahhat, R., and santa cruz, S. (2016). "Methodology to characterize and quantify debris generation in residential buildings after seismic events." *Resources, Conservation and Recycling*, 117.

GEER (n.d.). "Geotechnical Extreme Events Reconnaissance." Accessed March 13, 2020 http://www.geerassociation.org/.

Geoportale (2018). "GEOPORTALE del Comune di Torino." Accessed, http://www.comune.torino.it/geoportale/.

Geoportale (2021). "Geoportale e governo del territorio." Accessed, 2021 https://geoportale.comune.torino.it/.

Ghobarah, A. "On drift limits associated with different damage levels." *Proc., International workshop on performance-based seismic design*, Dept. of Civil Engineering, McMaster University, June 28–July 1.

Gilbert, S., and Ayyub, B. M. (2016). "Models for the Economics of Resilience." *ASCE-ASME Journal of Risk and Uncertainty in Engineering Systems, Part A: Civil Engineering*, 2(4), 04016003.

Giovinazzi, S., Austin, A., Ruiter, R., Foster, C., Nayyerloo, M., Nair, N.-K., and Wotherspoon, L. (2017). "Resilience and fragility of the telecommunication network to seismic events." *Bulletin of the New Zealand Society for Earthquake Engineering*, 50(2), 318-328.

Giovinazzi, S., Pollino, M., Kongar, I., Rossetto, T., Caiaffa, E., Di Pietro, A., La Porta, L., Rosato, V., and Tofani, A. "Towards a decision support tool for assessing, managing and mitigating seismic risk of electric power networks." *Proc., International Conference on Computational Science and Its Applications*, Springer, 399-414.

Giovinazzi, S., Wilson, T., Davis, C., Bristow, D., Gallagher, M., Schofield, A., Villemure, M., Eidinger, J., and Tang, A. (2011). "Lifelines performance and management following the 22 February 2011 Christchurch earthquake, New Zealand: highlights of resilience."

Goldberger, J., Roweis, S., Hinton, G., and Salakhutdinov, R. (2004). "Neighbourhood components analysis." *Proceedings of the 17th International Conference on Neural Information Processing Systems*, MIT Press, Vancouver, British Columbia, Canada, 513–520.

Gomes, T., Tapolcai, J., Esposito, C., Hutchison, D., Kuipers, F., Rak, J., De Sousa, A., Iossifides, A., Travanca, R., and André, J. "A survey of strategies for communication networks to protect against large-scale natural disasters." *Proc., 2016 8th international workshop on resilient networks design and modeling (RNDM)*, IEEE, 11-22.

Google (2021). "Google Maps." Accessed, 2021 https://maps.google.com/.

Guidotti, R., Gardoni, P., and Rosenheim, N. (2019). "Integration of physical infrastructure and social systems in communities' reliability and resilience analysis." *Reliability Engineering & System Safety*, 185, 476-492.

Hagberg, A., Swart, P., and S Chult, D. (2008). "Exploring network structure, dynamics, and function using NetworkX." Los Alamos National Lab.(LANL), Los Alamos, NM (United States).

Haklay, M., and Weber, P. (2008). "Openstreetmap: User-generated street maps." *IEEE Pervasive Computing*, 7(4), 12-18.

Hata, M. (1980). "Empirical formula for propagation loss in land mobile radio services." *IEEE transactions on Vehicular Technology*, 29(3), 317-325.

Hosseini, S., Barker, K., and Ramirez-Marquez, J. E. (2016). "A review of definitions and measures of system resilience." *Reliability Engineering & System Safety*, 145, 47-61.

IRETI (2016). "Rete e Impianti." Accessed, https://www.ireti.it/impianti.

ISTAT (2020). "Istituto Nazionale di statistica." Accessed, http://dati.istat.it/.

ISTAT, A. S. I. (2016). "Istituto Nazionale di statistica."

Kammouh, O., Dervishaj, G., and Cimellaro, G. P. (2018). "Quantitative framework to assess resilience and risk at the country level." *ASCE-ASME Journal of risk and uncertainty in engineering systems, part A: civil engineering*, 4(1), 04017033.

Kammouh, O., Noori, A. Z., Taurino, V., Mahin, S. A., and Cimellaro, G. P. (2018). "Deterministic and fuzzy-based methods to evaluate community resilience." *Earthquake Engineering and Engineering Vibration*, 17(2), 261-275.

Kammouh, O., Zamani Noori, A., Cimellaro, G. P., and Mahin, S. A. (2019). "Resilience assessment of urban communities." *ASCE-ASME Journal of Risk and Uncertainty in Engineering Systems, Part A: Civil Engineering*, 5(1), 04019002.

Khadem, A., and Hossein-Zadeh, G. A. (2014). "Estimation of direct nonlinear effective connectivity using information theory and multilayer perceptron." *J. Neurosci. Methods*, 229, 53-67.

Kongar, I., Esposito, S., and Giovinazzi, S. (2017). "Post-earthquake assessment and management for infrastructure systems: learning from the Canterbury (New Zealand) and L'Aquila (Italy) earthquakes." *Bulletin of earthquake engineering*, 15(2), 589-620.

Krishnamurthy, V., Kwasinski, A., and Duenas-Osorio, L. (2016). "Comparison of power and telecommunications dependencies and interdependencies in the 2011 tohoku and 2010 maule earthquakes." *Journal of Infrastructure Systems*, 22(3), 04016013.

Latora, V., and Marchiori, M. (2001). "Efficient behavior of small-world networks." *Physical review letters*, 87(19), 198701.

Lee, J., Han, J.-K., and Zhang, J. (2009). "MIMO technologies in 3GPP LTE and LTE-advanced." *EURASIP Journal on wireless communications and networking*, 2009, 1-10.

Leiserson, C. E. (1985). "Fat-trees: universal networks for hardware-efficient supercomputing." *IEEE transactions on Computers*, 100(10), 892-901.

Liu, X., Ferrario, E., and Zio, E. (2017). "Resilience analysis framework for interconnected critical infrastructures." *ASCE-ASME J Risk and Uncert in Engrg Sys Part B Mech Engrg*, 3(2).

Liu, X., Ferrario, E., and Zio, E. (2017). "Resilience analysis framework for interconnected critical infrastructures." *ASCE-ASME Journal of Risk and Uncertainty in Engineering Systems, Part B: Mechanical Engineering*, 3(2).

Lu, X., Yang, Z., Cimellaro, G. P., and Xu, Z. (2019). "Pedestrian evacuation simulation under the scenario with earthquake-induced falling debris." *Safety Science*, 114, 61-71.

Malandrino, F., Chiasserini, C.-F., and Kirkpatrick, S. (2017). "Cellular network traces towards 5G: Usage, analysis and generation." *IEEE Transactions on Mobile Computing*, 17(3), 529-542.

Marasco, S., Noori, A. Z., and Cimellaro, G. P. (2017). "Resilience Assessment for the Built Environment of a Virtual City." *compdyn 2017 Proceedings*, 1-13.

Marnay, C., Aki, H., Hirose, K., Kwasinski, A., Ogura, S., and Shinji, T. (2015). "Japan's pivot to resilience: how two microgrids fared after the 2011 earthquake." *IEEE Power and Energy Magazine*, 13(3), 44-57.

Martín-Sacristán, D., Monserrat, J. F., Cabrejas-Peñuelas, J., Calabuig, D., Garrigas, S., and Cardona, N. "3GPP long term evolution: Paving the way towards next 4G." *Proc., Waves*.

Maskrey, A., Peduzzi, P., Chatenoux, B., Herold, C., Dao, Q.-H., and Giuliani, G. (2011). "Revealing Risk, Redefining Development, Global Assessment Report on Disaster Risk Reduction." *United Nations Strategy for Disaster Reduction*, 17-51.

MATLAB. 2018. MATLAB, version R2018aThe MathWorks, Inc., https://www.mathworks.com/.

Mazzoni, S., McKenna, F., Scott, M. H., and Fenves, G. L. (2006). "OpenSees command language manual." *Pacific Earthquake Engineering Research (PEER) Center*, 264.

Miao, G., Zander, J., Sung, K. W., and Slimane, S. B. (2016). *Fundamentals of mobile data networks*, Cambridge University Press.

Miles, S. B., and Chang, S. E. (2011). "ResilUS: A community based disaster resilience model." *Cartography and Geographic Information Science*, 38(1), 36-51.

Mirza, S. A., and MacGregor, J. G. (1979). "Variability of mechanical properties of reinforcing bars." *Journal of the Structural Division*, 105(ASCE 14590 Proceeding).

Mogensen, P. E., and Wigard, J. (1999). "COST Action 231: Digital Mobile Radio Towards Future Generation System, Final Report." *Section 5.2: On antenna and frequency diversity in GSM. Section 5.3: Capacity study of frequency hopping GSM network*.

Mühleisen, M., Bültmann, D., Schoenen, R., and Walke, B. "Analytical evaluation of an IMT-advanced compliant LTE system level simulator." *Proc., 17th European Wireless 2011-Sustainable Wireless Technologies*, VDE, 1-5.

Nemoto, Y., and Hamaguchi, K. (2014). "Resilient ICT research based on lessons learned from the Great East Japan Earthquake." *IEEE Communications Magazine*, 52(3), 38-43.

NIST (2015). "Disaster Resilience Framework." National Institute of Standards and Technology, 75% Draft for San Diego, CA Workshop

Norris, F. H., Stevens, S. P., Pfefferbaum, B., Wyche, K. F., and Pfefferbaum, R. L. (2008). "Community Resilience as a Metaphor." *Theory, Set of Capacities*.

Olmos, J., Ruiz, S., García-Lozano, M., and Martín-Sacristán, D. "Link abstraction models based on mutual information for LTE downlink." *Proc., COST*, 1-18.

OSSPAC (2013). "The Oregon resilience plan: Reducing risk and improving recovery for the next Cascadia earthquake and tsunami." Seismic Safety Policy Advisory Commission, Oregon, US.

Ouyang, M. (2014). "Review on modeling and simulation of interdependent critical infrastructure systems." *Reliability engineering & System safety*, 121, 43-60.

Owada, Y., Byonpyo, J., Kumagai, H., Takahashi, Y., Inoue, M., Sato, G., Temma, K., and Kuri, T. "Resilient mesh network system utilized in areas affected by the Kumamoto earthquakes." *Proc., 2018 5th International Conference on Information and Communication Technologies for Disaster Management (ICT-DM)*, IEEE, 1-7.

Pamungkas, A., Bekessy, S. A., and Lane, R. (2014). "Vulnerability modelling to improve assessment process on community vulnerability." *Procedia-Social and Behavioral Sciences*, 135, 159-166.

Park, J., Seager, T. P., Rao, P. S. C., Convertino, M., and Linkov, I. (2013). "Integrating risk and resilience approaches to catastrophe management in engineering systems." *Risk analysis*, 33(3), 356-367.

Peric, S., and Callahan, T. (2013). "Challenges with microcell deployment & configuration."

Pfefferbaum, R. L., Pfefferbaum, B., Van Horn, R. L., Klomp, R. W., Norris, F. H., and Reissman, D. B. (2013). "The communities advancing resilience toolkit (CART): An intervention to build community resilience to disasters." *Journal of public health management and practice*, 19(3), 250-258.

Planning, S. S. F., and Association, U. R. (2009). "Defining what San Francisco needs from its seismic mitigation policies."

Prettico, G., Gangale, F., Mengolini, A., Lucas, A. & Fulli, G (2016). "Distribution System Operators Observatory: From Europe-an Electricity Distribution Systems to Representative Distri-bution Networks." Publications Office of the European Union, Luxembourg.

QGIS. 2019. QGIS Las Palmas, version 2.18.19Open Source Geospatial Foundation Project, https://qgis.org/en/site/.

Qi, C., Fourie, A., Ma, G., Tang, X., and Du, X. (2018). "Comparative Study of Hybrid Artificial Intelligence Approaches for Predicting Hangingwall Stability." *Journal of Computing in Civil Engineering*, 32(2), 04017086.

Quinlan, J. R. (1986). "Induction of decision trees." *Machine Learning*, 1(1), 81-106.

Rathi, S., Malik, N., Chahal, N., and Malik, S. (2014). "Throughput for TDD and FDD 4 G LTE Systems." *International Journal of Innovative Technology and Exploring Engineering (IJITEE), ISSN*, 2278-3075.

Renschler, C. S., Frazier, A. E., Arendt, L. A., Cimellaro, G. P., Reinhorn, A. M., and Bruneau, M. (2010). *A framework for defining and measuring resilience at the community scale: The PEOPLES resilience framework*, MCEER Buffalo, NY.

Romero, N., Nozick, L. K., Dobson, I., Xu, N., and Jones, D. A. (2015). "Seismic retrofit for electric power systems." *Earthquake Spectra*, 31(2), 1157-1176.

Saja, A. A., Goonetilleke, A., Teo, M., and Ziyath, A. M. (2019). "A critical review of social resilience assessment frameworks in disaster management." *International journal of disaster risk reduction*, 101096.

Scherzer, S., Lujala, P., and Rød, J. K. (2019). "A community resilience index for Norway: An adaptation of the Baseline Resilience Indicators for Communities (BRIC)." *International Journal of Disaster Risk Reduction*, 36, 101107.

Scikit-learn, d. (2018). "Scikit-learn user guide."

Series, M. (2009). "Guidelines for evaluation of radio interface technologies for IMT-Advanced." *Report ITU*, 638, 1-72.

Series, P. (2015). "Propagation data and prediction methods for the planning of short-range outdoor radiocommunication systems and radio local area networks in the frequency range 300 MHz to 100 GHz." *tech. rep., ITU, Tech. Rep. ITU-R*.

Sharma, N., Tabandeh, A., and Gardoni, P. (2018). "Resilience analysis: A mathematical formulation to model resilience of engineering systems." *Sustainable and Resilient Infrastructure*, 3(2), 49-67.

Takeda, T., Sozen, M. A., and Nielsen, N. N. (1970). "Reinforced concrete response to simulated earthquakes." *Journal of the Structural Division*, 96(12), 2557-2573.

Tibshirani, R. (1996). "Regression Shrinkage and Selection Via the Lasso." *Journal of the Royal Statistical Society: Series B (Methodological)*, 58(1), 267-288.

Travanca, R., Varum, H., and Real, P. V. (2013). "The past 20 years of telecommunication structures in Portugal." *Engineering Structures*, 48, 472-485.

Twigg, J. (2007). "Characteristics of a disaster-resilient community: A guidance note." Department for International Development (DFID).

Twigg, J. (2009). "Characteristics of a disaster-resilient community: a guidance note (version 2)."

UNISDR (2007). "Hyogo Framework for Action 2005–2015: Building the Resilience of Nations and

Communities to Disasters." *Extract from the final report of the World Conference on Disaster Reduction*.

USGS (2013). "United States Geological Survey." Accessed, 2019 http://earthquake.usgs.gov/hazards/designmaps/grdmotion.php.

van der Maaten, L., and Hinton, G. (2008). "Visualizing Data using t-SNE." *J. Mach. Learn. Res.*, 9, 2579-2605.

Vapnik, V. N. (1995). *The nature of statistical learning theory*, Springer-Verlag.

Vapnik, V. N. (1998). *Statistical Learning Theory*, Wiley-Interscience.

Vrouwenvelder, T., and Faber, M. (2001). "Probabilistic model code." *Joint Committee on Structural Safety, website http://www.jcss.ethz*.

Wagner, I., and Breil, P. (2013). "The role of ecohydrology in creating more resilient cities." *Ecohydrology & Hydrobiology*, 13(2), 113-134.

Wannstrom, J. (2013). "LTE-advanced." *Third Generation Partnership Project (3GPP)*.

White, R. K., Edwards, W. C., Farrar, A., and Plodinec, M. J. (2015). "A practical approach to building resilience in America's communities." *American Behavioral Scientist*, 59(2), 200-219.

Yokel, F. Y. (1990). "Earthquake resistant construction of electric transmission and telecommunication facilities serving the Federal government report." National Inst. of Standards and Technology (NEL), Gaithersburg, MD (United ….

Zhang, J., Dong, D., Liang, Y., Nie, X., Gao, X., Zhang, Y., Huang, C., and Liu, G. "Propagation characteristics of wideband MIMO channel in urban micro- and macrocells." *Proc., 2008 IEEE 19th International Symposium on Personal, Indoor and Mobile Radio Communications*, IEEE, 1-6.

Zhang, J., Perez, D. L., Song, H., de la Roche, G., Liu, E., and Chu, X. (2014). "Small Cells-Technologies and Deployment, Second and Expanded Edition." John Wiley & Sons, Limited.

Zhu, M., McKenna, F., and Scott, M. H. (2018). "OpenSeesPy: Python library for the OpenSees finite element framework." *SoftwareX*, 7, 6-11.

Zimmerman, R. D., Murillo-Sanchez, C. E. & Thomas, R. J. (2011). "Matpower: Steady-State Operations, Planning and Analysis Tools for Power Systems

Research and Education." *IEEE Transactions on Power Systems* 26(1), 12-19.

Zou, H., and Hastie, T. (2005). "Regularization and variable selection via the elastic net." *J. R. Stat. Soc. Ser. B-Stat. Methodol.*, 67, 301-320.